Institut für Theoretische Physik I
Universität Stuttgart
Pfaffenwaldring 57
70550 Stuttgart

Quantum Thermodynamics under Observation: The Influence of Quantum Measurements

Von der Fakultät Mathematik und Physik der Universität Stuttgart zur Erlangung der Würde eines Doktors der Naturwissenschaften (Dr. rer. nat.) genehmigte Abhandlung

Vorgelegt von

Thomas Jahnke

aus Ludwigsburg

Hauptberichter:	Prof. Dr. Günter Mahler
Mitberichter:	Prof. Dr. Hans Peter Büchler
Tag der mündlichen Prüfung:	28. Februar 2011

Institut für Theoretische Physik der Universität Stuttgart

2011

(Dissertation Universität Stuttgart)

Danksagung

Ich möchte mich bei einigen Personen bedanken, die mich bei dieser Dissertation auf vielfältige Weise unterstützt haben.

Zuallererst bedanke ich mich ganz herzlich bei Prof. Dr. Günter Mahler dafür, dass er mir die Forschung in seiner Arbeitsgruppe ermöglicht hat. Seine sehr gute Betreuung und sein Interesse an meiner Arbeit, welches zu zahlreichen anregenden Diskussionen führte, haben maßgeblich zu dieser Dissertation beigetragen.

Prof. Dr. Hans Peter Büchler danke ich herzlich für die Übernahme des Mitberichts.

Ebenso danke ich Prof. Dr. Clemens Bechinger für die Übernahme des Prüfungsvorsitzes.

Bedanken möchte ich mich auch bei meinen ehemaligen Kollegen Suzanne Lanéry, Kilian Rambach, Florian Rempp, Heiko Schröder, Jens Teifel, Pedro Vidal, Gerald Waldherr und Hendrik Weimer für viele interessante Diskussionen. Insbesondere danke ich Heiko, Jens und Hendrik für die vielen unterhaltsamen Stunden, die wir zusammen verbracht haben.

Ein besonderer Dank gilt meinen Eltern Manfred und Petra Jahnke sowie meiner Schwester Jasmin für ihre vielfältige Unterstützung während meines gesamten Studiums und der Promotion.

Contents

1. Introduction **1**

I. Quantum thermodynamics under the influence of periodic measurements **5**

2. The quantum thermodynamical model **7**
2.1. General properties of quantum thermodynamical models 7
2.2. The concrete model 8
2.2.1. Spectrum of the modular environment 8
2.2.2. Interaction between system and environment 9
2.3. Numerical illustration of the thermalization 10
2.4. Quantum thermodynamics and observation 13

3. Quantum measurement theory **15**
3.1. The measurement postulate for projective measurements 15
3.1.1. Measurements on bipartite systems: The co-jump 16
3.2. POVM measurement 17
3.3. Concrete measurement models 18

4. Influence of periodic measurements of the environment **21**
4.1. Effects of the measurement of the environmental energy 21
4.2. Short-time dynamics 23
4.2.1. Diagonal elements of the TLS state 25
4.2.2. Off-diagonal elements of the TLS state 31
4.2.3. Probabilities for the measurement results 34
4.3. Normalization of the interaction 36
4.4. Trajectories due to periodic measurements 38
4.5. Analytical calculation of the ensemble average 40
4.5.1. Off-diagonal elements 40
4.5.2. Diagonal elements: General properties 43
4.5.3. Attractor state for the resonant case 44
4.5.4. Attractor state for the off-resonant case 46

4.5.5. Test of the analytical results 49
4.5.6. Long-time average and ergodicity 49
4.6. Entropy and lack of knowledge 52
4.6.1. Information in thermodynamics 52
4.6.2. Measurement logic 53

5. Measurements on a small spin-environment 59
5.1. Dynamics without external disturbance 59
5.2. Dynamics with measurements of the environment 60
5.3. Dynamics with direct measurements of the TLS 68
5.4. Explicit measurement model based on a CNOT-gate 71
5.4.1. Hamiltonian for the CNOT gate 72
5.4.2. Dynamics of the TLS under periodic application of the CNOT-operation 74

6. Comparison with the model of Kurizki et al. 79

II. Temperature estimation: Fluctuations arising from quantum measurements 83

7. Temperature estimation for modular systems 85
7.1. Repeated temperature estimations: Average and fluctuations . 86
7.1.1. Bounds for the validity of the fluctuation formula 91
7.1.2. Temperature estimation by using more than one measurement 92
7.2. Example: The n spin model 92
7.2.1. Average temperature estimate 93
7.2.2. Fluctuations of the estimated temperature 96
7.2.3. Temperature estimation with several measurements . . 99

8. Conclusion 103

III. Appendices 107

A. Numerical test of the approximations 109

B. Short-time approximation 113

C. Interaction energy 117

D. Evolution of ρ_{00} for periodic measurement of the same energy band 119

E. Vanishing of the off-diagonal elements 121

F. POVM measurements of the TLS 125

G. Lower limit for the Gaussian approximation 127

H. German summary - Deutsche Zusammenfassung 129
H.1. Das quantenthermodynamische Modell 130
H.2. Der Einfluss periodischer Messungen 132
H.2.1. Kurzzeitdynamik und Trajektorien 132
H.2.2. Ensemblemittelung: Relaxation und Attraktorzustand . 135
H.2.3. Periodische Messungen bei kleinen Spin-Umgebungen . 136
H.2.4. Vergleich mit dem Modell von Kurizki et al. 138
H.3. Temperaturschätzung und Fluktuationen 138
H.3.1. Temperaturschätzung durch Energiemessung: Erwartungswert und Fluktuationen 139
H.3.2. Konkretes Beispiel: Das n-Spin System 141
H.4. Fazit 141

List of Symbols 143

Bibliography 147

1. Introduction

Observations not only disturb what has to be measured, they produce it.

—Pascual Jordan [27]

Thermodynamics [8, 47] as developed mainly in the 19th century, is a powerful theory with a large range of applications. Originally being developed to describe heat engines, its concepts are for example also applicable to chemical reactions or even in cosmology. However, this theory is purely phenomenological, based on the axiomatic laws of thermodynamics. Thus, the question arises, whether thermodynamics could be derived from a more fundamental theory.

Originally, classical mechanics has been considered as such an underlying theory, which led to the development of statistical mechanics. But such classical approaches did not get along without additional assumptions as, e.g., the ergodic hypothesis.

In the 20th century quantum mechanics [4, 44] was developed to describe systems at atomic and subatomic scales. It turned out that classical behavior can be obtained from quantum mechanics as a special limiting case, implying that quantum theory is more fundamental than the classical theories. Concerning thermodynamics, this led to two main questions:

- Is it possible to derive thermodynamics directly from quantum mechanics, without any further assumptions?
- Are the concepts of thermodynamics in some sense also applicable for quantum systems beyond the classical limit?

The answers to these questions are searched within the rather new field of quantum thermodynamics [15, 17, 41]. It turns out that, indeed, thermal properties can arise from quantum mechanics: A system typically relaxes to a stationary, thermal state due to the coupling to an appropriate environment. Remarkably, this even holds for very small quantum systems as for example a single two-level system.

However, in quantum thermodynamics the total system – consisting of system and environment – is considered to be closed. In particular, there exists

no interaction with an external observer. As we know, quantum measurements lead to a disturbance of the measured system according to the measurement postulate. Thus, the question arises, how an external observation effects the properties of a quantum thermodynamical system.

In this thesis, we provide such a connection to an external observer by including quantum measurements (i.e. information aspects) into the quantum thermodynamical model. As we will see, various concepts known from statistical mechanics arise from such a "quantum thermodynamics under observation", although they do not have any meaning in the isolated quantum thermodynamical setting:

In statistical mechanics, the systems are supposed to pass trough a trajectory in phase space. In contrast to quantum thermodynamics, thermal properties emerge only by averaging over an ensemble of such systems or as a long-time average over a single trajectory. The above mentioned ergodic hypothesis then states that both of these averages should be equal. In our model we will, indeed, recover quasi-classical trajectories and observe thermalization in the sense of statistical mechanics. Furthermore, we will prove the ergodicity of the system.

Another issue concerns the interpretation of entropy as a measure of lack of knowledge. As long as the underlying theory is classical, this lack of knowledge can only be subjective, since the exact micro state at any point in time is well defined and therefore – at least in principle – can be known. In contrast, the von Neumann entropy of a system in quantum thermodynamics is based on a fundamental lack of knowledge due to the entanglement with the environment. Based on the measurement logic, we will find a possibility to connect the objective entropy of the system with the subjective lack of knowledge of the observer carrying out the measurements.

A further apparent contradiction between statistical mechanics and quantum thermodynamics is related to fluctuations of thermodynamic variables. Especially, there have been long-standing controversies [29, 35] concerning the existence and the meaning of temperature fluctuations [30]. From the point of quantum thermodynamics, such fluctuations cannot exist, since the system – as mentioned above – relaxes to a stationary state, leaving no room for any fluctuations in time. However, we will be able to demonstrate, how the well known and controversial formula for temperature fluctuations can be recovered for quantum thermodynamical systems including measurements.

Going beyond the quantum thermodynamical model, we will show how the measurements may be used to freeze the initial state or to create thermal states of – in principle – almost arbitrary temperatures, even inversion becomes possible.

This thesis is divided into two main parts, corresponding to two different

physical scenarios. In the first part (Chap. 2 and Chap. 4 to 6), we consider a typical quantum thermodynamical model consisting of a two-level system (TLS) coupled to an environment of n spins. In Chap. 2, we introduce this model and recapitulate its properties without measurements included.

In Chap. 3, we give a brief overview over quantum measurement theory.

In Chap. 4, we implement periodic measurements of the environment into our model. Using perturbation theory, we analyze the dynamics of the TLS under the influence of these measurements. We study the appearance of quasi-classical trajectories and calculate the ensemble and long time average to prove ergodicity. The appearing attractor state is shown to depend on the time between the measurements. Allowing a detuning between the TLS and the environmental spins, we demonstrate the possibility to cool the system or even create inversion using periodic measurements. At the end of this chapter we discuss the relation between entropy and the lack of knowledge of the observer.

In Chap. 5, we test the validity of our analytically obtained results for relatively small environments, for which the dynamics can be solved numerically exact. Here, we also study the evolution under direct projective measurements of the TLS, as well as the realization of the measurement using a controlled-NOT gate [23, 39]. This allows us to test whether our results are also applicable for these alternative measurement procedures.

In Chap. 6, we compare our findings with the results for a related model, presented in some recent papers by the group of G. Kurizki [5, 12, 18, 19].

In the second part of the thesis (Chap. 7), we consider a typical class of models, namely modular systems. For these, we will be able to demonstrate that trying to estimate the temperature by a single energy measurement of the system typically leads to fluctuations of this temperature estimate, which fulfill the well known formula $\Delta T^2 = \frac{k_B T^2}{\mathfrak{C}}$ with k_B being the Boltzmann constant and $\mathfrak{C}$ being the heat capacity of the system. We also investigate the validity limits of this formula. Finally we discuss a n spin system as a concrete example illustrating our general considerations.

Part of this work has already been published in [25, 26].

Part I.

Quantum thermodynamics under the influence of periodic measurements

2. The quantum thermodynamical model

2.1. General properties of quantum thermodynamical models

One of the main achievements of quantum thermodynamics has been to explain how thermal properties may arise solely from quantum mechanics [15, 17, 41]. It is clear that an isolated quantum system initially in a pure state can never thermalize – its state will stay pure forever. However, completely isolated quantum systems are an idealization, the interaction with environment is practically unavoidable. This interaction with the environment, indeed, can cause a thermalization of the coupled system. Therefore, some conditions have to be fulfilled:

- To be able to meaningfully speak of system and environment at all, the interaction between both parts of the total system has to be weak compared to the energies of the subsystems. This weak coupling also ensures that the spectrum of the total system is approximately the same as the joined spectrum of the uncoupled subsystems. The weak coupling limit is a typical assumption also in usual thermodynamic considerations.

- Since the system typically has to change its energy to thermalize, the interaction has to allow for energy exchange between the system and environment. Since the interaction is weak, such an energy exchange can only occur between resonant transitions or at least close to resonance.

- To get a thermal state for the coupled system, which is independent of its initial state, the state density of the environment has to increase exponentially with energy. This is typically the case for modular systems [15].

2.2. The concrete model

In the following, we will consider such a typical quantum thermodynamical model. Our system S consists of a single two-level system (TLS) with energy splitting δ coupled via $\hat{V}$ (strength λ) to an environment B consisting of n spins. Thus, the Hamiltonian of the total system reads

$$\hat{H}_{\text{tot}} = \frac{\delta}{2}\hat{\sigma}_z \otimes \hat{1}_B + \hat{1}_S \otimes \hat{H}_B + \lambda \hat{V} \,. \tag{2.1}$$

In the following, we discuss the key properties of this model, which justify to call it a typical quantum thermodynamical one.

2.2.1. Spectrum of the modular environment

Due to the resonance condition mentioned in the last section, the splitting δ_B of the environmental spins has to be equal or at least close to δ in order to serve as a thermalizing environment. In case of non-interacting spins and setting the ground state energy to 0, the energy of level k is just given by

$$E_k = \delta_B k \,, \quad k = 0, 1, \ldots, n \tag{2.2}$$

and has the binomial degeneracy

$$N_k = \binom{n}{k} \,. \tag{2.3}$$

Including a weak interaction between the spins, each energy level k broadens into an energy band of width $\Delta\varepsilon_k \ll \delta_B$.

Thus, the state density of the environment is not exponential, as it is expected for a thermalizing environment. However, one may ask, if it can can be approximated by an exponential of the form

$$N_k \approx \mathcal{N} \mathrm{e}^{\beta \delta_B k} \tag{2.4}$$

around a certain point k_0 in energy space. This would mean that the environment – although not being in a thermal state itself but only occupying a certain energy level k_0 initially – may cause a thermalization of the embedded system to a state with inverse temperature β. Such a state of the environment arises, for example, due to a measurement of the environmental energy or magnetization, which will be included into the model in Chap. 4.

To derive the relation $\beta(k_0)$, we first replace the discrete binomial coefficient by a continuous function, which can be done using $n! = \Gamma(n+1)$ with $\Gamma(x)$

being the gamma function. Thus, the binomial coefficient is rewritten as

$$\binom{n}{k} = \frac{\Gamma(n+1)}{\Gamma(n-k+1)\Gamma(k+1)}\,. \tag{2.5}$$

Now, we can apply a Taylor expansion around k_0, which reads

$$\begin{aligned}\binom{n}{k} &= \frac{\Gamma(n+1)}{\Gamma(n-k_0+1)\Gamma(k_0+1)}\left(1+(\digamma(n-k_0+1)-\digamma(k_0+1))(k-k_0)\right)\\ &\quad +\mathcal{O}\left((k-k_0)^2\right)\end{aligned} \tag{2.6}$$

where $\digamma(x) := \frac{\mathrm{d}}{\mathrm{d}x}\log(\Gamma(x))$ is the so-called digamma function [1]. Comparing this with the Taylor expansion of $\mathcal{N}\mathrm{e}^{\beta\delta_B k}$ yields in zeroth order

$$\frac{n!}{k_0!(n-k_0)!} \stackrel{!}{=} \mathcal{N}\mathrm{e}^{\beta\delta_B k_0} \tag{2.7}$$

and in first order

$$\frac{n!}{k_0!(n-k_0)!}(\digamma(n-k_0+1)-\digamma(k_0+1)) \stackrel{!}{=} \mathcal{N}\beta\delta_B\mathrm{e}^{\beta\delta_B k_0} \tag{2.8}$$

Hence, with (2.8)/(2.7) we get

$$\beta\delta_B = \digamma(n-k_0+1)-\digamma(k_0+1) \tag{2.9}$$

For large x the digamma function can be approximated by $\digamma(x) \approx \ln(x)-\frac{1}{2x} \approx \ln(x)$ [1], which finally leads to

$$\beta(k_0) \approx \frac{1}{\delta_B}\ln\left(\frac{n}{k_0}-1\right)\,, \tag{2.10}$$

for sufficiently large environments.

This means that introducing an appropriate interaction, as will be done in the next section, the environment B will cause a relaxation of S to a thermal state of temperature $T = 1/\beta(k_0)$, depending on its energy $E(k_0)$.

2.2.2. Interaction between system and environment

As already mentioned in Sect. 2.1, the second key ingredient for a quantum thermodynamical setting is an appropriate interaction of system and environment: It has to be weak, i.e., $\lambda\langle\hat{V}\rangle \ll \langle\hat{H}_S\rangle, \langle\hat{H}_B\rangle$ and – in order to enable thermalization – it has to allow energy exchange. The interaction we consider here is of the form

$$\hat{V} = \left(\hat{\sigma}^+ + \hat{\sigma}^-\right)\otimes\hat{B}\,, \tag{2.11}$$

where $\hat{\sigma}^+ = |1\rangle\langle 0|$ is the creation and $\hat{\sigma}^- = |0\rangle\langle 1|$ the annihilation operator for the TLS and

$$\hat{B} = \sum_k \sum_{n_k, m_{k+1}} C_{k+1,k}(m_{k+1}, n_k)\, |n_k\rangle\langle m_{k+1}| + C_{k,k+1}(n_k, m_{k+1})\, |m_{k+1}\rangle\langle n_k| \,. \tag{2.12}$$

Such an interaction may, indeed, be called "canonical coupling", since non-zero entries cause transitions within the TLS as well as in the environment, thus allowing for thermalization. In the environment, only transitions between next neighbor bands are possible. To keep the model as unbiased as possible, we consider the $C_{i,j}$ as a set of random matrices whose entries are taken from a Gaussian distribution and are normalized to $\overline{|C_{i,j}(a,b)|^2} = \tilde{c}_{i,j}$. Due to the Hermiticity of $\hat{V}$, we have $C_{i,j} = C_{j,i}^\dagger$. The special choice of the normalization $\tilde{c}_{i,j}$ is not essential for the quantum thermodynamical model, but will become important when including measurements as discussed in Sect. 4.3.

As one can see, our interaction does not only contain terms of the form $\hat{\sigma}^+ |n_k\rangle\langle m_{k+1}|$ and $\hat{\sigma}^- |m_{k+1}\rangle\langle n_k|$, which are responsible for the energy exchange between system and environment, but also includes the so-called anti-resonant terms $\hat{\sigma}^+ |m_{k+1}\rangle\langle n_k|$ and $\hat{\sigma}^- |n_k\rangle\langle m_{k+1}|$. These terms are often neglected (rotating wave approximation) and, indeed, are not important for the usual quantum thermodynamical behavior. However, these terms will become crucial for the dynamics including measurements, which will be discussed in Chap. 4.

2.3. Numerical illustration of the thermalization

In this section we illustrate the idea of thermalization of a TLS due to its environment by solving the Von-Neumann equation of the total system using numerical exact diagonalization.

If we considered the complete environment consisting of many spins, the dimension of Hilbert-space would be much too large to allow exact diagonalization. However, if initially only one energy band k_0 of the environment is occupied, then due to the interaction with the TLS only the occupied energy band and its next neighbor bands ($k_0 + 1$ and $k_0 - 1$) are involved in the dynamics. Therefore, one can reduce the model by just considering a TLS coupled to three energy bands with exponentially increasing number of states. The result of such simulations can also be found in [13–15]. However, we recapitulate these results to point out the main differences between this situation without measurements and the situation including measurements, which will be discussed later. Furthermore, a difference to previous simulations is

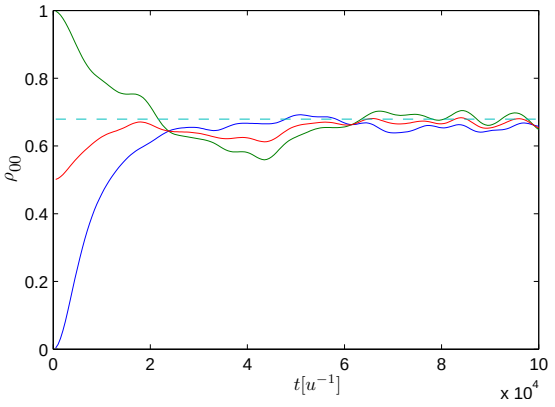

Figure 2.1.: Relaxation of the TLS to a thermal state with temperature $T = 1/\beta$ for different initial states of the TLS and a pure initial state (2.13) of the environment.

that we do not restrict ourselves to pure states of the total system but also allow for mixed initial states. Such states will typically arise when including measurements of the environment.

For our simulations the environment consists of 500 energy levels separated in three bands with distance $\delta_B = \delta = 1\,u$ (u being some arbitrary energy unit) with $N_1 = 66$, $N_2 = 139$ and $N_3 = 295$ levels, respectively. The number of levels is chosen such that it increases exponentially according to (2.4) with $\beta = 0.75\,u^{-1}$. The width of each band is chosen to be $\Delta\varepsilon = 0.001\,u$. We choose a random interaction of the form (2.11) with interaction strength $\lambda = 10^{-4}\,u$.

In order to be able to act as a thermalizing environment for any initial state of the TLS, initially only the central band has to be occupied. For the first simulations we choose a pure initial state for the environment:

$$\hat{\rho}_B(0) = |\psi_0\rangle\langle\psi_0| \;, \quad |\psi_0\rangle = \frac{1}{\sqrt{N_2}} \sum_{n_2} |n_2\rangle \;. \tag{2.13}$$

The relaxation of the occupation probability of the ground state for different initial states is shown in Fig. 2.1. As expected, ρ_{00} approximately relaxes to the value

$$\rho_{00}^{\text{final}} = \frac{\mathrm{e}^{\beta\delta/2}}{\mathrm{e}^{\beta\delta/2} + \mathrm{e}^{-\beta\delta/2}} \approx 0.679\,, \tag{2.14}$$

marked by the dashed line.

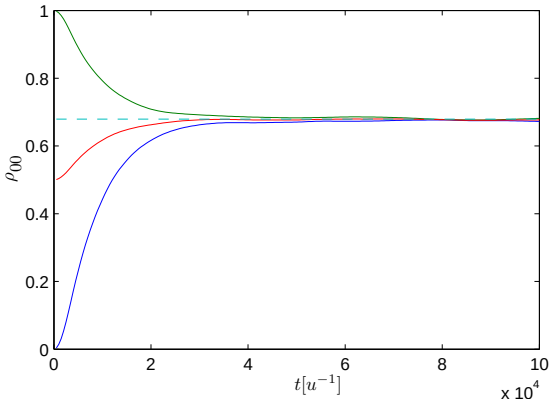

Figure 2.2.: Relaxation of the TLS with the same parameters as in Fig. 2.1, but now with a mixed initial state (2.15) of the environment.

Due to the finite size of the environment, some kind of fluctuations of the occupation probability around this value survive. However, these fluctuations are reduced drastically, when choosing a mixed initial state of the form

$$\hat{\rho}_B(0) = \frac{1}{N_2} \sum_{n_2} |n_2\rangle\langle n_2| \ . \tag{2.15}$$

The relaxation of the TLS with this initial state is shown in Fig. 2.2. As one can see, the fluctuations around the expected state have almost vanished here.

If the initial state of the TLS is not diagonal but contains some coherences, these vanish due to the interaction with the environment, i.e., the TLS really relaxes to a thermal state. This is shown in Fig. 2.3 for both initial states of the environment (2.13) and (2.15), whereas the TLS is starting in the pure state $|\psi_0\rangle = \frac{1}{\sqrt{2}}(|0\rangle + |1\rangle)$. Again, for the pure initial state (2.13) the fluctuations around $\rho_{10} = 0$ are much larger than for the mixed state (2.15).

Anyway, these simulations demonstrate how pure Schrödinger dynamics or rather von Neumann dynamics of the total system can lead to a thermalization of a subsystem. We point out here that, indeed, a single subsystem can relax to such a thermal state according to quantum thermodynamics. No ensembles have to be considered here, as it is common practice in statistical mechanics. In the following we will see, how this situation changes when including measurements.

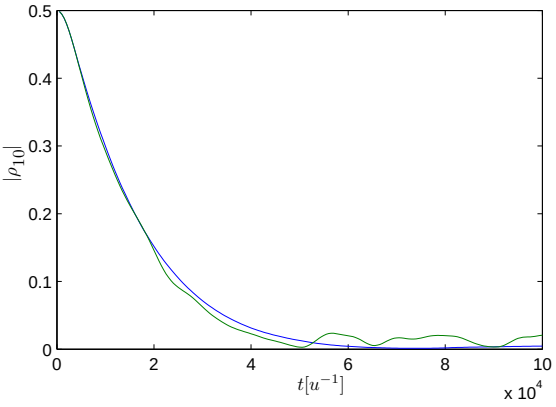

Figure 2.3.: Vanishing of the off-diagonal element ρ_{10} for with a mixed initial state (2.15) (blue) and a pure initial state (2.13) (green) of the environment.

2.4. Quantum thermodynamics and observation

Just like Schrödinger dynamics, quantum thermodynamics as such does not give us any access to its internal workings. As a remedy we will have to include additional measurement procedures subject to external control.

While single measurements are typically invoked for preparation and probe scenarios, we will focus here on (periodically) repeated measurements. These are needed to follow up dynamical evolutions or fluctuations (see Chap. 7). They are also needed to study the back-action of measurements giving rise to new quasi-stationary states (dynamical attractor states): This is what we mean by "quantum thermodynamics under observation" (Chap. 4 to 6). The resulting measurement protocols (time series) will be analyzed statistically.

3. Quantum measurement theory

Measurements play a central role in quantum mechanics, since they provide the connection of the abstract theory to experimentally accessible quantities. Here, an important point is that quantum measurements – in contrast to measurements in the classical regime – typically will disturb the measured system, i.e., change its state. This leads to an irreversibility, which opposes the unitary Schrödinger dynamics of closed quantum systems.

3.1. The measurement postulate for projective measurements

Let us first consider the so-called projective or von Neumann measurements. The most general formulation of measurements will be discussed briefly in Sect. 3.2.

In quantum mechanics all observables are associated with a Hermitian operator $\hat{A}$. The possible outcomes of a measurement of this observable are the real eigenvalues a_i of the operator.

We can rewrite the operator by the spectral decomposition

$$\hat{A} = \sum_i a_i \hat{P}_i \,, \tag{3.1}$$

where $\hat{P}_i$ denotes the projector onto the eigenspace of $\hat{A}$ corresponding to the eigenvalue a_i.

Let $|\psi'\rangle$ be the state of the system immediately before the measurement, then the probability to obtain the value a_i reads

$$p_i = \langle\psi'| \hat{P}_i |\psi'\rangle \,. \tag{3.2}$$

After measuring a_i, the state of the system is given by

$$|\psi\rangle = \frac{\hat{P}_i |\psi'\rangle}{\sqrt{p_i}} \,, \tag{3.3}$$

i.e., the measurement causes a projection of the state of the system into the eigenspace corresponding to the measured value. This is often referred to as

the "collapse of the wave function". In the simplest case of a non-degenerate spectrum, the state after measuring a_i is simply given by the the corresponding eigenvector $|\alpha_i\rangle$. An important consequence of this projection due to the measurement is that only observables associated with commuting operators can be measured at the same time, because they have common eigenvectors.

The measurement postulate can also be formulated by means of the density matrix, e.g., when dealing with mixed states. Let us suppose the system to be in the state $\hat{\rho}'$ before the measurement, then the state after measuring a_i reads

$$\hat{\rho} = \frac{\hat{P}_i \hat{\rho}' \hat{P}_i}{\mathrm{Tr}\left\{\hat{P}_i \hat{\rho}'\right\}}, \tag{3.4}$$

where the denominator ensures the normalization of $\hat{\rho}$ and also provides the probabilities for each measurement outcome

$$p_i = \mathrm{Tr}\left\{\hat{P}_i \hat{\rho}'\right\}. \tag{3.5}$$

3.1.1. Measurements on bipartite systems: The co-jump

An interesting feature of quantum measurements occurs when considering bipartite systems: Let us assume that our total system consists of two subsystems A and B. If we perform a measurement of a property of B, this will not only change the state of B due to the corresponding projection operator $\hat{P}_i$, but typically will also influence the state of A, as shown in the following.

To obtain the state of A we have to consider the state of the total system after the measurement and trace out subsystem B, which yields

$$\hat{\rho} = \frac{\mathrm{Tr}_B\left\{\hat{\tilde{P}}_i \hat{\rho}'_{\mathrm{tot}}\right\}}{\mathrm{Tr}_B\left\{\hat{P}_i \hat{\rho}'_B\right\}}. \tag{3.6}$$

Here, we $\hat{\tilde{P}}_i$ denotes the projection operator defined in the Hilbert space of the total system

$$\hat{\tilde{P}}_i := \hat{1}_A \otimes \hat{P}_i. \tag{3.7}$$

Splitting the state of the total system before the measurement into a product state $\hat{\rho}' \otimes \hat{\rho}'_B$ and the correlation $\hat{C}_{AB}$

$$\hat{\rho}'_{\mathrm{tot}} := \hat{\rho}' \otimes \hat{\rho}'_B + \hat{C}_{AB}, \tag{3.8}$$

we can rewrite (3.6) as

$$\hat{\rho} = \frac{\mathrm{Tr}_B\left\{\hat{\rho}' \otimes \hat{P}_i \hat{\rho}'_B \hat{P}_i + \hat{\bar{P}}_i \hat{C}_{AB} \hat{\bar{P}}_i\right\}}{\mathrm{Tr}_B\left\{\hat{P}_i \hat{\rho}'_B\right\}} = \hat{\rho}' + \frac{\mathrm{Tr}_B\left\{\hat{\bar{P}}_i \hat{C}_{AB}\right\}}{\mathrm{Tr}_B\left\{\hat{P}_i \hat{\rho}'_B\right\}}\,, \tag{3.9}$$

i.e., the state of A after the measurement equals the state before the measurement only, if the the total system has been in a product state. Correlations between both subsystems before the measurement will influence the state of the A after the measurement of B according to the second term in (3.9), the so-called co-jump [20].

3.2. POVM measurement

Measurements can also be discussed from a more general point of view (cf., e.g., [3, 39]). Let us assume that for a measurement only the measurement results a_i and their respective probabilities p_i are known. Then, we can assign a linear operator $\hat{E}_i$ to each measurement result, such that

$$p_i = \langle\psi'|\, \hat{E}_i\, |\psi'\rangle\ , \tag{3.10}$$

where $|\psi'\rangle$ again denotes the state of the system before the measurement. Describing this state by the density operator $\hat{\rho}'$, we get

$$p_i = \mathrm{Tr}\left\{\hat{\rho}' \hat{E}_i\right\}\ . \tag{3.11}$$

Because of $p_i \geq 0$, the operators $\hat{E}_i$ have to be positive and – due to $\sum_i p_i = 1$ – they have to fulfill the condition

$$\sum_i \hat{E}_i = \hat{1}\,. \tag{3.12}$$

Therefore, the set $\{\hat{E}_i\}$ is called a POVM which is a acronym standing for "Positive Operator-Valued Measure".

The state of the system after the measurement cannot directly be obtained from the $\{\hat{E}_i\}$. If one wants to calculate this state, one first has to determine the measurement operators $\{\hat{M}_i\}$, which are related to the POVM elements by

$$\hat{M}_i^\dagger \hat{M}_i = \hat{E}_i\,. \tag{3.13}$$

Note, that these measurement operators do not have to be Hermitian and that there are infinitely many $\hat{M}_i$ which fulfill (3.13), i.e., $\hat{M}_i$ is not unique if only

the $\{\hat{E}_i\}$ are known. However, given the measurement operators $\hat{M}_i$, the state after the measurement reads

$$\hat{\rho} = \frac{\hat{M}_i \hat{\rho}' \hat{M}_i^\dagger}{\mathrm{Tr}\left\{\hat{M}_i \hat{\rho}' \hat{M}_i^\dagger\right\}} . \tag{3.14}$$

The projective measurement discussed in Sect. 3.1 is a special case of a POVM measurement. Here the POVM elements are simply given by the projectors

$$\hat{E}_i = \hat{P}_i^\dagger \hat{P}_i = \hat{P}_i . \tag{3.15}$$

However, in general the POVM elements $\hat{E}_i$ are not projectors and do not have to be orthogonal, which means that the number of elements can be larger than the dimension of the considered Hilbert space.

The formalism of POVM measurements can, for example, be used to describe a projective measurement applied on the total system with respect to a certain subsystem. For such a subsystem the effect of this measurement typically cannot be described by a projection but by a POVM measurement.

3.3. Concrete measurement models

In Sect. 3.1, we have discussed how measurements can be mathematically described by means of projection operators. In doing so, one restricts oneself on the effect of the (ideal) measurement on the measured system, but does not model the detection as such.

Concrete measurement models, which include the description of the detector have to face the problem that quantum measurements are irreversible, in contrast to the unitary Schrödinger dynamics. Thus, the question arises, how to explain this irreversibility based on a reversible theory. It turns out that this can be done by including the environment-induced decoherence [46].

To explain this concept, let us briefly discuss the main elements of such concrete measurement models. These models are divided into three parts: First, the system being measured, second, the measurement apparatus/detector and third, the environment. The first step of the measurement is then described by the interaction of the system and the detector leading to an entanglement between both of them ("pre-measurement"). This pre-measurement thus provides a correlation between the state of the system and some macroscopic distinguishable pointer states of the detector.

However, this would typically lead to a superposition of the macroscopic pointer states, which is not observed in nature. The reason for this is the

unavoidable interaction of the detector with its environment, which causes decoherence, i.e., a vanishing of the macroscopic superposition, leading to a mixed state of the detector. Thus, a concrete measurement model including detector and environment is able to describe the outcome of a measurement in ensemble average.[1]

[1] Note however that decoherence cannot explain the "collapse" of the wave function for a single measurement. This so-called "measurement problem" is the main conceptual difficulty of quantum mechanics.

4. Influence of periodic measurements of the environment

The individual measurement will be assumed to be instantaneous. The periodic measurement sequence can be characterized by the waiting time Δt between subsequent measurements. In the following we will restrict ourselves to the short-time limit.

4.1. Effects of the measurement of the environmental energy

Concretely, we consider measurements of the environmental energy/magnetization, which are repeated after some time Δt and study their effect on the coupled TLS (system S). As we have discussed in Chap. 3, a quantum measurement causes a projection of the state into an eigenstate/eigenspace of the measured observable corresponding to the measured eigenvalue. Thus, these measurements lead to a projection of the environment into one of its energy bands. The pertinent projection operator reads

$$\hat{\tilde{P}}_k = \hat{1}_S \otimes \hat{P}_k \,, \tag{4.1}$$

with

$$\hat{P}_k = \sum_{n_k} |n_k\rangle\langle n_k| \,, \tag{4.2}$$

where we sum over all levels of the measured energy band k. The state of the total system after the measurement can be calculated according to

$$\hat{\rho}_{\mathrm{tot}} = \frac{\hat{\tilde{P}}_k \hat{\rho}'_{\mathrm{tot}} \hat{\tilde{P}}_k}{\mathrm{Tr}_B\left\{\hat{P}_k \hat{\rho}'_B\right\}} \,. \tag{4.3}$$

As we have seen inSect. 3.1.1, such measurements also have an indirect effect on the state of the TLS which is obtained by tracing out the environment

$$\hat{\rho} = \frac{\mathrm{Tr}_B\left\{\hat{\tilde{P}}_k \hat{\rho}'_{\mathrm{tot}}\right\}}{\mathrm{Tr}_B\left\{\hat{P}_k \hat{\rho}'_B\right\}} . \tag{4.4}$$

For the following analytical discussion of the dynamics due to the periodic measurements we have to apply two approximations concerning the state of the environment and the total system:

Since the measurement is incomplete, i.e., does not project into a pure state, there may still be some correlations left between S and B after the measurement. However, these correlations have negligible effect on the dynamics of the system for weak coupling and small width of the bands, as verified numerically in App. A.

Also the second approximation is related to the incompleteness of the measurements: The state of the environment after the measurement $\mathrm{Tr}_S\{\hat{\rho}_{\mathrm{tot}}\}$ may be rather complicated, depending on details of the interaction between S and B before the measurement. However, if we are mainly interested in the dynamics of the TLS and not on the details of the occupation probabilities of each energy level within the measured band, we can apply some kind of coarse graining by replacing the complicated state after the measurement by the simple form

$$\hat{\rho}^0_B(k) = \frac{1}{N_k} \sum_{n_k} |n_k\rangle\langle n_k| . \tag{4.5}$$

In App. A we test the validity of this approximation. It turns out that this approximation is justified as long as the environment is large enough.

Applying both of these approximations, the state of the total system after the measurement can be written as

$$\hat{\rho}_{\mathrm{tot}} \approx \hat{\rho} \otimes \hat{\rho}^0_B(k) . \tag{4.6}$$

Thus, the effect of the measurements is threefold: First, it prepares the environment in a certain energy band. Second, it causes a change of the TLS state due to the co-jump. And third, it destroys correlations between system and environment. All these effects will influence the dynamics of the TLS, as will be discussed in the following.

4.2. Short-time dynamics

The main goal in this section will be to determine the state of the TLS after measurement j according to (4.4), assuming that initially the total system is in a state of the form (4.6) prepared by measurement $j-1$. Therefore, we introduce a special notation for the states by labeling them by the measurement number instead of the time, i.e., the initial state for our dynamics is denoted by $\hat{\rho}_{\rm tot}(j-1) := \hat{\rho}_{\rm tot}(t=0)$, accordingly the initial state of S and B are denoted by $\hat{\rho}(j-1) := \hat{\rho}(t=0)$ and $\hat{\rho}_B(j-1) := \hat{\rho}_B(t=0)$, respectively. The respective states after applying the measurement at time Δt are then denoted by $\hat{\rho}_{\rm tot}(j) = \hat{\rho}_{\rm tot}(t=\Delta t)$, $\hat{\rho}(j) = \hat{\rho}(t=\Delta t)$ and $\hat{\rho}_B(j) = \hat{\rho}_B(t=\Delta t)$. Although we are only considering a single step from $t=0$ to $t=\Delta t$ in this section, this notion will be useful for the later discussion of periodic measurements, since it allows for an easy iteration.

The following calculation of the short-time dynamics is based on perturbation theory. Starting point is the von Neumann equation in the interaction picture, which reads ($\hbar = 1$)

$$\frac{\partial}{\partial t}\hat{\rho}_{\rm tot}(t) = {\rm i}[\hat{\rho}_{\rm tot}(t), \lambda\hat{V}(t)] \tag{4.7}$$

with

$$\hat{V}(t) = \hat{\sigma}^+\hat{B}(t) + \hat{\sigma}^-\hat{B}^\dagger(t)\,, \tag{4.8}$$

where the time dependence is written in the environmental part of the interaction

$$\begin{aligned}\hat{B}(t) &= {\rm e}^{{\rm i}\hat{H}_B t}\hat{B}{\rm e}^{-{\rm i}\hat{H}_B t}{\rm e}^{{\rm i}\delta t} \\ &= \sum_k \sum_{n_k, m_{k+1}} C_{k+1,k}(m_{k+1}, n_k){\rm e}^{-{\rm i}(\Omega+\omega(m_{k+1},n_k))t}\,|n_k\rangle\langle m_{k+1}| \\ &\quad + C_{k,k+1}(n_k, m_{k+1}){\rm e}^{{\rm i}(2\delta+\Omega+\omega(m_{k+1},n_k))t}\,|m_{k+1}\rangle\langle n_k|\,. \end{aligned} \tag{4.9}$$

Here, $\omega(m_{k+1}, n_k)$ denotes the energy difference of level m in band $k+1$ and level n in band k minus δ_B, i.e., $\omega(m_{k+1}, n_k)$ is always much smaller than δ for small band width. $\Omega := \delta_B - \delta$ is the detuning between TLS splitting and splitting of the environmental spins. In the quantum thermodynamical setting Ω has to be zero or at least to be small (in the order of the interaction energy) to allow thermalization as mentioned in Sect. 2.2.1. Nevertheless, we will keep our analysis as general as possible by allowing for $\Omega \neq 0$. As we will see later, varying the parameter Ω yields interesting effects in our model including measurements.

In case of $\Omega \ll \delta$ the so called anti-resonant terms in the second sum oscillate with a higher frequency than the other terms. In rotating wave approximation these terms are neglected. However, these terms will become important especially for fast measurements.

Following from (4.7) the density operator of the total system after time Δt (immediately before the measurement) reads up to second order in interaction strength

$$\begin{aligned}\hat{\rho}'_{\rm tot}(j) &\approx \hat{\rho}_{\rm tot}(j-1) + \mathrm{i}\lambda \int_0^{\Delta t} [\hat{\rho}_{\rm tot}(j-1), \hat{V}(t')]\mathrm{d}t' \\ &\quad -\lambda^2 \int_0^{\Delta t}\int_0^{t'} [[\hat{\rho}_{\rm tot}(j-1), \hat{V}(t'')], \hat{V}(t')]\mathrm{d}t''\mathrm{d}t' \,. \end{aligned} \tag{4.10}$$

As discussed below, the first order term is only relevant for calculating the interaction energy, while it does not contribute to the state of the TLS.

The double commutator appearing in the second order term (in the following abbreviated by $\hat{\mathfrak{c}}$) reads

$$\begin{aligned}&[[\hat{\rho}_{\rm tot}(j-1), \hat{V}(t'')], \hat{V}(t')] = \\ &\quad \hat{\rho}_{\rm tot}(j-1)\hat{\sigma}^+\hat{B}(t'')\hat{\sigma}^-\hat{B}^\dagger(t') + \hat{\rho}_{\rm tot}(j-1)\hat{\sigma}^-\hat{B}^\dagger(t'')\hat{\sigma}^+\hat{B}(t') \\ &\quad -\hat{\sigma}^+\hat{B}(t'')\hat{\rho}_{\rm tot}(j-1)\hat{\sigma}^+\hat{B}(t') - \hat{\sigma}^+\hat{B}(t'')\hat{\rho}_{\rm tot}(j-1)\hat{\sigma}^-\hat{B}^\dagger(t') \\ &\quad -\hat{\sigma}^-\hat{B}^\dagger(t'')\hat{\rho}_{\rm tot}(j-1)\hat{\sigma}^+\hat{B}(t') - \hat{\sigma}^-\hat{B}^\dagger(t'')\hat{\rho}_{\rm tot}(j-1)\hat{\sigma}^-\hat{B}^\dagger(t') \\ &\quad -\hat{\sigma}^+\hat{B}(t')\hat{\rho}_{\rm tot}(j-1)\hat{\sigma}^+\hat{B}(t'') - \hat{\sigma}^-\hat{B}^\dagger(t')\hat{\rho}_{\rm tot}(j-1)\hat{\sigma}^+\hat{B}(t'') \\ &\quad -\hat{\sigma}^+\hat{B}(t')\hat{\rho}_{\rm tot}(j-1)\hat{\sigma}^-\hat{B}^\dagger(t'') - \hat{\sigma}^-\hat{B}^\dagger(t')\hat{\rho}_{\rm tot}(j-1)\hat{\sigma}^-\hat{B}^\dagger(t'') \\ &\quad +\hat{\sigma}^-\hat{B}^\dagger(t')\hat{\sigma}^+\hat{B}(t'')\hat{\rho}_{\rm tot}(j-1) + \hat{\sigma}^+\hat{B}(t')\hat{\sigma}^-\hat{B}^\dagger(t'')\hat{\rho}_{\rm tot}(j-1) \\ &\quad =: \hat{\mathfrak{c}} \,. \end{aligned} \tag{4.11}$$

Since $\hat{\rho}_{\rm tot}(j-1)$ is a product state $\hat{\rho}_{\rm tot}(j-1) = \hat{\rho}(j-1)\otimes\hat{\rho}_B(j-1)$, we can split the terms into system and environmental parts, i.e.,

$$\hat{\rho}_{\rm tot}(j-1)\hat{\sigma}^+\hat{B}(t'')\hat{\sigma}^-\hat{B}^\dagger(t') = \hat{\rho}(j-1)\hat{\sigma}^+\hat{\sigma}^-\hat{\rho}_B(j-1)\hat{B}(t'')\hat{B}^\dagger(t') \,,$$

and so forth.

Our main aim is to determine the state of the TLS after the measurement according to (4.4). Some of the 2nd order terms contribute only to the diagonal elements of this state, others contribute only to the off-diagonal elements, and some contribute to both diagonal and off-diagonal elements. In the next section we will focus on calculating the diagonal elements, whereas the off-diagonal elements will be discussed in Sect. 4.2.2.

4.2.1. Diagonal elements of the TLS state

The first order term of (4.10) does not contribute to the state (4.4) of the TLS after the measurement, since

$$\begin{aligned}
\mathrm{Tr}_B\left\{\hat{P}_{k_j}\hat{\rho}_B(j-1)\hat{B}(t')\right\} &= 0\,, && (4.12)\\
\mathrm{Tr}_B\left\{\hat{P}_{k_j}\hat{\rho}_B(j-1)\hat{B}^\dagger(t')\right\} &= 0\,, && (4.13)\\
\mathrm{Tr}_B\left\{\hat{P}_{k_j}\hat{B}(t')\hat{\rho}_B(j-1)\right\} &= 0\,, && (4.14)\\
\mathrm{Tr}_B\left\{\hat{P}_{k_j}\hat{B}^\dagger(t')\hat{\rho}_B(j-1)\right\} &= 0\,. && (4.15)
\end{aligned}$$

Analyzing the system part of (4.11), we find that only the following terms contribute to the 00 component of the state of S:

$$\begin{aligned}
\hat{\sigma}^-\hat{\sigma}^+\hat{\rho}(j-1) &= \begin{pmatrix} 0 & 0 \\ \rho_{01}(j-1) & \rho_{00}(j-1)\end{pmatrix}\,,\\
\hat{\rho}(j-1)\hat{\sigma}^-\hat{\sigma}^+ &= \begin{pmatrix} 0 & \rho_{10}(j-1) \\ 0 & \rho_{00}(j-1)\end{pmatrix}\,,\\
\hat{\sigma}^-\hat{\rho}(j-1)\hat{\sigma}^+ &= \begin{pmatrix} 0 & 0 \\ 0 & \rho_{11}(j-1)\end{pmatrix}\,.
\end{aligned} \qquad (4.16)$$

This leads to the following 00 component of the numerator $\mathrm{Tr}_B\left\{\hat{\tilde{P}}_{k_j}\hat{\rho}'_{\mathrm{tot}}(j)\right\}$ in (4.4)

$$\begin{aligned}
\mathrm{Tr}_B\left\{\hat{\tilde{P}}_{k_j}\hat{\rho}'_{\mathrm{tot}}(j)\right\}_{00} \approx\ & \rho_{00}(j-1)\delta_{k_{j-1}k_j}\\
& -\lambda^2\int_0^{\Delta t}\int_0^{t'}\rho_{00}(j-1)\xi_0(t',t'')\\
& \qquad -\rho_{11}(j-1)\xi_1(t',t'')\mathrm{d}t''\mathrm{d}t' \qquad (4.17)
\end{aligned}$$

with

$$\begin{aligned}
\xi_0(t',t'') &:= \mathrm{Tr}_B\Big\{\hat{P}_{k_j}\hat{\rho}_B(j-1)\hat{B}^\dagger(t'')\hat{B}(t') + \hat{P}_{k_j}\hat{B}^\dagger(t')\hat{B}(t'')\hat{\rho}_B(j-1)\Big\} \\
&= \frac{2\delta_{k_{j-1}k_j}}{N_{k_j}} \sum_{m_{k_j},n_{k_j-1}} |C_{k_j,k_j-1}(m_{k_j},n_{k_j-1})|^2 \\
&\qquad \times \cos(\Omega + \omega(m_{k_j},n_{k_j-1})(t'-t'')) \\
&\quad + \frac{2\delta_{k_{j-1}k_j}}{N_{k_j}} \sum_{m_{k_j},n_{k_j+1}} |C_{k_j,k_j+1}(m_{k_j},n_{k_j+1})|^2 \\
&\qquad \times \cos((2\delta + \Omega + \omega(n_{k_j+1},m_{k_j}))(t'-t''))\,, \\
\xi_1(t',t'') &:= \mathrm{Tr}_B\Big\{\hat{P}_{k_j}\hat{B}^\dagger(t'')\hat{\rho}_B(j-1)\hat{B}(t') + \hat{P}_{k_j}\hat{B}^\dagger(t')\hat{\rho}_B(j-1)\hat{B}(t'')\Big\} \\
&= \frac{2\delta_{k_{j-1}+1k_j}}{N_{k_j-1}} \sum_{m_{k_j},n_{k_j-1}} |C_{k_j,k_j-1}(m_{k_j},n_{k_j-1})|^2 \\
&\qquad \times \cos(\Omega + \omega(m_{k_j},n_{k_j-1})(t'-t'')) \\
&\quad + \frac{2\delta_{k_{j-1}-1k_j}}{N_{k_j+1}} \sum_{m_{k_j},n_{k_j+1}} |C_{k_j,k_j+1}(m_{k_j},n_{k_j+1})|^2 \\
&\qquad \times \cos((2\delta + \Omega + \omega(n_{k_j+1},m_{k_j}))(t'-t''))\,.
\end{aligned} \tag{4.18}$$

Here, we have used that $\hat{\rho}_B(j-1) = \hat{\rho}_B^0(k_{j-1})$ according to (4.5) and $\hat{B}(t)$ given by (4.9). δ_{ab} denotes the Kronecker delta, being 1 for $a = b$ and zero otherwise. For example, the term with $\delta_{k_{j-1}-1k_j}$ is non-vanishing only, if at step j one band higher is measured than in the previous measurement, etc.

ξ_0 as well as ξ_1 both consist of two double sums over many oscillating terms with normal distributed amplitudes and approximately uniformly distributed frequencies. This allows us to apply an additional short-time approximation (more details and a numerical verification can be found in App. B):

$$\sum_{m_a,n_b} |C_{a,b}(m_a,n_b)|^2 \cos((\alpha+\omega(m_a,n_b))(t'-t'')) \approx A_{a,b}\cos(\alpha(t'-t'')) \tag{4.19}$$

where we defined

$$A_{a,b} := N_a N_b \overline{|C_{a,b}(m_a,n_b)|^2} = A_{b,a} \tag{4.20}$$

and α being Ω or $2\delta + \Omega$.

Thus, for sufficiently small width of the bands (or rather short enough times) the terms ξ_0 and ξ_1 can be approximated by

$$\begin{aligned}
\xi_0(t',t'') &\approx \frac{2\delta_{k_{j-1}k_j}}{N_{k_j}}\big(A_{k_j,k_j-1}\cos(\Omega(t'-t'')) \\
&\quad +A_{k_j,k_j+1}\cos((2\delta+\Omega)(t'-t''))\big)\,, \\
\xi_1(t',t'') &\approx \frac{2\delta_{k_{j-1}+1k_j}}{N_{k_j-1}}A_{k_j,k_j-1}\cos(\Omega(t'-t'')) \\
&\quad +\frac{2\delta_{k_{j-1}-1k_j}}{N_{k_j+1}}A_{k_j,k_j+1}\cos((2\delta+\Omega)(t'-t''))\,.
\end{aligned} \tag{4.21}$$

With this, the integrals in (4.17) can easily be calculated, leading to the final expression for the 00 component of the numerator of (4.4)

$$\begin{aligned}
\mathrm{Tr}_B\Big\{\hat{\tilde{P}}_{k_j}\hat{\rho}'_{\mathrm{tot}}\Big\}_{00} &\approx \rho_{00}(j-1)\delta_{k_{j-1}k_j} \\
&\quad +4\lambda^2\Bigg[-\rho_{00}(j-1)\frac{\delta_{k_{j-1}k_j}}{N_{k_j}}\left(A_{k_j,k_j-1}\zeta_1+A_{k_j,k_j+1}\zeta_2\right) \\
&\quad +\rho_{11}(j-1) \\
&\quad \times\left(\frac{A_{k_j,k_j-1}}{N_{k_j-1}}\delta_{k_{j-1}+1k_j}\zeta_1+\frac{A_{k_j,k_j+1}}{N_{k_j+1}}\zeta_2\delta_{k_{j-1}-1k_j}\right)\Bigg]\,,
\end{aligned} \tag{4.22}$$

where we have introduced the abbreviations

$$\zeta_1 := \frac{\sin^2\left(\frac{\Omega}{2}\Delta t\right)}{\Omega^2}\,, \tag{4.23}$$

$$\zeta_2 := \frac{\sin^2\left(\left(\delta+\frac{\Omega}{2}\right)\Delta t\right)}{(2\delta+\Omega)^2}\,. \tag{4.24}$$

In order to get the occupation probability of the ground state after measurement j, we finally have to determine the denominator of (4.4), which is given by $\mathrm{Tr}_B\Big\{\hat{P}_{k_j}\hat{\rho}'_B(j)\Big\}$. Therefore, we need to calculate $\hat{\rho}'_B$ using the expansion of the state of the total system (4.10) and trace out the TLS. Then we have to apply the projector $\hat{P}_{k_j}$ and calculate the trace.

Again, according to (4.12)–(4.15) the first order term does not contribute here.

Using $\mathrm{Tr}_S\{\sigma^+\sigma^-\hat{\rho}(j-1)\} = \rho_{11}(j-1)$ and $\mathrm{Tr}_S\{\sigma^-\sigma^+\hat{\rho}(j-1)\} = \rho_{00}(j-1)$ we can trace out the TLS in the 2nd order commutator (4.11), which leads to

$$\mathrm{Tr}_S\{\hat{\mathfrak{c}}\} = \rho_{00}(j-1)\hat{\Xi}_0(t',t'') + \rho_{11}(j-1)\hat{\Xi}_1(t',t'') \tag{4.25}$$

with

$$\begin{aligned}
\hat{\Xi}_0(t',t'') &:= \hat{\rho}_B(j-1)\hat{B}^\dagger(t'')\hat{B}(t') - \hat{B}(t'')\hat{\rho}_B(j-1)\hat{B}^\dagger(t') \\
&\quad -\hat{B}(t')\hat{\rho}_B(j-1)\hat{B}^\dagger(t'') + \hat{B}^\dagger(t')\hat{B}(t'')\hat{\rho}_B(j-1))\,, \qquad (4.26)\\
\hat{\Xi}_1(t',t'') &:= \hat{\rho}_B(j-1)\hat{B}(t'')\hat{B}^\dagger(t') - \hat{B}^\dagger(t'')\hat{\rho}_B(j-1)\hat{B}(t') \\
&\quad -\hat{B}^\dagger(t')\hat{\rho}_B(j-1)\hat{B}(t'') + \hat{B}(t')\hat{B}^\dagger(t'')\hat{\rho}_B(j-1)\,. \qquad (4.27)
\end{aligned}$$

We now apply the projector $\hat{P}_{k_j}$ on (4.26) and (4.27) and then calculate the trace. This leads to the following expressions

$$\begin{aligned}
\mathrm{Tr}_B\Big\{\hat{P}_{k_j}\hat{\Xi}_0(t',t'')\Big\} &= \frac{2\delta_{k_{j-1}k_j}}{N_{k_j}}\Big(\sum_{m_{k_j},n_{k_j-1}} |C_{k_j,k_j-1}(m_{k_j},n_{k_j-1})|^2 \\
&\quad \times\cos((\Omega+\omega(m_{k_j},n_{k_j-1}))(t'-t'')) \\
&\quad + \sum_{m_{k_j},n_{k_j+1}} |C_{k_j,k_j+1}(m_{k_j},n_{k_j+1})|^2 \\
&\quad \times\cos((2\delta+\Omega+\omega(n_{k_j+1},m_{k_j}))(t'-t''))\Big) \\
&\quad -\frac{2\delta_{k_{j-1}-1k_j}}{N_{k_j+1}}\sum_{m_{k_j+1},n_{k_j}} |C_{k_j+1,k_j}(m_{k_j+1},n_{k_j})|^2 \\
&\quad \times\cos((\Omega+\omega(m_{k_j+1},n_{k_j}))(t'-t'')) \\
&\quad -\frac{2\delta_{k_{j-1}+1k_j}}{N_{k_j-1}}\sum_{m_{k_j-1},n_{k_j}} |C_{k_j-1,k_j}(m_{k_j-1},n_{k_j})|^2 \\
&\quad \times\cos((2\delta+\Omega+\omega(n_{k_j},m_{k_j-1}))(t'-t''))
\end{aligned} \tag{4.28}$$

and

$$\begin{aligned}
\mathrm{Tr}_B\Big\{\hat{P}_{k_j}\hat{\Xi}_1(t',t'')\Big\} &= \frac{2\delta_{k_{j-1}k_j}}{N_{k_j}}\Big(\sum_{m_{k_j+1},n_{k_j}}|C_{k_j+1,k_j}(m_{k_j+1},n_{k_j})|^2 \\
&\quad\times\cos((\Omega+\omega(m_{k_j+1},n_{k_j}))(t'-t'')) \\
&\quad+\sum_{m_{k_j-1},n_{k_j}}|C_{k_j-1,k_j}(m_{k_j-1},n_{k_j})|^2 \\
&\quad\times\cos((2\delta+\Omega+\omega(n_{k_j},m_{k_j-1}))(t'-t''))\Big) \\
&\quad-\frac{\delta_{k_{j-1}-1k_j}}{N_{k_j+1}}\sum_{m_{k_j},n_{k_j+1}}|C_{k_j,k_j+1}(m_{k_j},n_{k_j+1})|^2 \\
&\quad\times\cos((2\delta+\Omega+\omega(n_{k_j+1},m_{k_j}))(t'-t'')) \\
&\quad-\frac{\delta_{k_{j-1}+1k_j}}{N_{k_j-1}}\sum_{m_{k_j},n_{k_j-1}}|C_{k_j,k_j-1}(m_{k_j},n_{k_j-1})|^2 \\
&\quad\times\cos((\Omega+\omega(m_{k_j},n_{k_j-1}))(t'-t'')). \quad (4.29)
\end{aligned}$$

Using the short-time approximation (4.19) yields

$$\begin{aligned}
&\mathrm{Tr}_B\Big\{\hat{P}_{k_j}\,\mathrm{Tr}_S\{\hat{\mathfrak{c}}\}\Big\}\approx \\
&\quad\rho_{11}(j-1) \\
&\quad\times\Big(\frac{2\delta_{k_{j-1}k_j}}{N_{k_j}}\left(A_{k_j,k_j+1}\cos(\Omega(t'-t''))+A_{k_j,k_j-1}\cos((2\delta+\Omega)(t'-t''))\right) \\
&\qquad-\frac{2\delta_{k_{j-1}+1k_j}}{N_{k_j-1}}A_{k_j,k_j-1}\cos(\Omega(t'-t'')) \\
&\qquad-\frac{2\delta_{k_{j-1}-1k_j}}{N_{k_j+1}}A_{k_j,k_j+1}\cos((2\delta+\Omega)(t'-t''))\Big) \\
&\quad+\rho_{00}(j-1) \\
&\quad\times\Big(\frac{2\delta_{k_{j-1}k_j}}{N_{k_j}}\left(A_{k_j,k_j-1}\cos(\Omega(t'-t''))+A_{k_j,k_j+1}\cos((2\delta+\Omega)(t'-t''))\right) \\
&\qquad-\frac{2\delta_{k_{j-1}-1k_j}}{N_{k_j+1}}A_{k_j,k_j+1}\cos(\Omega(t'-t'')) \\
&\qquad-\frac{2\delta_{k_{j-1}+1k_j}}{N_{k_j-1}}A_{k_j,k_j-1}\cos((2\delta+\Omega)(t'-t''))\Big). \quad (4.30)
\end{aligned}$$

With this, we can calculate the denominator of (4.4) according to

$$\begin{aligned}
\mathrm{Tr}_B\left\{\hat{P}_{k_j}\hat{\rho}'_B(j)\right\} &\approx \delta_{k_{j-1}k_j} - \lambda^2 \int_0^{\Delta t}\int_0^{t'} \mathrm{Tr}_B\left\{\hat{P}_{k_j}\,\mathrm{Tr}_S\{\hat{\mathfrak{c}}\}\right\}\mathrm{d}t''\mathrm{d}t' \\
&\approx \delta_{k_{j-1}k_j} - 4\lambda^2\Bigg\{\Bigg[\rho_{11}(j-1)\left(\frac{A_{k_j,k_j+1}}{N_{k_j}}\zeta_1 + \frac{A_{k_j,k_j-1}}{N_{k_j}}\zeta_2\right) \\
&\quad +\rho_{00}(j-1)\left(\frac{A_{k_j,k_j-1}}{N_{k_j}}\zeta_1 + \frac{A_{k_j,k_j+1}}{N_{k_j}}\zeta_2\right)\Bigg]\delta_{k_{j-1}k_j} \\
&\quad -\frac{A_{k_j,k_j-1}}{N_{k_j-1}}\left(\rho_{11}(j-1)\zeta_1 + \rho_{00}(j-1)\zeta_2\right)\delta_{k_{j-1}+1k_j} \\
&\quad -\frac{A_{k_j,k_j+1}}{N_{k_j+1}}\left(\rho_{00}(j-1)\zeta_1 + \rho_{11}(j-1)\zeta_2\right)\delta_{k_{j-1}-1k_j}\Bigg\}.
\end{aligned} \tag{4.31}$$

Equations (4.22) and (4.31) lead to three different values for $\rho_{00}(j)$ after the measurement, depending on the whether the same ($k_{j+1} = k_j$), a higher ($k_{j+1} = k_j + 1$) or a lower energy ($k_{j+1} = k_j - 1$) has been measured compared to the last measurement. To distinguish these three cases, we denote $\rho_{00}(j)$ by the additional index 0, + and −.

In case of measuring the same energy again, we get

$$\rho_{00,0}(j) \approx \rho_{00}(j-1)\left(1 - \frac{4\frac{\lambda^2}{N_{k_j}}\rho_{11}(j-1)(A_{k_j,k_j+1} - A_{k_j,k_j-1})\,(\zeta_1-\zeta_2)}{1 - 4\frac{\lambda^2}{N_{k_j}}\left(A_{k_j,k_j-1}\zeta_1 + A_{k_j,k_j+1}\zeta_2\right)}\right)^{-1}, \tag{4.32}$$

Up to 2nd order in interaction strength λ this expression reads

$$\rho_{00,0}(j) \approx \rho_{00}(j-1)\left(1 - 4\frac{\lambda^2}{N_{k_j}}\rho_{11}(j-1)(A_{k_j,k_j-1} - A_{k_j,k_j+1})\,(\zeta_1-\zeta_2)\right), \tag{4.33}$$

Measuring one band higher than before yields

$$\rho_{00,+}(j) \approx \frac{\rho_{11}(j-1)\zeta_1}{\rho_{11}(j-1)\zeta_1 + \rho_{00}(j-1)\zeta_2}, \tag{4.34}$$

whereas measuring one band lower leads to

$$\rho_{00,-}(j) \approx \frac{\rho_{11}(j-1)\zeta_2}{\rho_{11}(j-1)\zeta_2 + \rho_{00}(j-1)\zeta_1}. \tag{4.35}$$

As one can see, the state of the TLS strongly depends on the measurement result. Interestingly, it is independent of the interaction strength λ and the choice of the normalization of the interaction (i.e., independent of the $A_{a,b}$) in case of measuring an energy different from in the previous measurement. Only when measuring the same energy band again, the change of the TLS state depends on the special choice of the interaction. However, even in this case, the behavior is rather general, namely the TLS monotonically approaches its ground or excited state. Which of the cases occurs, depends on the chosen parameters. The proof of the monotonicity can be found in App. D. Since the interaction strength enters (4.32), the changes of ρ_{00} will be relatively small when measuring the same band. This is completely different in the other two cases: measuring a different band typically causes significant changes in the occupation probabilities of the TLS. For example, if ρ_{00} has been close to 1 after the last measurement it will be almost 0 after such a measurement and vice versa. Combining this aspect with the monotonicity for measuring the same band, one can expect that periodically repeated measurements after sufficiently long time will lead to some kind of quasi-classical trajectory for the TLS, always jumping between its ground and excited state.

Before we start the detailed discussion of these trajectories in Sect. 4.4, we first investigate the short-time dynamics of the off-diagonal elements of $\hat{\rho}$ in a similar way as done for the diagonal elements.

4.2.2. Off-diagonal elements of the TLS state

Since the density operator is Hermitian ($\rho_{10} = \rho_{01}^*$), we only have to calculate one of the off-diagonal elements. Choosing the 10 component, we first have to identify the contributing terms in the 2nd order commutator (4.11) (the first order does not contribute as discussed in Sect. 4.2.1). These are all terms which contain one of the following expressions

$$\begin{aligned}
\hat{\sigma}^+\hat{\sigma}^-\hat{\rho}(j-1) &= \begin{pmatrix} \rho_{11}(j-1) & \rho_{10}(j-1) \\ 0 & 0 \end{pmatrix}, \\
\hat{\rho}(j-1)\hat{\sigma}^-\hat{\sigma}^+ &= \begin{pmatrix} 0 & \rho_{10}(j-1) \\ 0 & \rho_{00}(j-1) \end{pmatrix}, \\
\hat{\sigma}^+\hat{\rho}(j-1)\hat{\sigma}^+ &= \begin{pmatrix} 0 & \rho_{01}(j-1) \\ 0 & 0 \end{pmatrix}.
\end{aligned} \tag{4.36}$$

Thus, the 10 component of the numerator $\mathrm{Tr}_B\left\{\hat{\tilde{P}}_{k_j}\hat{\rho}'_{\mathrm{tot}}(j)\right\}$ in (4.4) reads

$$\begin{aligned}\mathrm{Tr}_B\left\{\hat{\tilde{P}}_{k_j}\hat{\rho}'_{\mathrm{tot}}(j)\right\}_{10} &\approx \rho_{10}(j-1)\delta_{k_{j-1}k_j} \\ &\quad -\lambda^2\int_0^{\Delta t}\int_0^{t'}\rho_{10}(j-1)\xi_{10}(t',t'') \\ &\quad -\rho_{01}(j-1)\xi_{01}(t',t'')\mathrm{d}t''\mathrm{d}t' \qquad (4.37)\end{aligned}$$

with

$$\begin{aligned}\xi_{10}(t',t'') &:= \mathrm{Tr}_B\left\{\hat{P}_{k_j}\hat{\rho}_B(j-1)\hat{B}^\dagger(t'')\hat{B}(t') + \hat{P}_{k_j}\hat{B}(t')\hat{B}^\dagger(t'')\hat{\rho}_B(j-1)\right\} \\ &= \frac{\delta_{k_{j-1}k_j}}{N_{k_j}}\sum_{m_{k_j},n_{k_j-1}}|C_{k_j,k_j-1}(m_{k_j},n_{k_j-1})|^2 \\ &\quad\times\left(\mathrm{e}^{-\mathrm{i}(\Omega+\omega(m_{k_j},n_{k_j-1}))(t'-t'')} + \mathrm{e}^{\mathrm{i}(2\delta+\Omega+\omega(m_{k_j},n_{k_j-1}))(t'-t'')}\right) \\ &\quad+\frac{\delta_{k_{j-1}k_j}}{N_{k_j}}\sum_{m_{k_j},n_{k_j+1}}|C_{k_j,k_j+1}(m_{k_j},n_{k_j+1})|^2 \\ &\quad\times\left(\mathrm{e}^{-\mathrm{i}(\Omega+\omega(m_{k_j+1},n_{k_j}))(t'-t'')} + \mathrm{e}^{\mathrm{i}(2\delta+\Omega+\omega(m_{k_j+1},n_{k_j}))(t'-t'')}\right), \\ \xi_{01}(t',t'') &:= \mathrm{Tr}_B\left\{\hat{P}_{k_j}\hat{B}(t'')\hat{\rho}_B(j-1)\hat{B}(t') + \hat{P}_{k_j}\hat{B}(t')\hat{\rho}_B(j-1)\hat{B}(t'')\right\} \\ &= \frac{\delta_{k_{j-1}-1k_j}}{N_{k_j+1}}\sum_{m_{k_j},n_{k_j+1}}|C_{k_j,k_j+1}(m_{k_j},n_{k_j+1})|^2 \\ &\quad\times\Bigg(\mathrm{e}^{2\mathrm{i}\delta t'}\mathrm{e}^{\mathrm{i}(\Omega+\omega(n_{k_j+1},m_{k_j}))(t'-t'')} \\ &\quad\quad+\mathrm{e}^{2\mathrm{i}\delta t''}\mathrm{e}^{-\mathrm{i}(\Omega+\omega(n_{k_j+1},m_{k_j}))(t'-t'')}\Bigg) \\ &\quad+\frac{\delta_{k_{j-1}+1k_j}}{N_{k_j-1}}\sum_{m_{k_j},n_{k_j-1}}|C_{k_j,k_j-1}(m_{k_j},n_{k_j-1})|^2 \\ &\quad\times\Bigg(\mathrm{e}^{2\mathrm{i}\delta t'}\mathrm{e}^{\mathrm{i}(\Omega+\omega(m_{k_j},n_{k_j-1}))(t'-t'')} \\ &\quad\quad+\mathrm{e}^{2\mathrm{i}\delta t''}\mathrm{e}^{-\mathrm{i}(\Omega+\omega(m_{k_j},n_{k_j-1}))(t'-t'')}\Bigg). \qquad (4.38)\end{aligned}$$

As for the diagonal element discussed in Sect. 4.2.1 we can again apply the short-time approximation, which yields

$$\begin{aligned}
\xi_{10}(t',t'') &\approx \frac{\delta_{k_{j-1}k_j}}{N_{k_j}}\left(A_{k_j,k_j+1}+A_{k_j,k_j-1}\right)\left(\mathrm{e}^{-\mathrm{i}\Omega(t'-t'')}+\mathrm{e}^{\mathrm{i}(2\delta+\Omega)(t'-t'')}\right),\\
\xi_{01}(t',t'') &\approx \left(\frac{\delta_{k_{j-1}-1k_j}}{N_{k_j+1}}A_{k_j,k_j+1}+\frac{\delta_{k_{j-1}+1k_j}}{N_{k_j-1}}A_{k_j,k_j-1}\right)\\
&\quad\times\left(\mathrm{e}^{2\mathrm{i}\delta t'}\,\mathrm{e}^{\mathrm{i}\Omega(t'-t'')}+\mathrm{e}^{2\mathrm{i}\delta t''}\,\mathrm{e}^{-\mathrm{i}\Omega(t'-t'')}\right). \qquad (4.39)
\end{aligned}$$

With this, we can calculate the integrals in (4.37), leading us to

$$\begin{aligned}
\mathrm{Tr}_B\left\{\hat{\tilde{P}}_{k_j}\hat{\rho}'_{\mathrm{tot}}(j)\right\}_{10} &\approx \rho_{10}(j-1)\delta_{k_{j-1}k_j}-\lambda^2\Bigg[\frac{\delta_{k_{j-1}k_j}}{N_k}\left(A_{k_j,k_j+1}+A_{k_j,k_j-1}\right)\\
&\quad\times\left(\frac{1-\mathrm{e}^{\mathrm{i}\Omega\Delta t}+\mathrm{i}\Omega\Delta t}{\Omega^2}+\frac{1-\mathrm{e}^{\mathrm{i}(2\delta+\Omega)\Delta t}+\mathrm{i}(2\delta+\Omega)\Delta t}{(2\delta+\Omega)^2}\right)\\
&\quad\times\rho_{10}(j-1)\\
&\quad+\frac{1+\mathrm{e}^{2\mathrm{i}\delta\Delta t}(1-2\cos((\delta+\Omega)\Delta t))}{2\delta\Omega+\Omega^2}\\
&\quad\times\left(\frac{\delta_{k_{j-1}-1k_j}}{N_{k_j+1}}A_{k_j,k_j+1}+\frac{\delta_{k_{j-1}+1k_j}}{N_{k_j-1}}A_{k_j,k_j-1}\right)\\
&\quad\times\rho_{01}(j-1)\Bigg]. \qquad (4.40)
\end{aligned}$$

Together with the denominator (4.31), we are now able to calculate the off-diagonal elements of the TLS state after the measurement according to (4.4). As for the diagonal elements, we get three different values depending on the

measurement result:

$$\begin{aligned}\rho_{10,0}(j) \;\approx\; \rho_{10}(j-1)\Bigg[1 - \frac{\lambda^2(A_{k_j,k_j+1} + A_{k_j,k_j-1})}{N_{k_j}} \\ \times\left(\frac{1-\mathrm{e}^{\mathrm{i}\Omega\Delta t}+\mathrm{i}\Omega\Delta t}{\Omega^2} + \frac{1-\mathrm{e}^{\mathrm{i}(2\delta+\Omega)\Delta t}+\mathrm{i}(2\delta+\Omega)\Delta t}{(2\delta+\Omega)^2}\right)\Bigg] \\ \times\Bigg[1 - 4\frac{\lambda^2}{N_{k_j}}\big(\left(\rho_{11}(j-1)A_{k_j,k_j+1} + \rho_{00}(j-1)A_{k_j,k_j-1}\right)\zeta_1 \\ + \left(\rho_{11}(j-1)A_{k_j,k_j-1} + \rho_{00}(j-1)A_{k_j,k_j+1}\right)\zeta_2\big)\Bigg]^{-1}, \quad (4.41)\end{aligned}$$

$$\rho_{10,+}(j) \;\approx\; \rho_{01}(j-1)\frac{1+\mathrm{e}^{2\mathrm{i}\delta\Delta t} - 2\mathrm{e}^{\mathrm{i}\delta\Delta t}\cos((\delta+\Omega)\Delta t)}{4(2\delta\Omega+\Omega^2)\left(\rho_{11}(j-1)\zeta_1 + \rho_{00}(j-1)\zeta_2\right)}, \quad (4.42)$$

$$\rho_{10,-}(j) \;\approx\; \rho_{01}(j-1)\frac{1+\mathrm{e}^{2\mathrm{i}\delta\Delta t} - 2\mathrm{e}^{\mathrm{i}\delta\Delta t}\cos((\delta+\Omega)\Delta t)}{4(2\delta\Omega+\Omega^2)\left(\rho_{11}(j-1)\zeta_2 + \rho_{00}(j-1)\zeta_1\right)}. \quad (4.43)$$

Again, the expression obtained for measuring the same band can be rewritten by expanding up to 2nd order in λ, obtaining

$$\begin{aligned}\rho_{10,0}(j) \;\approx\; \rho_{10}(j-1)\Bigg[1 + \frac{\lambda^2}{N_{k_j}}\Bigg(\left(A_{k_j,k_j-1}\rho_{00}(j-1) + A_{k_j,k_j+1}\rho_{11}(j-1)\right)4\zeta_1 \\ + \left(A_{k_j,k_j+1}\rho_{00}(j-1) + A_{k_j,k_j-1}\rho_{11}(j-1)\right)4\zeta_2 \\ - \left(A_{k_j,k_j-1} + A_{k_j,k_j+1}\right) \\ \times\left(\frac{1-\mathrm{e}^{\mathrm{i}\Omega\Delta t}+\mathrm{i}\Omega\Delta t}{\Omega^2} + \frac{1-\mathrm{e}^{\mathrm{i}(2\delta+\Omega)\Delta t}+\mathrm{i}(2\delta+\Omega)\Delta t}{(2\delta+\Omega)^2}\right)\Bigg)\Bigg]. \quad (4.44)\end{aligned}$$

This expression is still rather complicated, but one can see that – as for the diagonal elements – the changes of the off-diagonals in this case also are relatively small due to the weak coupling ($\propto \lambda^2$), whereas the expressions (4.42) and (4.43) for measuring a different energy band are again independent of the details of the chosen interaction.

4.2.3. Probabilities for the measurement results

In the preceding sections, we have calculated the state of the TLS after measuring the energy of the environment. We have seen that this state strongly depends on the measurement result. In order to be able to discuss the evolution of the TLS under the influence of periodic measurements, we thus also have to determine the probabilities with which each of these measurement results occur.

Since we measure the energy of the environment, these probabilities are just given by the occupation probabilities of the energy bands directly before the measurement. As already mentioned, if band k_{j-1} has been measured at step $j-1$, there exist three possible results for measurement j, which correspond to three non-vanishing occupation probabilities of the bands $k_j = \{k_{j-1}, k_{j-1}+1, k_{j-1}-1\}$. These probabilities are given by

$$p_{k_j}(j) = \sum_{n_{k_j}} \langle n_{k_j}| \operatorname{Tr}_S\{\hat{\rho}'_{\rm tot}(j)\} |n_{k_j}\rangle \ . \tag{4.45}$$

Using the projection operator (4.2), we can rewrite (4.45) as

$$p_{k_j}(j) = \operatorname{Tr}_B\left\{\hat{P}_{k_j}\hat{\rho}'_B(j)\right\} , \tag{4.46}$$

which is exactly the denominator of (4.4) calculated in Sect. 4.2.1. According to (4.31), we get

$$\begin{aligned} p_{k_j}(j) \quad \approx \quad & \delta_{k_{j-1}k_j} - 4\lambda^2 \Bigg\{ \Bigg[\rho_{11}(j-1) \left(\frac{A_{k_j,k_j+1}}{N_{k_j}}\zeta_1 + \frac{A_{k_j,k_j-1}}{N_{k_j}}\zeta_2 \right) \\ & + \rho_{00}(j-1) \left(\frac{A_{k_j,k_j-1}}{N_{k_j}}\zeta_1 + \frac{A_{k_j,k_j+1}}{N_{k_j}}\zeta_2 \right) \Bigg] \delta_{k_{j-1}k_j} \\ & - \frac{A_{k_j,k_j-1}}{N_{k_j-1}} \left(\rho_{11}(j-1)\zeta_1 + \rho_{00}(j-1)\zeta_2\right) \delta_{k_{j-1}+1k_j} \\ & - \frac{A_{k_j,k_j+1}}{N_{k_j+1}} \left(\rho_{00}(j-1)\zeta_1 + \rho_{11}(j-1)\zeta_2\right) \delta_{k_{j-1}-1k_j} \Bigg\} . \end{aligned} \tag{4.47}$$

Thus, for given energy band k_{j-1} determined at the preceding measurement $j-1$, the probabilities for measuring one band higher, one band lower or the same band read

$$p_+(k_{j-1}) \quad \approx \quad 4\lambda^2 \frac{A_{k_{j-1},k_{j-1}+1}}{N_{k_{j-1}}} \left(\rho_{11}(j-1)\zeta_1 + \rho_{00}(j-1)\zeta_2\right) , \tag{4.48}$$

$$p_-(k_{j-1}) \quad \approx \quad 4\lambda^2 \frac{A_{k_{j-1},k_{j-1}-1}}{N_{k_{j-1}}} \left(\rho_{00}(j-1)\zeta_1 + \rho_{11}(j-1)\zeta_2\right) , \tag{4.49}$$

$$p_0(k_{j-1}) \quad \approx \quad 1 - p_+(k_{j-1}) - p_-(k_{j-1}) . \tag{4.50}$$

As one can see, the probabilities for measuring a different band are proportional to λ^2, i.e., much smaller than for measuring the same band due to the weak coupling. That is, in the majority of cases, the same band as in the previous measurement will be measured again.

4.3. Normalization of the interaction

Up to this point the normalization $\overline{|C_{i,j}(a,b)|^2} := \tilde{c}_{i,j}$ of the blocks in the interaction has not been specified. As mentioned in Sect. 2.2.2 this choice is not important for the quantum thermodynamical model without measurements but becomes important now, when including measurements. The reason for this is that in the model without measurements, there are only three energy bands involved in the relaxation and for these the interaction can always be chosen to be weak, by choosing an appropriate λ. However, if we include measurements, the band index k can change. Thus, there will be an interaction with many different bands during the dynamics. Therefore, we have to be careful in our choice of the normalization in order to ensure that the interaction always stays weak, i.e., that the interaction energy always stays small compared to the energy of the system. The interaction energy can be calculated in a similar way as done for the state of the TLS in the previous sections: Denoting the initial state of the TLS (or rather its state after the previous measurement) by ρ_{ij} and the initially occupied band by k, the interaction energy between system and environment for times t until the next measurement reads (cf. App. C)

$$\begin{aligned} E_{\mathrm{int}}(t) \quad &\approx \quad \frac{4\lambda^2}{N_k}\Bigg[\left(\rho_{11}A_{k,k-1} - \rho_{00}A_{k,k+1}\right) \frac{1}{2\delta+\Omega} \sin^2\left(\frac{2\delta+\Omega}{2}t\right) \\ &\qquad + \left(\rho_{00}A_{k,k-1} - \rho_{11}A_{k,k+1}\right) \frac{1}{\Omega} \sin^2\left(\frac{\Omega}{2}t\right)\Bigg] . \end{aligned} \tag{4.51}$$

Let us first consider the simplest possible normalization $\tilde{c}_{i,j} = 1$, i.e., the case where all non-vanishing entries of the interaction matrix were determined by the same Gaussian distribution. Such a normalization was chosen, for example, in [14] to demonstrate the thermalization of a TLS by a finite bath. For this choice, the interaction energy as well as the measurement probabilities (4.48)–(4.50) strongly depend on the index of the occupied band before the measurement according to (2.4) and (4.20)

$$\frac{A_{k,k-1}}{N_k} = \frac{N_k N_{k-1}\cdot 1}{N_k} = N_{k-1} = \mathcal{N}\mathrm{e}^{\beta\delta_B(k-1)} , \tag{4.52}$$

$$\frac{A_{k,k+1}}{N_k} = \frac{N_k N_{k+1}\cdot 1}{N_k} = N_{k+1} = \mathcal{N}\mathrm{e}^{\beta\delta_B(k+1)} . \tag{4.53}$$

Thus, for increasing band number, this would eventually lead to a very strong coupling, even if λ was chosen such that the coupling was weak initially. In this case, our whole calculations based on perturbation theory would break down. Furthermore, such an exponential dependency on the band index can hardly be justified on physical grounds.

In order to ensure that the interaction stays weak independent of the actual band index, a better choice for the normalization is $\tilde{c}_{i,j} = (N_i N_j)^{-1/2}$. This normalization leads to

$$\frac{A_{k,k-1}}{N_k} = \frac{N_k N_{k-1} \cdot (N_k N_{k-1})^{-1/2}}{N_k} = \mathrm{e}^{-\beta\delta_B/2}\,, \tag{4.54}$$

$$\frac{A_{k,k+1}}{N_k} = \frac{N_k N_{k+1} \cdot (N_k N_{k+1})^{-1/2}}{N_k} = \mathrm{e}^{\beta\delta_B/2}\,, \tag{4.55}$$

which, indeed, is independent of the actual band index k. Hence, it is possible to choose λ such that it guaranties a weak coupling at any time of the dynamics. Furthermore, this choice allows us also to calculate the ensemble average analytically, which will be done in the next section.

The dynamics following from this normalization can also be expected to appear for other concrete choices of the interaction as, e.g., for a $\sigma_x \otimes \sigma_x$-coupling between the TLS and the n environmental spins: In this case, the number of entries 1 in the interaction block $C_{k,k+1}$ is given by the number of levels N_k within the band k times the number of spins down $n-k$ in this band, whereas the rest of the entries is 0, i.e, the average over the whole block with $N_k N_{k+1}$ entries reads

$$\overline{|C_{k,k+1}(a,b)|^2} = \frac{N_k(n-k)}{N_k N_{k+1}} = \frac{n-k}{N_{k+1}}\,. \tag{4.56}$$

The same considerations apply for the block $C_{k,k-1}$ where the number of non-vanishing entries is given by $N_k \cdot k$ and therefore

$$\overline{|C_{k,k-1}(a,b)|^2} = \frac{N_k k}{N_k N_{k-1}} = \frac{k}{N_{k-1}}\,. \tag{4.57}$$

This leads to

$$\frac{A_{k,k-1}}{N_k} = \frac{N_k N_{k-1} \cdot \frac{k}{N_{k-1}}}{N_k} = k\,, \tag{4.58}$$

$$\frac{A_{k,k+1}}{N_k} = \frac{N_k N_{k+1} \cdot \frac{n-k}{N_{k+1}}}{N_k} = n-k\,. \tag{4.59}$$

Thus, for $\sigma_x \otimes \sigma_x$-coupling we get a linear dependency on the band index k. However, for the large environments we are considering here to be able to talk about quantum thermodynamics, the change of the band index during the dynamics will be much smaller than the band index itself, i.e, (4.58) and (4.59) will stay approximately constant. Thus, one can expect that the calculations assuming $\tilde{c}_{i,j} = (N_i N_j)^{-1/2}$ should also apply to this model.

4.4. Trajectories due to periodic measurements

In Sect. 4.2 we have calculated how the state of the TLS changes depending on the result of the energy measurement of the environment. We also determined the probabilities with which each of these results will occur. In this section we will use these results to discuss the trajectories of the TLS arising from periodic measurements.

Before we show some results of numerical simulations, let us first contemplate the dynamics expected from the results of the last sections. We have seen, that in most cases the same energy band as in the last measurement will be measured. In these cases the state of the TLS slowly approaches its ground state or exited state (depending on the concrete parameters of the model as discussed in App. D). In the much less frequent cases of measuring a different band, the state of the TLS was shown to change drastically, jumping from close to the ground state almost to the exited state and vice versa. Bringing all these aspects together, one can thus expect, that after sufficiently many measurements, the TLS will show some kind of quasi-classical trajectories, jumping between its ground and exited state.

Let us now test this consideration by a numerical simulation. The result of each measurement is determined by a generated pseudo-random number $0 \leq z_j \leq 1$:

- For $z_j \leq p_-(k_{j-1})$, the lower band is "measured", i.e., $k_j = k_{j-1} - 1$ and the state of the TLS changes according to (4.35) and (4.43).

- In case of $z_j \geq 1 - p_+(k_{j-1})$, the measurement of a higher band is simulated ($k_j = k_{j-1} + 1$) where the state of the TLS is determined by (4.34) and (4.42).

- For all other cases $p_-(k_{j-1}) < z_j < 1 - p_+(k_{j-1})$ we simulate the measurement of the same band $k_j = k_{j-1}$ leading to the TLS state given by (4.33) and (4.44).

Two examples for such trajectories following from eqs. (4.33)–(4.35), (4.42)–(4.44) and (4.48)–(4.50) are shown in Fig. 4.1 and Fig. 4.2. As expected, the single TLS no longer relaxes to a thermal state as it would in the quantum thermodynamical setting without measurements. The arising quasi-classical trajectories of the TLS under periodic measurements of the environment are typical for any chosen norm $\overline{|C_{i,j}(a,b)|^2}$ of the interaction, as long as the weak coupling assumption remains fulfilled. Thus, this kind of classicality arises under rather general conditions.

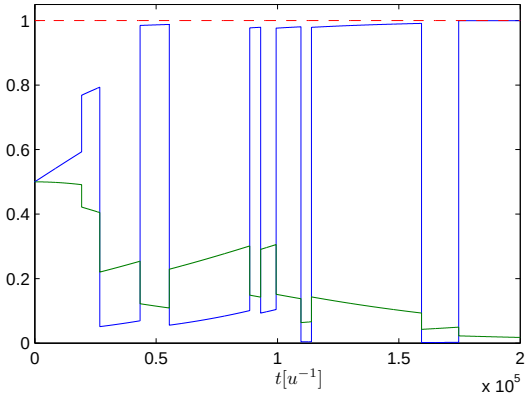

Figure 4.1.: Trajectory of the TLS for the initial pure state $|\psi\rangle = 1/\sqrt{2}(|1\rangle + |0\rangle)$: After some transient, the TLS always jumps between ground and excited state. The blue line corresponds to ρ_{00}. The off-diagonal elements (the green line shows $|\rho_{10}|$) vanish such that the purity $\mathcal{P} := \mathrm{Tr}\{\hat{\rho}^2\}$ (dashed red line) always stays close to 1. Used parameters: $\delta = 1\,u$, $\Delta t = 2\,u^{-1}$, $\beta = 0.75\,u^{-1}$, $\lambda = 4 \cdot 10^{-3}\,u$, $\Omega = 0\,u$.

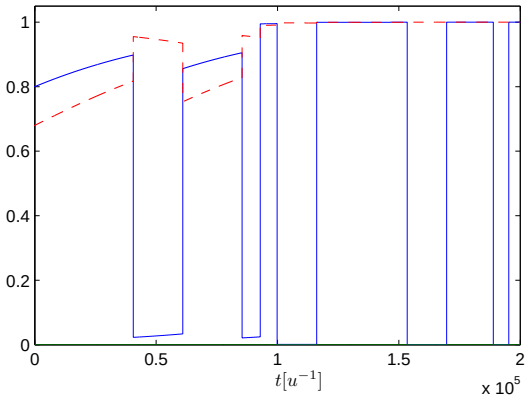

Figure 4.2.: Same as Fig. 4.1 but for an initial diagonal state with $\rho_{00} = 0.8$. Here the off-diagonal elements (green) are zero all the time, whereas the diagonal elements (blue) again approach the classical trajectory. Therefore, the purity (dashed red) increases until it reaches $\mathcal{P} = 1$.

An interesting point is that for an initial pure state, the state of the TLS stays pure or at least very close to a pure state over the whole trajectory, whereas an initial thermal state will always stay diagonal.

Thus there exists no thermal state for the single system, but one may wonder if there exists a thermal state for an ensemble of systems, as thermalization is typically defined in statistical mechanics. Hence, our goal in the following discussion is to determine the ensemble average over these trajectories to search for a possible attractor state. Numerically this can be done easily by just simulating many of those trajectories for fixed parameters and then calculating the average. A comparison of the analytical obtained ensemble average and this numerical average can be found in Sect. 4.5.5.

4.5. Analytical calculation of the ensemble average

In this section, we investigate the dynamics of the ensemble average analytically. As we have seen in the previous section, this average is basically independent of the chosen normalization $\overline{|C_{i,j}(a,b)|^2}$. However, for the analytical discussion it is helpful to pick a special case, namely $\tilde{c}_{i,j} = (N_i N_j)^{-1/2}$. As already discussed in Sect. 4.3, this choice is a good approximation for concrete physical interactions like the $\hat{\sigma}_x \otimes \hat{\sigma}_x$ coupling. The main advantage of this normalization is that – according to (4.54) and (4.55) – the dynamics becomes independent of the actual band index k. This allows us to calculate the ensemble average of the TLS state at step j for fixed initial state $\hat{\rho}(0)$ by calculating the ensemble average after a single step and then iterating this result.

4.5.1. Off-diagonal elements

Before we discuss the diagonal elements in the next section, we first study the off-diagonal elements. As we will see, these off-diagonals vanish in almost all cases for sufficiently many measurements. Thus periodic measurements typically lead to a diagonal state for the TLS, which will allow us to assign a temperature to the ensemble of TLS.

Let us start with the ensemble average after step j, assuming the state at step $j-1$ is known. This average then is simply given by the probabilities for each of the three measurement results times the corresponding state of the TLS, i.e., the ensemble average for the off-diagonal element ρ_{10} reads

$$\overline{\rho}_{10}(j) = p_0(j)\rho_{10,0}(j) + p_+(j)\rho_{10,+}(j) + p_-(j)\rho_{10,-}(j)\,. \tag{4.60}$$

Using (4.54) and (4.55) the probabilities (4.48)–(4.50) read

$$p_+(j) \approx 4\lambda^2 \mathrm{e}^{\beta\delta_B/2}\left(\rho_{11}(j-1)\zeta_1 + \rho_{00}(j-1)\zeta_2\right), \tag{4.61}$$

$$p_-(j) \approx 4\lambda^2 \mathrm{e}^{-\beta\delta_B/2}\left(\rho_{00}(j-1)\zeta_1 + \rho_{11}(j-1)\zeta_2\right), \tag{4.62}$$

$$p_0(j) \approx 1 - p_+(k_{j-1}) - p_-(k_{j-1}). \tag{4.63}$$

Applying (4.54) and (4.55) also to (4.41)–(4.43) then leads to

$$\begin{aligned}\overline{\rho}_{10}(j) = \; & \rho_{10}(j-1) + 2\lambda^2\cosh(\beta\delta_B/2) \\ & \times\Big[-\rho_{10}(j-1) \\ & \times\left(\frac{1-\mathrm{e}^{\mathrm{i}\Omega\Delta t}+\mathrm{i}\Omega\Delta t}{\Omega^2} + \frac{1-\mathrm{e}^{\mathrm{i}(2\delta+\Omega)\Delta t}+\mathrm{i}(2\delta+\Omega)\Delta t}{(2\delta+\Omega)^2}\right) \\ & +\rho_{01}(j-1)\frac{1+\mathrm{e}^{2\mathrm{i}\delta\Delta t}-2\mathrm{e}^{\mathrm{i}\delta\Delta t}\cos((\delta+\Omega)\Delta t)}{2\delta\Omega+\Omega^2}\Big]. \end{aligned} \tag{4.64}$$

Interestingly, this expression for the ensemble average does not depend on the diagonal elements of the density matrix. Therefore, the dynamics of the off-diagonal elements can be calculated independently of the diagonal elements. We now iterate this result: the ensemble average after measurement 1 is taken as initial state for the next time step leading to the average after measurement 2 and so forth. In order to obtain an analytical expression for the ensemble average after measurement j, we rewrite (4.64) in the form

$$\overline{\rho}_{10}(j) - \overline{\rho}_{10}(j-1) = \overline{\rho}_{10}(j-1)(c_1 + \mathrm{i}c_2) + \overline{\rho}_{01}(j-1)(c_3 + \mathrm{i}c_4) \tag{4.65}$$

where we defined the real coefficients

$$c_1 := -2\lambda^2\cosh(\beta\delta_B/2)\left(\frac{1-\cos(\Omega\Delta t)}{\Omega^2} + \frac{1-\cos((2\delta+\Omega)\Delta t)}{(2\delta+\Omega)^2}\right), \tag{4.66}$$

$$\begin{aligned} c_2 := \; & -2\lambda^2\cosh(\beta\delta_B/2) \\ & \times\left(\frac{\Omega\Delta t - \sin(\Omega\Delta t)}{\Omega^2} + \frac{(2\delta+\Omega)\Delta t - \sin((2\delta+\Omega)\Delta t)}{(2\delta+\Omega)^2}\right), \end{aligned} \tag{4.67}$$

$$c_3 := -4\lambda^2\cosh(\beta\delta_B/2)\frac{\cos(\delta\Delta t)\cos((\delta+\Omega)\Delta t) - \cos^2(\delta\Delta t)}{2\delta\Omega+\Omega^2}, \tag{4.68}$$

$$c_4 := -2\lambda^2\cosh(\beta\delta_B/2)\frac{2\sin(\delta\Delta t)\cos((\delta+\Omega)\Delta t) - \sin(2\delta\Delta t)}{2\delta\Omega+\Omega^2}. \tag{4.69}$$

The left-hand side of (4.65) can be approximated as a derivative with respect to j, if the change of $\overline{\rho}_{10}$ from one measurement to the next one is small, which is guaranteed by the weak coupling assumption. Considering the real

and imaginary parts of $\overline{\rho}_{10}$ as two variables $\Re(j) := \mathrm{Re}\,(\overline{\rho}_{10}(j))$ and $\Im(j) := \mathrm{Im}\,(\overline{\rho}_{10}(j))$, then leads to two coupled differential equations of the form

$$\frac{\mathrm{d}\Re(j)}{\mathrm{d}j} = (c_1 + c_3)\Re(j) + (c_4 - c_2)\Im(j)\,, \tag{4.70}$$

$$\frac{\mathrm{d}\Im(j)}{\mathrm{d}j} = (c_1 - c_3)\Im(j) + (c_2 + c_4)\Re(j)\,. \tag{4.71}$$

The solution of this system of differential equations reads

$$\begin{aligned}\Re(j) &= \frac{1}{2\gamma}\mathrm{e}^{(c_1-\gamma)j}\Big[\Big(c_3\left(\mathrm{e}^{2\gamma j}-1\right)+\gamma\left(\mathrm{e}^{2\gamma j}+1\right)\Big)\Re(0)\\ &\quad +(c_4-c_2)\left(\mathrm{e}^{2\gamma j}-1\right)\Im(0)\Big]\,,\end{aligned} \tag{4.72}$$

$$\begin{aligned}\Im(j) &= \frac{1}{2\gamma}\mathrm{e}^{(c_1-\gamma)j}\Big[\left(c_2+c_4\right)\left(\mathrm{e}^{2\gamma j}-1\right)\Re(0)\\ &\quad +\left(-c_3\left(\mathrm{e}^{2\gamma j}-1\right)+\gamma\left(\mathrm{e}^{2\gamma j}+1\right)\right)\Im(0)\Big]\,,\end{aligned} \tag{4.73}$$

where we introduced the abbreviation $\gamma := \sqrt{-c_2^2 + c_3^2 + c_4^2}$. Considering the absolute value of $\overline{\rho}_{10}$, we get

$$\begin{aligned}|\overline{\rho}_{10}(j)| &= \left(\Re(j)^2 + \Im(j)^2\right)^{1/2}\\ &= \frac{\mathrm{e}^{c_1 j}}{\gamma}\Big[\big(\left(c_3\sinh(\gamma j) + \gamma\cosh(\gamma j)\right)\Re(0) + (c_4 - c_2)\sinh(\gamma j)\Im(0)\big)^2\\ &\quad +\big(\left(c_2+c_4\right)\sinh(\gamma j)\Re(0) + \left(-c_3\sinh(\gamma j) + \gamma\cosh(\gamma j)\right)\Im(0)\big)^2\Big]^{1/2}.\end{aligned} \tag{4.74}$$

This is an important result, describing the dynamics of the off-diagonal elements of the TLS under the influence of periodic measurements of the environment. As one directly can see, a diagonal initial state (i.e., $\Re(0) = \Im(0) = 0$) will stay diagonal forever. Furthermore, as discussed in App. E, for arbitrary initial states, the off-diagonal elements will vanish in the limit of many measurements

$$\lim_{j\to\infty} |\overline{\rho}_{10}(j)| = 0, \tag{4.75}$$

for almost any choice of the parameters: In the resonant case ($\delta = \delta_B$) this is always true, whereas in the off-resonant case one may suppress the dynamics of the TLS by choosing appropriate values for the parameters Δt and Ω. As we will see in the next section, in this very special case not only the off-diagonal elements but also the diagonal elements stay constant, i.e., the state

becomes stationary. The exact parameters for which this freezing of the TLS state occurs can be found in App. E. However, for all other situations the off-diagonals will vanish, i.e., the measurements lead to a thermal state for the TLS. Hence, all we yet need to completely characterize the attractor state is the occupation probability of the ground state. This will be subject of the next section.

4.5.2. Diagonal elements: General properties

The ensemble average of the diagonal element ρ_{00} after step j – given the state after measurement $j-1$ – can be calculated in the same way as done in (4.60) for the off-diagonal element ρ_{10}, namely

$$\overline{\rho}_{00}(j) = p_0(j)\rho_{00,0}(j) + p_+(j)\rho_{00,+}(j) + p_-(j)\rho_{00,-}(j)\,. \tag{4.76}$$

Using again (4.61)–(4.63) and applying (4.54) and (4.55) to (4.32)–(4.35) yields

$$\begin{aligned}\overline{\rho}_{00}(j) &= \rho_{00}(j-1) + 4\lambda^2\Big[\left(\mathrm{e}^{\beta\delta_B/2}\rho_{11}(j-1) - \mathrm{e}^{-\beta\delta_B/2}\rho_{00}(j-1)\right)\zeta_1 \\ &\quad + \left(\mathrm{e}^{-\beta\delta_B/2}\rho_{11}(j-1) - \mathrm{e}^{\beta\delta_B/2}\rho_{00}(j-1)\right)\zeta_2\Big]\,. \end{aligned}\tag{4.77}$$

As done for the off-diagonal elements, this result can be iterated: To derive the analytical expression for $\overline{\rho}_{00}(j)$, we first rewrite (4.77) as

$$\overline{\rho}_{00}(j+1) - \overline{\rho}_{00}(j) = -R\overline{\rho}_{00}(j) + d \tag{4.78}$$

with

$$R := 8\lambda^2\cosh(\beta\delta_B/2)\,(\zeta_1+\zeta_2)\,, \tag{4.79}$$

$$d := 4\lambda^2\left(\mathrm{e}^{\beta\delta_B/2}\zeta_1 + \mathrm{e}^{-\beta\delta_B/2}\zeta_2\right)\,. \tag{4.80}$$

Again, the left-hand side can be approximated by a derivative with respect to j, as long as $\overline{\rho}_{00}$ only chances slowly with j, which is guaranteed by the weak coupling. Thus, we can reinterpret (4.78) as a differential equation of the form

$$\frac{\mathrm{d}\overline{\rho}_{00}(j)}{\mathrm{d}j} = -R\overline{\rho}_{00}(j) + d\,, \tag{4.81}$$

keeping in mind that the measurement number j of course is always an integer. The solution of this differential equation reads

$$\overline{\rho}_{00}(j) = \left(\rho_{00}(0) - \frac{d}{R}\right)\mathrm{e}^{-Rj} + \frac{d}{R}\,, \tag{4.82}$$

i.e., in ensemble average the occupation probability of the ground state relaxes exponentially from the initial state $\overline{\rho}_{00}(0) = \rho_{00}(0)$ to an attractor state, given by

$$\begin{aligned} \overline{\rho}_{00}^{\mathrm{attr}} &= \frac{d}{R} \\ &= \frac{\mathrm{e}^{\beta\delta_B/2}\zeta_1 + \mathrm{e}^{-\beta\delta_B/2}\zeta_2}{2\cosh(\beta\delta_B/2)\,(\zeta_1+\zeta_2)}\,. \end{aligned} \tag{4.83}$$

This relaxation has some interesting properties: First, it is noteworthy that due to the measurements a relaxation becomes possible not only in the resonant case but also for $\delta_B \neq \delta$. In this case (but without measurements) the interaction would induce almost no change of the state, as already mentioned in Sect. 2.1.

Considering the relaxation constant

$$R = 8\lambda^2 \cosh(\beta\delta_B/2)\left(\frac{\sin^2\left(\frac{\Omega}{2}\Delta t\right)}{\Omega^2} + \frac{\sin^2\left(\left(\delta+\frac{\Omega}{2}\right)\Delta t\right)}{(2\delta+\Omega)^2}\right), \tag{4.84}$$

one can see that it depends on the time Δt between the measurements. In particular, one gets

$$\lim_{\Delta t\to 0} R = 0\,, \tag{4.85}$$

which means that the relaxation is slowed down for very fast repeated measurements. Such a suppression of decay due to fast, periodic measurements is well known as the so-called quantum Zeno effect [22, 37]. Furthermore, R also vanishes for $\Delta t = n\frac{\pi}{\delta}$ and $\Omega = \frac{2m\pi}{\Delta t}$, $n = 0, 1, 2, .., m = 1, 2, ...$ For this special choice of the parameters, also the off-diagonal elements stay constant as shown in App. E. Thus, it is also possible to freeze the state of the TLS by periodic measurements carried out with finite frequency.

4.5.3. Attractor state for the resonant case

Before we discuss the influence of the detuning Ω on the attractor state in Sect. 4.5.4, let us first study in detail the case $\Omega = 0$, i.e., the case corresponding to the quantum thermodynamical situation, where a thermalization to a state of temperature $1/\beta$ would happen without measurements.

For the resonant case, we have

$$\zeta_1 = \lim_{\Omega\to 0}\frac{\sin^2\left(\frac{\Omega}{2}\Delta t\right)}{\Omega^2} = \frac{\Delta t^2}{4}\,, \tag{4.86}$$

$$\zeta_2 = \lim_{\Omega\to 0}\frac{\sin^2\left(\left(\delta+\frac{\Omega}{2}\right)\Delta t\right)}{(2\delta+\Omega)^2} = \frac{\sin^2(\delta\Delta t)}{4\delta^2}\,. \tag{4.87}$$

Thus, the attractor state reads

$$\overline{\rho}_{00}^{\mathrm{attr}}(\Delta t) = \frac{\mathrm{e}^{-\beta\delta/2}\sin^2(\delta\Delta t) + \mathrm{e}^{\beta\delta/2}\delta^2\Delta t^2}{2\cosh(\beta\delta/2)\left(\sin^2(\delta\Delta t) + \delta^2\Delta t^2\right)}\,. \tag{4.88}$$

Remarkably, this attractor state depends not only on the parameters β and δ as in the quantum thermodynamical setting, but also on the time Δt between the measurements, i.e., the ensemble average of the TLS state depends on how often one "looks" at the environment. Therefore, this attractor is a dynamical one: As soon as one stops the periodic measurements, the TLS would start to relax to a thermal state of temperature $1/\beta$ due to the coupled environment. Considering the dependency on Δt, the attractor has two interesting bounds:

- In the limit of very fast measurements, because of

$$\lim_{\Delta t\to 0}\frac{\sin^2(\delta\Delta t)}{\Delta t^2} = \delta^2\,, \tag{4.89}$$

we get

$$\lim_{\Delta t\to 0}\overline{\rho}_{00}^{\mathrm{attr}} = \frac{\mathrm{e}^{-\beta\delta/2}\delta^2 + \mathrm{e}^{\beta\delta/2}\delta^2}{2\cosh(\beta\delta/2)\,(\delta^2+\delta^2)} = \frac{1}{2}\,. \tag{4.90}$$

That is, the TLS is heated up to infinite temperature in this limit. This may seem to be contradicting with the fact that in this limit we also have suppression of the dynamics due to the Zeno effect, i.e., the state of the TLS should not change. Indeed, for $\Delta t \to 0$ it would take infinitely long time to reach the attractor state, but this limit is of course not reachable. Nevertheless, for any short but finite Δt we obtain the interesting feature that an initial state with low temperature ($T < 1/\beta$) will be kept at low temperature for a time much longer than the relaxation time without measurements due to the Zeno effect, but finally the TLS will be heated up to a temperature higher than the quantum thermodynamical one ($T > 1/\beta$).

- The other limit, i.e, the lowest possible temperature can be determined by the condition $\frac{\mathrm{d}}{\mathrm{d}\Delta t}\overline{\rho}_{00}^{\mathrm{attr}}(\Delta t) \stackrel{!}{=} 0$. Calculation the derivative of (4.88) leads to

$$\begin{aligned}\frac{\mathrm{d}}{\mathrm{d}\Delta t}\overline{\rho}_{00}^{\mathrm{attr}}(\Delta t) &= \frac{2(\mathrm{e}^{\beta\delta}-1)\delta^2\Delta t\sin(\delta\Delta t)(\sin(\delta\Delta t) - \delta\Delta t\cos(\delta\Delta t))}{(\mathrm{e}^{\beta\delta}+1)\left(\delta^2\Delta t^2 + \sin^2(\delta\Delta t)\right)^2} \\ &\stackrel{!}{=} 0\end{aligned} \tag{4.91}$$

This condition is fulfilled, if $\sin(\delta\Delta t) = 0$ or $(\sin(\delta\Delta t) - \delta\Delta t\cos(\delta\Delta t)) = 0$. By checking the change of sign of the derivative, one can see that $\sin(\delta\Delta t) = 0$ determines the maxima whereas the transcendental equation determines the local minimal of $\overline{\rho}_{00}^{\mathrm{attr}}$. Thus, the minimal temperature (maximal $\overline{\rho}_{00}^{\mathrm{attr}}$) is reached for $\Delta t = \frac{n\pi}{\delta}$, $n = 1, 2, 3, ...$ Entering this into (4.88), we find

$$\max\left(\overline{\rho}_{00}^{\mathrm{attr}}(\Delta t)\right) = \frac{\mathrm{e}^{\beta\delta/2}}{\mathrm{e}^{\beta\delta/2} + \mathrm{e}^{-\beta\delta/2}}\,, \tag{4.92}$$

which corresponds to the temperature $T = 1/\beta$. Hence, the lowest possible temperature reachable in the resonant case under the influence of periodic measurements is exactly the temperature, the TLS would get also without any measurements in the quantum thermodynamical setting. However, we emphasize once again that there is still a crucial difference between both situations, since in the case without measurements already a single TLS will be in a quasi-stationary thermal state whereas in the case including measurements, the TLS will always be in $|0\rangle$ or $|1\rangle$ and obtains the temperature $1/\beta$ only in terms of an ensemble average, as mentioned before.

Fig. 4.3 shows an example for the dependency of the attractor state on the time Δt between the measurements in the resonant case.

As already mentioned, fast measurements lead to a heating of the TLS whereas at times $\Delta t = \frac{n\pi}{\delta}$, $n = 1, 2, 3, ...$ the temperature $1/\beta$ is reached. As one can see, this temperature is also approximately approached for sufficiently large values of Δt. However, we have to keep in mind that our calculations are based on the short-time approximation, thus one cannot expect these results to be valid for arbitrary large Δt. For too large Δt (in terms of the relaxation time), there will be a significant change of the TLS state between the measurements, i.e., there won't be quasi-classical trajectories for the TLS any more.[1]

4.5.4. Attractor state for the off-resonant case

As already mentioned in Sect. 2.1, without the resonance condition $\delta = \delta_B$ being fulfilled, there would be almost no dynamics, i.e., no thermalization of the TLS, if the total system is closed. This situation changes drastically, if we disturb the total system by including our periodic measurements: Since the measurements destroy correlations between system and environment, they also

[1] For $\Delta t \to \infty$ we expect, in fact, independent individual measurements, cf. Chap. 7.

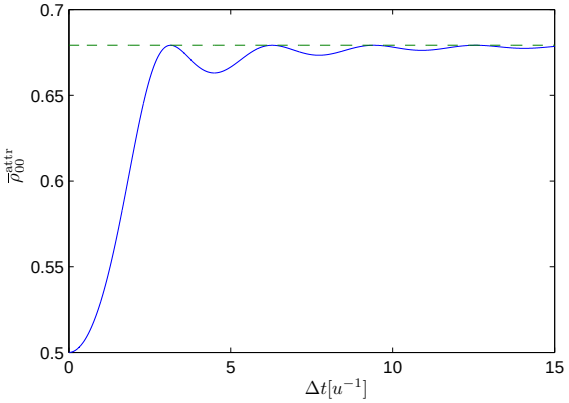

Figure 4.3.: Attractor for the occupation probability of the ground state of system S, depending on the time Δt between the measurements in the resonant case. The dashed line marks the occupation probability of the ground state for a thermal state with temperature $1/\beta$. Used parameters: $\delta = 1\,u$, $\beta = 0.75\,u^{-1}$.

change the interaction energy (for a product state after the measurement this interaction energy is zero). During the evolution after the measurement, the interaction energy is rebuild at the expense of the systems and environmental energy, leading to a change of the state of system and environment. Repeating this mechanism by applying periodic measurements thus allows to change the state of the TLS significantly even in the off-resonant case. As our analytical considerations have shown, there exists also an attractor state in this off-resonant case given by (4.83)

$$\overline{\rho}_{00}^{\mathrm{attr}} = \frac{\mathrm{e}^{\beta\delta_B/2}\frac{\sin^2\left(\frac{\Omega}{2}\Delta t\right)}{\Omega^2} + \mathrm{e}^{-\beta\delta_B/2}\frac{\sin^2\left(\left(\delta+\frac{\Omega}{2}\right)\Delta t\right)}{(2\delta+\Omega)^2}}{2\cosh(\beta\delta_B/2)\left(\frac{\sin^2\left(\frac{\Omega}{2}\Delta t\right)}{\Omega^2} + \frac{\sin^2\left(\left(\delta+\frac{\Omega}{2}\right)\Delta t\right)}{(2\delta+\Omega)^2}\right)}\,. \tag{4.93}$$

The main difference to the resonant attractor state is an additional dependency on the detuning Ω. For given Ω, the maxima with respect to Δt are reached for $\Delta t = n\pi/(\delta + \Omega/2)$, $n = 1, 2, 3, ...$ and given by

$$\max\left(\overline{\rho}_{00}^{\mathrm{attr}}(\Delta t)\right) = \frac{\mathrm{e}^{\beta\delta_B/2}}{\mathrm{e}^{\beta\delta_B/2} + \mathrm{e}^{-\beta\delta_B/2}}\,. \tag{4.94}$$

This result appears to be almost the same as for the resonant case, but the crucial difference is that here we have δ_B instead of δ in the exponents. For

$\delta_B > \delta$ this means that the temperature of the TLS will be smaller than $1/\beta$, namely

$$T_{\min} = \frac{\delta}{\delta_B}\frac{1}{\beta}\,. \tag{4.95}$$

Thus, the off-resonance may be used for cooling the TLS down to very low temperatures by choosing proper values for Δt and Ω. Both parameters should also experimentally be well controllable: Δt by adjusting the frequency of measurements and Ω by applying an appropriate magnetic field to change the splitting of the environmental spins. Thus, this may be a useful method for cooling.

After having identified the lowest possible temperature, we now determine the highest possible temperature in the off-resonant case. In the limit of very fast measurements, we again approach the limit

$$\lim_{\Delta t\to 0} \overline{\rho}_{00}^{\text{attr}} = \frac{1}{2}\,, \tag{4.96}$$

i.e., $T \to \infty$. However, this is actually not the lowest possible occupation probability of the ground state. Indeed, the lowest values of $\overline{\rho}_{00}^{\text{attr}}$ are reached for $\Delta t = 2n\pi/|\Omega|$ and given by

$$\min\left(\overline{\rho}_{00}^{\text{attr}}(\Delta t)\right) = \frac{\mathrm{e}^{-\beta\delta_B/2}}{\mathrm{e}^{\beta\delta_B/2} + \mathrm{e}^{-\beta\delta_B/2}}\,. \tag{4.97}$$

Hence, in the off-resonant case it is also possible to create population inversion, i.e., a state where the temperature of the TLS becomes negative [32]

$$T_{\max} = -\frac{\delta}{\delta_B}\frac{1}{\beta}\,. \tag{4.98}$$

Also this upper bound can be set at will by adjusting the parameters Ω and Δt. Thus, by controlling Ω and Δt we can – at least in principle – prepare the TLS in an any thermal state between $T = +0$ and $T = -0$. Fig. 4.4 shows the dependency of the ground state occupation probability on the parameters Ω and Δt. Note that there exist also some special points at $\Delta t = n\frac{\pi}{\delta}$ and $\Omega = \frac{2m\pi}{\Delta t}$, $n = 0, 1, 2, ..,\ m = 1, 2, ...$ around which a small change of the parameters Δt and Ω causes an extreme change of the attractor state. These are the points, where the state is frozen due to the measurements, since the relaxation constant (4.84) vanishes here and also the off-diagonal elements stay constant (cf. Sect. 4.5.2 and App. E). Thus, relaxation to the attractor state at these points would take infinitely long time.

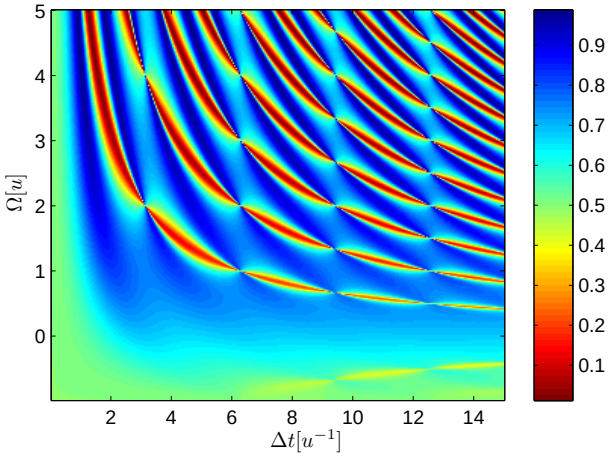

Figure 4.4.: Attractor for the occupation probability of the ground state $\overline{\rho}_{00}^{\mathrm{attr}}$ as a function of the parameters Δt and Ω. States with low temperature are dark blue and such with high (negative) temperatures are red. Used parameters: $\delta = 1\,u$, $\beta = 0.75\,u^{-1}$.

4.5.5. Test of the analytical results

To check our analytical results for the ensemble averages, we compare them with the numerically calculated average over many of the trajectories discussed in Sect. 4.4. As one can see in Fig. 4.5 and Fig. 4.6 for the resonant case as well as in Fig. 4.7 and Fig. 4.8 for the off-resonant case, our analytical results are in accordance with the numerically obtained average. The fluctuations are due to the finite number of calculated trajectories and thus can be further reduced by increasing the number of simulations. This demonstrates that the approximation we used to derive the analytical expressions for the ensemble average, namely replacing the difference $\overline{\rho}_{mn}(j+1) - \overline{\rho}_{mn}(j)$ by the derivative $\frac{\mathrm{d}\overline{\rho}_{mn}(j)}{\mathrm{d}j}$, is well justified under weak coupling.

4.5.6. Long-time average and ergodicity

In the previous sections we have discussed the ensemble average over many trajectories for the TLS. The ergodic hypothesis, which is often assumed in statistical mechanics, states that the average over such a statistical ensemble equals the long-time average over a single trajectory. However, there exist also systems, which are not ergodic. A pertinent example are, e.g., ferromagnetic

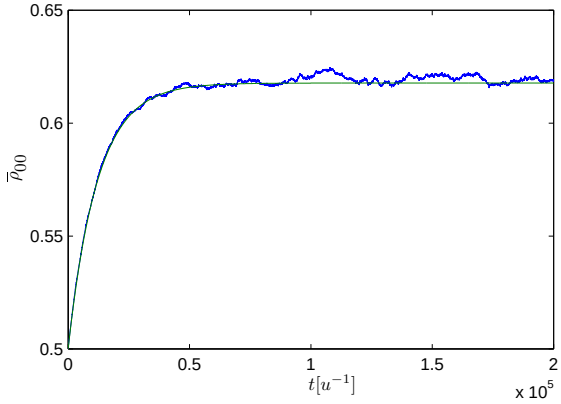

Figure 4.5.: Analytical result for the dynamics of the ensemble average $\overline{\rho}_{00}$ according to (4.82) (green line), compared with an average over $5 \cdot 10^4$ trajectories (blue line) starting with the initial pure state $|\psi\rangle = 1/\sqrt{2}(|1\rangle + |0\rangle)$. Used parameters: $\delta = 1\,u$, $\Delta t = 2\,u^{-1}$, $\beta = 0.75\,u^{-1}$, $\lambda = 4 \cdot 10^{-3}\,u$, $\Omega = 0\,u$.

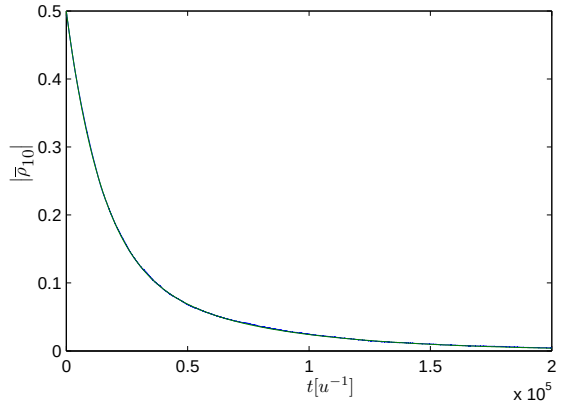

Figure 4.6.: Comparison of the analytical result $|\overline{\rho}_{10}|$ given by (4.74) (green line) with the numerical average over $5 \cdot 10^4$ trajectories (blue line) with the same parameters as in Fig. 4.5. The accordance is already very good in this case: Both curves are almost the same.

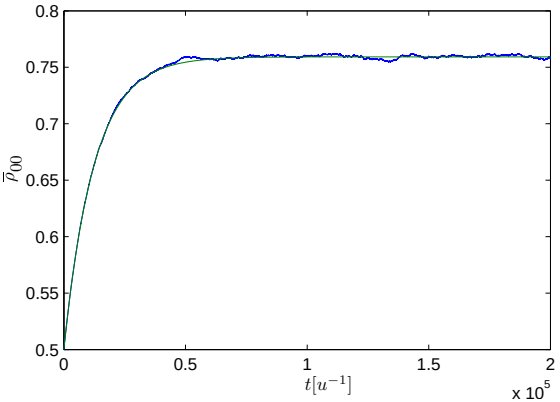

Figure 4.7.: Analytical result for the dynamics of the ensemble average $\overline{\rho}_{00}$ for the off-resonant case according to (4.82) (green line), compared with an average over $5 \cdot 10^4$ trajectories (blue line) starting with the initial pure state $|\psi\rangle = 1/\sqrt{2}(|1\rangle + |0\rangle)$. Used parameters: $\delta = 1\,u$, $\Delta t = 4\,u^{-1}$, $\beta = 0.75\,u^{-1}$, $\lambda = 4 \cdot 10^{-3}\,u$, $\Omega = 0.7\,u$.

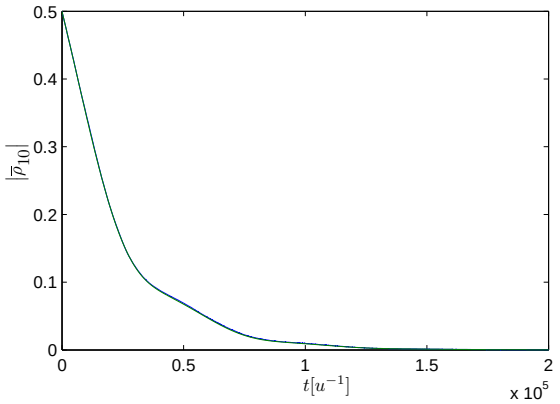

Figure 4.8.: Comparison of the analytical result $|\overline{\rho}_{10}|$ for the off-resonant case given by (4.74) (green line) with the numerical average over $5 \cdot 10^4$ trajectories (blue line) with the same parameters as in Fig. 4.7. The accordance is again very good.

systems which exhibit a spontaneous magnetization below the Curie temperature [51]. Thus, we investigate the long-time average over a single trajectory to test whether the ergodic hypothesis is valid in our model.

We have seen that the TLS passes through some kind of quasi-classical trajectory, jumping between its ground and excited state. If we want to calculate the long-time average for such a trajectory, we have to determine the probabilities of the jumps $|0\rangle \to |1\rangle$ and $|1\rangle \to |0\rangle$. Since such jumps happen only if we measure a different energy band, these probabilities are just given by the probabilities of measuring a different band for $\rho_{00} = 1$ and $\rho_{00} = 0$, respectively. Using (4.61) and (4.62) yields

$$p_{|0\rangle\to|1\rangle} = 4\lambda^2 \left(\mathrm{e}^{-\beta\delta_B/2}\zeta_1 + \mathrm{e}^{\beta\delta_B/2}\zeta_2\right) , \tag{4.99}$$

$$p_{|1\rangle\to|0\rangle} = 4\lambda^2 \left(\mathrm{e}^{\beta\delta_B/2}\zeta_1 + \mathrm{e}^{-\beta\delta_B/2}\zeta_2\right) . \tag{4.100}$$

$$\tag{4.101}$$

The long-time average for the probability of being in the ground state then is given by the probability to jump from the excited state to the ground state divided by the probability for any jump:

$$\begin{aligned} \langle\rho_{00}\rangle_t &= \frac{p_{|1\rangle\to|0\rangle}}{p_{|0\rangle\to|1\rangle} + p_{|1\rangle\to|0\rangle}} \\ &= \frac{\mathrm{e}^{\beta\delta_B/2}\zeta_1 + \mathrm{e}^{-\beta\delta_B/2}\zeta_2}{2\cosh(\beta\delta_B/2)\,(\zeta_1+\zeta_2)} \\ &= \overline{\rho}_{00}^{\mathrm{attr}} . \end{aligned} \tag{4.102}$$

Thus, we get the remarkable result that the long time average exactly equals the ensemble average, i.e., we obtain ergodicity arising from the quantum thermodynamical model under the influence of periodic measurements.

4.6. Entropy and lack of knowledge

4.6.1. Information in thermodynamics

The correspondence between information and thermodynamics has long since been a topic of remarkable interest. The probably most famous character within this discussion is "Maxwell's demon" [36, 43], which originally was introduced by Maxwell to examine the "limitations of the second law of thermodynamics". The main idea behind Maxwell's demon is that a smart being (the demon) could reduce the entropy of a system by using its knowledge about the trajectories of the particles within the system.

A concrete model illustrating this idea is the Szilard's engine, consisting of a box of volume V, which contains a one-particle gas and is connected to a heat bath of temperature T. This box is partitioned into two halves by entering a massless, movable wall. Then, the demon determines the position of the particle and – "using his knowledge" (i.e. feed-back of the measurement result) – connects a load to one side of the wall, such that he can extract work from the system by a quasi-static isothermal expansion. Finally, the gas returns to its initial state. After such a cycle, the work $W = k_B T \ln(2)$ has been extracted, which leads to an entropy reduction of $\Delta S = Q/T = W/T = k_B \ln(2)$. This apparently contradicts to the second law, which states that the total entropy has to increase or at least stays constant for a cyclic process.

However, the process just described is not cyclic, since also the memory of the demon has to be reset to really return to the initial state. Landauer argued that the erasure of 1 bit of information is connected with an increase of the entropy given by $\Delta S_{\text{erasure}} = k_B \ln(2)$ (Landauers principle) [31]. Thus, the entropy decrease due to the work extraction described before is counterbalanced by the entropy increase due to the erasure of the information in the demon's memory and the second law remains valid. This demonstrates that thermodynamical entropy and information are somehow connected. This is further supported by the mathematical resemblance between the information theoretical Shannon entropy and the thermodynamical entropy [34].

Therefore, in statistical mechanics, entropy is often argued to be a measure of the lack of knowledge about the considered system [21]. However, as far as the system is described by classical mechanics, this lack of knowledge can be only subjective, since the exact micro-state in principle is well defined at any time. This is different in the quantum thermodynamical setting. Since a single system can be in a mixed state due to the entanglement with its environment, the lack of knowledge about the system, indeed, is fundamental.

In the following section we discuss how the entropy of the TLS can be associated with the subjective lack of knowledge of the observer of our quantum thermodynamical model, although the subjective lack of knowledge – of course – is not the origin of the thermodynamical entropy.

4.6.2. Measurement logic: Correlations between measurement result and state of the TLS

Previously we have derived the averaged attractor state for the TLS under the influence of the indirect periodic measurements. We have seen that increasing the frequency of measurements leads to an increase of entropy for the TLS. Thinking of measurements as providing information about the system, this is counterintuitive since one may expect that more measurements provide

more information. Indeed, as we will see, the opposite is the case: Fast measurements reduce the ("useful") information gained about the system, which is in accordance with the increase of the entropy in this limit.

Hence, we like to discuss the following question: What do we learn about the state of the TLS by our indirect measurements? Or in other words, how is the measurement result correlated with the state of the TLS? Therefore, we restrict ourselves to times after the transient, i.e., to times where the TLS is already jumping between its ground and excited state. Since measuring the same band does not provide any new information, we repeat the measurements until a change of the energy band is obtained. We then are interested in the correlations between measuring band up or down and the state of the TLS ($|0\rangle$ or $|1\rangle$).

Therefore, we consider the so-called correlation coefficient, which in general is defined as [40]

$$\begin{aligned} \mathrm{Corr}\,(X,Y) &:= \frac{\langle X\cdot Y\rangle - \langle X\rangle\langle Y\rangle}{\sigma_X\sigma_Y} \\ &= \frac{\langle (X-\langle X\rangle)(Y-\langle Y\rangle)\rangle}{\sigma_X\sigma_Y}\,, \end{aligned} \tag{4.103}$$

where $\langle\ldots\rangle$ denotes the expectation value and $\sigma_{X,Y}$ the standard deviation of the random variable X or Y, respectively. $\mathrm{Corr}\,(X,Y)$ is a normalized measure for the linear dependence between the variables X and Y: Possible values of the correlation coefficient lie between -1 and 1. For perfect correlation $\mathrm{Corr}\,(X,Y)=1$ is reached, whereas $\mathrm{Corr}\,(X,Y)=-1$ implies perfect anticorrelation. If X and Y are uncorrelated, the correlation coefficient vanishes ($\mathrm{Corr}\,(X,Y)=0$).

In our case, the two variables are the measurement result (band up or band down) and the state of the TLS after the measurement ($|0\rangle$ or $|1\rangle$). To derive the correlation coefficient, we first have to calculate some conditional probabilities: At first, let us assume the TLS to be in its ground state before the measurement (to distinguish between the state before and after the measurement, we denote them by $|0\rangle_b$ and $|0\rangle_a$). Then, the relative probability to measure band up when measuring a different band following from (4.61) and (4.62) is given by

$$\begin{aligned} \tilde{p}\,(+|\,|0\rangle_b) &= \left.\frac{p_+}{p_+ + p_-}\right|_{\rho_{00}=1} \\ &= \frac{\mathrm{e}^{\beta\delta_B/2}\zeta_2}{\mathrm{e}^{-\beta\delta_B/2}\zeta_1 + \mathrm{e}^{\beta\delta_B/2}\zeta_2}\,. \end{aligned} \tag{4.104}$$

Accordingly, the probability to measure band up when the TLS is in its excited

state reads

$$\begin{aligned}\tilde{p}\left(+\left|\left|1\right\rangle_b\right.\right) &= \left.\frac{p_+}{p_+ + p_-}\right|_{\rho_{00}=0} \\ &= \frac{\mathrm{e}^{\beta\delta_B/2}\zeta_1}{\mathrm{e}^{\beta\delta_B/2}\zeta_1 + \mathrm{e}^{-\beta\delta_B/2}\zeta_2}\,. \end{aligned} \tag{4.105}$$

Thus, if the TLS was in the ground state with probability $p(\left|0\right\rangle_b)$, the relative probability to measure band up can be calculated as

$$\tilde{p}_+ = p(\left|0\right\rangle_b)\tilde{p}\left(+\left|\left|0\right\rangle_b\right.\right) + p(\left|1\right\rangle_b)\tilde{p}\left(+\left|\left|1\right\rangle_b\right.\right)\,. \tag{4.106}$$

Otherwise, the conditional probability for the TLS being in its ground state after measuring band up (i.e., it has been in the excited state before the measurement) reads

$$\tilde{p}\left(\left|0\right\rangle_a\left|+\right.\right) = \frac{p(\left|1\right\rangle_b)\tilde{p}\left(+\left|\left|1\right\rangle_b\right.\right)}{p(\left|0\right\rangle_b)\tilde{p}\left(+\left|\left|0\right\rangle_b\right.\right) + p(\left|1\right\rangle_b)\tilde{p}\left(+\left|\left|1\right\rangle_b\right.\right)}\,. \tag{4.107}$$

Analog considerations for measuring band down lead to the conditional probabilities

$$\begin{aligned}\tilde{p}\left(-\left|\left|0\right\rangle_b\right.\right) &= \left.\frac{p_-}{p_+ + p_-}\right|_{\rho_{00}=1} \\ &= \frac{\mathrm{e}^{-\beta\delta_B/2}\zeta_1}{\mathrm{e}^{-\beta\delta_B/2}\zeta_1 + \mathrm{e}^{\beta\delta_B/2}\zeta_2}\,, \end{aligned} \tag{4.108}$$

$$\begin{aligned}\tilde{p}\left(-\left|\left|1\right\rangle_b\right.\right) &= \left.\frac{p_-}{p_+ + p_-}\right|_{\rho_{00}=0} \\ &= \frac{-\mathrm{e}^{\beta\delta_B/2}\zeta_2}{\mathrm{e}^{\beta\delta_B/2}\zeta_1 + \mathrm{e}^{-\beta\delta_B/2}\zeta_2}\,. \end{aligned} \tag{4.109}$$

Consistently, the relative probability to measure band down for given $p(\left|0\right\rangle_b)$ reads

$$\tilde{p}_- = p(\left|0\right\rangle_b)\tilde{p}\left(-\left|\left|0\right\rangle_b\right.\right) + p(\left|1\right\rangle_b)\tilde{p}\left(-\left|\left|1\right\rangle_b\right.\right) = 1 - \tilde{p}_+\,. \tag{4.110}$$

Finally, the conditional probability for the TLS being in its ground state after measuring band down is given by

$$\tilde{p}\left(\left|0\right\rangle_a\left|-\right.\right) = \frac{p(\left|1\right\rangle_b)\tilde{p}\left(-\left|\left|1\right\rangle_b\right.\right)}{p(\left|0\right\rangle_b)\tilde{p}\left(-\left|\left|0\right\rangle_b\right.\right) + p(\left|1\right\rangle_b)\tilde{p}\left(-\left|\left|1\right\rangle_b\right.\right)}\,. \tag{4.111}$$

This leads us to the joint probability distribution

	$\left\|0\right\rangle_a$	$\left\|1\right\rangle_a$
+	$p(\left\|1\right\rangle_b)\tilde{p}\,(+\left\|\,\right\|1\rangle_b)$	$p(\left\|0\right\rangle_b)\tilde{p}\,(+\left\|\,\right\|0\rangle_b)$
−	$p(\left\|1\right\rangle_b)\tilde{p}\,(-\left\|\,\right\|1\rangle_b)$	$p(\left\|0\right\rangle_b)\tilde{p}\,(-\left\|\,\right\|0\rangle_b)$

Assigning the value $X = 0$ to the ground state $\left|0\right\rangle_a$ and $X = 1$ to the excited state $\left|1\right\rangle_a$ as well as $Y = 1$ to measuring band up and $Y = -1$ to measuring band down, this leads us to the following expectation values:

$$\begin{aligned}
\langle X\rangle &= 0\cdot p(\left|1\right\rangle_b) + 1\cdot p(\left|0\right\rangle_b) = p(\left|0\right\rangle_b)\,, && (4.112)\\
\langle Y\rangle &= \tilde{p}_+ - \tilde{p}_-\,, && (4.113)\\
\langle X\cdot Y\rangle &= 1\cdot 0\cdot p(\left|1\right\rangle_b)\tilde{p}\,(+\left|\,\right|1\rangle_b) + 1\cdot 1\cdot p(\left|0\right\rangle_b)\tilde{p}\,(+\left|\,\right|0\rangle_b)\\
&\quad +(-1)\cdot 0\cdot p(\left|1\right\rangle_b)\tilde{p}\,(-\left|\,\right|1\rangle_b) + (-1)\cdot 1\cdot p(\left|0\right\rangle_b)\tilde{p}\,(-\left|\,\right|0\rangle_b)\\
&= p(\left|0\right\rangle_b)\tilde{p}\,(+\left|\,\right|0\rangle_b) - p(\left|0\right\rangle_b)\tilde{p}\,(-\left|\,\right|0\rangle_b)\,. && (4.114)
\end{aligned}$$

For the standard deviations, we get

$$\begin{aligned}
\sigma_X &= \left[(0-p(\left|0\right\rangle_b))^2\,p(\left|1\right\rangle_b) + (1-p(\left|0\right\rangle_b))^2\,p(\left|0\right\rangle_b)\right]^{1/2}\\
&= \sqrt{p(\left|0\right\rangle_b)p(\left|1\right\rangle_b)}\,, && (4.115)\\
\sigma_Y &= \left[(1-\tilde{p}_+ + \tilde{p}_-)^2\,\tilde{p}_+ + (-1-\tilde{p}_+ + \tilde{p}_-)^2\,\tilde{p}_-\right]^{1/2}\\
&= 2\sqrt{\tilde{p}_+\tilde{p}_-}\,. && (4.116)
\end{aligned}$$

Entering (4.112)–(4.116) into (4.103) leads to the correlation coefficient

$$\mathrm{Corr} = \frac{p(\left|0\right\rangle_b)\,(\tilde{p}_- - \tilde{p}_+ - \tilde{p}\,(-\left|\,\right|0\rangle_b) + \tilde{p}\,(+\left|\,\right|0\rangle_b))}{2\sqrt{p(\left|0\right\rangle_b)p(\left|1\right\rangle_b)}\sqrt{\tilde{p}_+\tilde{p}_-}}\,. \qquad (4.117)$$

Using (4.104)–(4.106) and (4.108)–(4.110) and some further conversions finally yield

$$\begin{aligned}
\mathrm{Corr} &= \mathrm{e}^{\beta\delta_B/2}(p(\left|0\right\rangle_b) - p(\left|0\right\rangle_b)^2)^{1/2}\,\left(\zeta_2^2 - \zeta_1^2\right)\\
&\quad\times\big[\,\left(\mathrm{e}^{\beta\delta_B}p(\left|0\right\rangle_b)\zeta_1^2 + \zeta_1\zeta_2 + \mathrm{e}^{\beta\delta_B}(1-p(\left|0\right\rangle_b))\zeta_2^2\right)\\
&\qquad\times\left((1-p(\left|0\right\rangle_b))\zeta_1^2 + \mathrm{e}^{\beta\delta_B}\zeta_1\zeta_2 + p(\left|0\right\rangle_b)\zeta_2^2\right)\big]^{-1/2}\,. \qquad (4.118)
\end{aligned}$$

Thus, we have derived an expression describing the correlations between measurement result and the state of the TLS, i.e., a measure for the "usefulness" of the indirect measurement to determine the state of the TLS.

To check, how this is related to the attractor state of the TLS discussed in Sect. 4.5, let us consider the interesting limits. We have seen that the lowest temperature of the TLS is reached for $\Delta t = n\pi/(\delta + \Omega/2)$, $n = 1, 2, 3, ...$ (or

rather $\Delta t = n\pi/\delta$ for the resonant case). Since $\zeta_2 = 0$ holds for these Δt, we find for the correlation coefficient

$$\mathrm{Corr}\,(\Delta t = n\pi/(\delta + \Omega/2)) = -1\,, \tag{4.119}$$

i.e., a strict anticorrelation, which means, whenever band up is measured, one knows for sure that the TLS will be in its ground state after the measurement and vice versa. In the limit of the highest (negative) temperature, which only exists in the off-resonant case, the correlation coefficient is given by

$$\mathrm{Corr}\,(\Delta t = 2n\pi/|\Omega|) = 1\,, \tag{4.120}$$

since $\zeta_1 = 0$. This means, for this choice of Δt we get a strict correlation between measurement result and TLS state: Measuring band up here means that the TLS is in its excited state after the measurement and vise versa. This can also be seen by describing the measurements as POVM measurements of the TLS (cf. App. F). Thus, in both limits with minimal entropy of the ensemble averaged TLS state, the measurement logic is optimal, i.e., the measurements are providing full information about the TLS.

Of course, now the question arises, what is happening in the limit of fast measurements ($\Delta t \to 0$). This limit is not so easy to analyze, since both, numerator and denominator of the correlation coefficient (4.118) vanish for $\Delta t \to 0$. Indeed, as a calculation using `Mathematica` shows, one needs to apply l'Hospital's rule four times to be able to calculate the limit. Since these high order derivatives would fill many pages and would not give any physical insight, we skip the calculation here and only present the result: One finds that for $\Delta t \to 0$ the fourth order derivative of the numerator still vanishes whereas for the denominator we get the finite value $\frac{2}{3}\mathrm{e}^{\beta\delta_B/2}\left(1 + \mathrm{e}^{\beta\delta_B}\right)$, which means that

$$\lim_{\Delta t \to 0} \mathrm{Corr}\,(\Delta t) = 0\,. \tag{4.121}$$

Thus, we obtain the remarkable result that for very fast repeated measurements the correlation between measurement result and state of the TLS vanishes, i.e., the indirect measurements no longer give any information about the state of the TLS. This agrees with the obtained attractor state of the TLS in this limit, which is a totally mixed state of maximum entropy (cf. (4.96)).

Hence, in our model there exists, indeed, a connection between the objective entropy of the TLS in ensemble average and the subjective lack of knowledge of the observer due to his indirect measurements: If the environment serves as a perfect measurement device, he obtains the same entropy as in the quantum

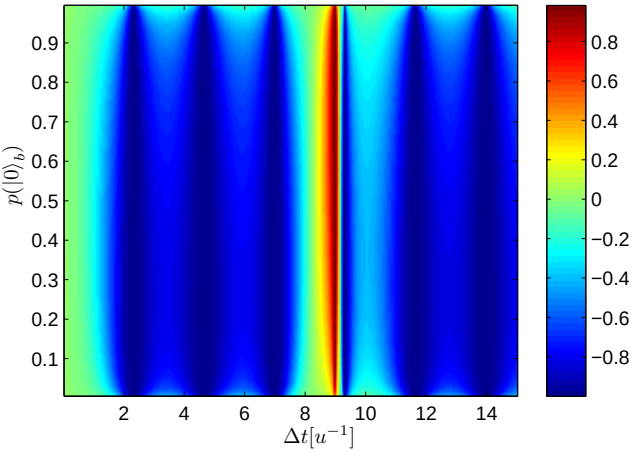

Figure 4.9.: The correlation coefficient (4.103) as a function of the parameters Δt and $p(|0\rangle_b)$. For times $\Delta t = n\pi/(\delta + \Omega/2)$, Corr $= -1$ is reached (dark blue), whereas for $\Delta t = 2n\pi/|\Omega|$ we have perfect correlation Corr $= 1$ (dark red). For fast measurements the correlations vanish Corr $\to 0$ (green). Other parameters: $\delta = 1\,u$, $\beta = 0.75\,u^{-1}$, $\Omega = 0.7\,u$.

thermodynamical model without measurements, whereas imperfect measurements are related to a higher entropy, (and additional perturbations of the system state).

In the limits we have discussed, the correlation coefficient is independent of the probability $p(|0\rangle_b)$, but for all other choices of Δt, it also depends on this parameter. This dependency of the correlation coefficient on $p(|0\rangle_b)$ and Δt is illustrated in Fig. 4.9. Note, however, that $p(|0\rangle_b)$ is not a free parameter in the model with periodic measurements, but is determined by the attractor state (4.102).

5. Measurements on a small spin-environment

In the last chapter we have discussed the influence of periodic measurements applied to an environment consisting of many spins. We studied the dynamics of the density operator of the coupled TLS in ensemble average and analytically derived the relaxation to an attractor state. This final state was found to be independent of the initial one, but dependent on the time Δt between the measurements and the detuning Ω.

In this chapter we will consider a TLS which is coupled to a small environment, which only consists of a few spins. For these small systems it is possible to calculate the dynamics numerically exact, whereas an analytical treatment as for the large environment is no longer possible. However, one may wonder whether the effects of the periodic measurements we obtained for the large environments still occur in this regime. Furthermore, we will test some different measurement procedures as direct projective measurements of the TLS (Sect. 5.3) and "measurements" using a CNOT-gate (Sect. 5.4).

As just mentioned, the system we are studying here, consists of a TLS coupled to a few spins. The coupling between system and environment could in principle be chosen to be again the rather general random interaction introduced in Sect. 2.2.2. However, in this chapter we want to pick a concrete, intuitive interaction within this class, namely a $\sigma_x \otimes \sigma_x$-coupling between the TLS and each of the environmental spins. Since the strength of these $\sigma_x \otimes \sigma_x$-interactions may vary (for example due to different distances between the TLS and the spins), each interaction strength is chosen randomly from a Gaussian distribution. In analogy to the band width introduced in Sect. 2.2.1, we also allow for some small deviations of the energy splittings of the spins, again realized by picking values from a Gaussian distribution.

5.1. Dynamics without external disturbance

The main difference between a small spin-environment and a large one is – besides the obviously much smaller size of the Hilbert space – that the degeneracy structure no longer can be approximated by an exponential increasing

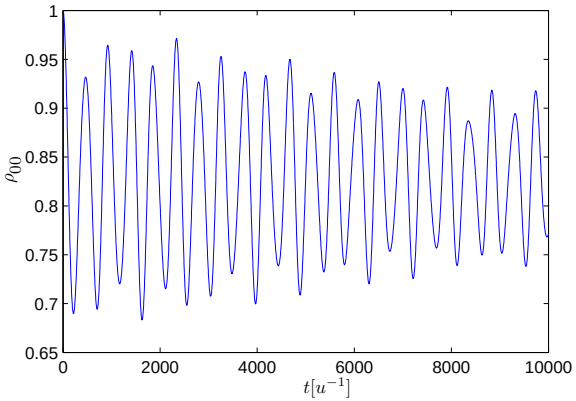

Figure 5.1.: Time evolution of the TLS coupled (interaction strength $\lambda = 0.003\,u$) to a small environment consisting of 7 spins in the resonant case ($\delta = \delta_B = 1\,u$). The environment starts in its third "energy band", which corresponds to two spins up.

one around a certain working point in energy space. Therefore, one cannot expect standard thermalization of the coupled TLS due to its environment. Indeed, if we consider pure Schrödinger dynamics of the total system without external disturbance, the TLS just exhibits some kind of oscillatory behavior as shown in Fig. 5.1, if the splitting of TLS and the environmental spins are approximately the same (resonant case). In the off-resonant case, we have only very small, fast oscillating changes in the occupation probabilities of the TLS (Fig. 5.2), since changing energy is only possible at the expense of the interaction energy, which is very small in the considered weak-coupling regime.

5.2. Dynamics with measurements of the environment

We have seen in the last section that – as expected – the small environments we consider here do not lead to a quasi-stationary state for the coupled TLS. Now we investigate, how this situation changes by including periodic measurements as discussed in Chap. 4 for large environments. Let us again consider the resonant case first. Fig. 5.3 shows the result of a simulation, where the dynamics was disturbed by measurements which were performed with period

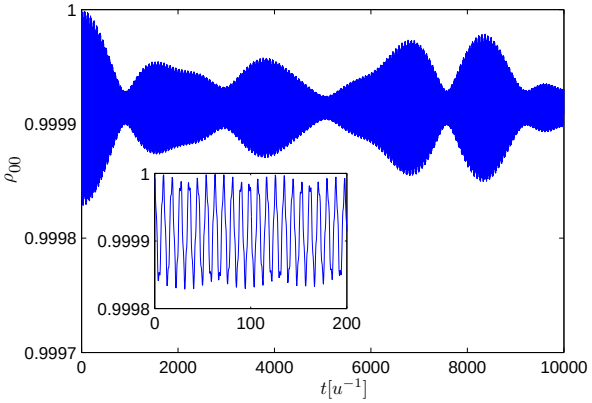

Figure 5.2.: Same as Fig. 5.1 but for the off-resonant case ($\Omega = 0.7\,u$). To display the very fast oscillations (frequency Ω), the inset shows the short interval $0\,u^{-1} \leq t \leq 200\,u^{-1}$.

$\Delta t = 4\,u^{-1}$. As one can see, in ensemble average the TLS, indeed, shows some kind of relaxation to a state with $\overline{\rho}_{00} = 1/2$, i.e. to a state with infinite temperature (the off-diagonal elements remain zero). This relaxation seems to be subdivided into two regimes: A fast initial relaxation to a state with finite temperature followed by a much slower relaxation to the final, totally mixed state.

To understand this behavior let us take a look on the evolution of the occupation probabilities of the environmental energy bands. As shown in Fig. 5.4 in the short first phase of the dynamics the energy increase of the TLS is connected to an energy decrease of the environment: Basically the occupation probability of the energy band ($k = 1$) below the initially occupied one is increasing. Then, in the second phase the occupation drifts towards the center bands. Finally a state is reached, where the occupation probabilities are given by a binomial distribution

$$\overline{p}\,(j) = \binom{n}{j} 2^{-n}\,. \tag{5.1}$$

This evolution is caused by the different probabilities to measure a higher or lower energy, as we will see below. This symmetric final state of the environment also explains the relaxation to a symmetric final state of the TLS with $\overline{\rho}_{00} = 1/2$. Indeed, this is the asymptotic stationary state for the TLS coupled to any spin environment of finite size under the influence of periodic measure-

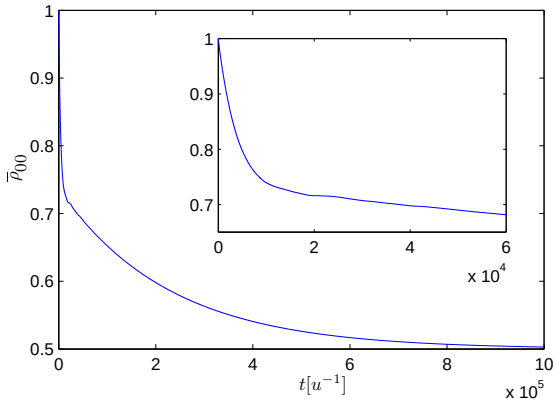

Figure 5.3.: Dynamics of the TLS given by the ensemble averaged $\overline{\rho}_{00}$ under periodic measurements ($\Delta t = 4\,u^{-1}$) of an environment consisting of 7 spins with initially two spins up. The inset shows the fast, initial relaxation (phase 1), followed by the much slower relaxation in phase 2. Other parameters: $\delta = \delta_B = 1\,u$, $\lambda = 0.003\,u$.

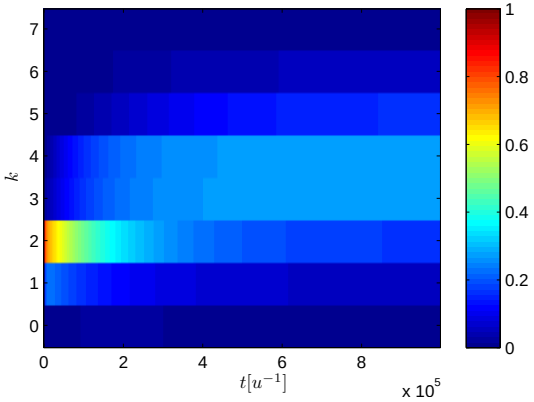

Figure 5.4.: Time evolution of the occupation probabilities p_k of the "energy bands" (in ensemble average) corresponding to the dynamics of the TLS shown in Fig. 5.3.

ments. However, if the number n of environmental spins is large as assumed in the last chapter, the relaxation to this final state will be much slower then the relaxation to the attractor state (4.83), since $\beta(k) \approx \frac{1}{\delta_B} \ln\left(\frac{n}{k} - 1\right)$ (cf. (2.10)) only changes slowly with the band index k.

Thus, we can conclude that the second phase of the dynamics becomes observable due to the small size of the environment whereas the first phase should be associated with the dynamics we have discussed in Chap. 4. One therefore may wonder if we can predict the value for this quasi-attractor state of the first phase (i.e., the value of $\overline{\rho}_{00}$ at the sharp bend in the relaxation curve) using our previous analytical results.

It is clear that we cannot expect that this value is independent of the initial state, since we do not have an exponential degeneracy structure in the environment. Nevertheless, we can apply our results due to the following considerations: Let us assume, the TLS initially is in its ground state. As long as the resonant terms of the interaction dominate the dynamics (the other case will be discussed below), an increase of energy of the TLS is linked to an energy decrease of the environment. Therefore, the dynamics will mainly be determined by the degeneracies of the initially occupied energy band k_0 and the band $k_0 - 1$. Hence, we can formally define an inverse temperature according to these two degeneracies

$$N_{k_0} = \mathcal{N}_- \mathrm{e}^{\beta_- \delta_B k_0}\,, \tag{5.2}$$

$$N_{k_0-1} = \mathcal{N}_- \mathrm{e}^{\beta_- \delta_B (k_0-1)}\,, \tag{5.3}$$

that is,

$$\beta_- = \frac{1}{\delta_B} \ln\left(\frac{N_{k_0}}{N_{k_0-1}}\right)\,. \tag{5.4}$$

According to (4.83) we then expect that the quasi-attractor state will be given by

$$\overline{\rho}_{00}^{(-)} = \frac{\mathrm{e}^{\beta_- \delta_B/2}\zeta_1 + \mathrm{e}^{-\beta_- \delta_B/2}\zeta_2}{2\cosh(\beta_- \delta_B/2)\,(\zeta_1 + \zeta_2)}\,. \tag{5.5}$$

Similarly, we can calculate the quasi-attractor for the TLS being initially in its excited state as

$$\overline{\rho}_{00}^{(+)} = \frac{\mathrm{e}^{\beta_+ \delta_B/2}\zeta_1 + \mathrm{e}^{-\beta_+ \delta_B/2}\zeta_2}{2\cosh(\beta_+ \delta_B/2)\,(\zeta_1 + \zeta_2)}\,, \tag{5.6}$$

with

$$\beta_+ = \frac{1}{\delta_B} \ln\left(\frac{N_{k_0+1}}{N_{k_0}}\right)\,. \tag{5.7}$$

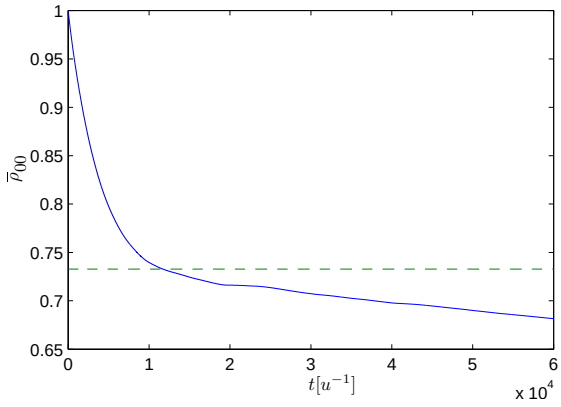

Figure 5.5.: Same as Fig. 5.3 (inset) but together with the corresponding quasi-attractor (dashed line) state according to (5.5). Since the environment starts with two spins up, we have $N_{k_0} = N_3 = 21$ and $N_{k_0-1} = N_2 = 7$ and therefore $\beta_- = \ln(21/7) = \ln(3)$, which leads to $\overline{\rho}_{00}^{(-)} \approx 0.7327$.

Fig. 5.5 and Fig. 5.6 show that both results, indeed, fit nicely with the sharp bends in the relaxation curves.

But what happens, if the initial state of the TLS is neither its ground nor its excited state but an arbitrary thermal state? In this case, both dynamics described above account for the final state – weighted by the initial occupation probabilities of the ground and excited state – which means the quasi-attractor state is approximately given as a linear combination of (5.5) and (5.6)

$$\overline{\rho}_{00}^{\text{attr}} = \rho_{00}(0)\overline{\rho}_{00}^{(-)} + (1 - \rho_{00}(0))\overline{\rho}_{00}^{(+)}\,, \tag{5.8}$$

as shown in Fig. 5.7.

Thus, the results we derived for the large environments allow us in some sense to predict the behavior of the TLS under the influence of periodic measurements even for very small environments down to only a few spins.

However, as we can see in Fig. 5.5 – Fig. 5.7, the final drift towards the totally mixed state is still relatively fast. Hence, it is an interesting question whether the quasi-attractor state could be stabilized, i.e., if we can prevent the relaxation to the state with $T = \infty$. To answer this question, we first have to understand the origin of this drift of the occupation towards higher energy bands in the environment. Therefore, let us consider our analytical results for the large environments: As we have discussed in Sect. 4.5.6 the

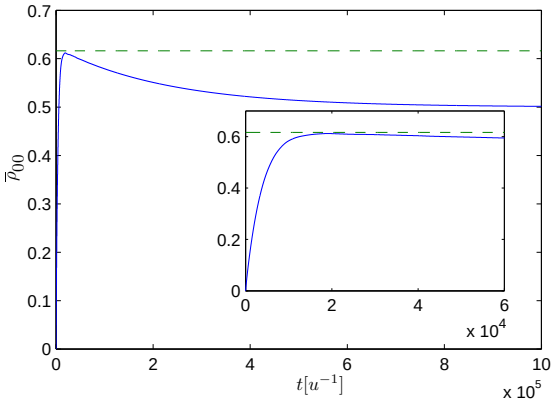

Figure 5.6.: Same as Fig. 5.3 but now with the TLS starting in the excited state. The quasi-attractor state is thus calculated according to (5.6), where $N_{k_0} = N_3 = 21$ and $N_{k_0+1} = N_4 = 35$ and therefore $\beta_+ = \ln(5/3)$ yields $\overline{\rho}_{00}^{(+)} \approx 0.6164$. The inset again shows the initial dynamics. Again we can clearly distinguish the two phases of the dynamics: The TLS first approaches the quasi-attractor state and then slowly relaxes to the final, totally mixed state.

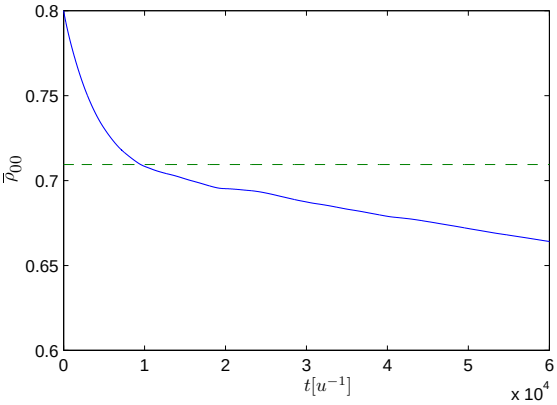

Figure 5.7.: Same as Fig. 5.3 but now the TLS initially is in a thermal state with $\rho_{00}(0) = 0.8$. According to (5.8), we obtain the quasi-attractor state $\overline{\rho}_{00}^{\text{attr}} \approx 0.7094$ (dashed line).

attractor state in ensemble average equals the long time average for the single TLS. That is, the TLS jumps between ground and excited state, being in the ground state with probability (4.102), which equals $\overline{\rho}_{00}^{\mathrm{attr}}$. The probabilities to measure band up or band down, if the TLS is in in its ground state with probability $\overline{\rho}_{00}^{\mathrm{attr}}$ (4.83) (and accordingly in the excited state with probability $\overline{\rho}_{11}^{\mathrm{attr}} = 1 - \overline{\rho}_{00}^{\mathrm{attr}}$) following from (4.61) and (4.62) are then given by

$$\begin{aligned} p_+ &= 4\lambda^2 \mathrm{e}^{\beta\delta_B/2} \left(\overline{\rho}_{11}^{\mathrm{attr}}\zeta_1 + \overline{\rho}_{00}^{\mathrm{attr}}\zeta_2\right) \\ &= 4\lambda^2 \mathrm{e}^{\beta\delta_B/2} \frac{\zeta_1^2 + 2\mathrm{e}^{\beta\delta_B}\zeta_1\zeta_2 + \zeta_2^2}{(1+\mathrm{e}^{\beta\delta_B})(\zeta_1+\zeta_2)}\,, \qquad (5.9) \\ p_- &= 4\lambda^2 \mathrm{e}^{-\beta\delta_B/2} \left(\overline{\rho}_{00}^{\mathrm{attr}}\zeta_1 + \overline{\rho}_{11}^{\mathrm{attr}}\zeta_2\right) \\ &= 4\lambda^2 \mathrm{e}^{-\beta\delta_B/2} \frac{2\zeta_1\zeta_2 + \mathrm{e}^{\beta\delta_B}\left(\zeta_1^2+\zeta_2^2\right)}{(1+\mathrm{e}^{\beta\delta_B})(\zeta_1+\zeta_2)}\,, \qquad (5.10) \end{aligned}$$

which are typically not equal. Indeed, calculating the difference $p_+ - p_-$ we find

$$p_+ - p_- = 16\lambda^2 \sinh(\beta\delta_B/2) \frac{\zeta_1\zeta_2}{\zeta_1+\zeta_2} \geq 0\,, \qquad (5.11)$$

where the equal sign holds if $\zeta_1 = 0$ or $\zeta_2 = 0$. In the resonant case, $\zeta_1 = \Delta t^2/4$ is always positive for finite Δt and $\zeta_2 = 0$ holds for $\Delta t = \frac{n\pi}{\delta}$, $n = 1, 2, 3, ...$, i.e., for the special times where the temperature of the TLS reaches its minimum $T = 1/\beta$ (cf. Sect. 4.5.3). In the off-resonant case, $\zeta_1 = 0$ holds for $\Delta t = 2n\pi/|\Omega|$ and $\zeta_2 = 0$ for $\Delta t = n\pi/(\delta + \Omega/2)$, $n = 1, 2, 3, ...$, for which the maximum (negative) and minimum temperature are reached (cf. Sect. 4.5.4). Thus, if we choose such a special time Δt between the measurements, there exists no drift towards higher bands in the environment, whereas for all other choices we, indeed, have such a drift since $p_+ > p_-$.[1]

Hence, using our analytical approach we are able to derive the drift which we had already observed for the finite environments. Our goal to stabilize the quasi-attractor state of the TLS should therefore be achievable by choosing the appropriate Δt. This, indeed, is the case as shown in Fig. 5.8. The corresponding evolution of the environmental band occupation probabilities is shown in Fig. 5.9. This demonstrates that it is possible to create a stable thermal state (in ensemble average) with finite temperature by coupling the TLS to a small environment under periodic measurements.

[1] At this point, we should mention that this argument only holds as long as $\beta > 0$. If β becomes negative, $\sinh(\beta\delta_B/2)$ becomes negative too, which means that $p_+ \leq p_-$ in this case, which changes the direction of the drift. Therefore, we always get a drift towards the center bands which correspond to $\beta = 0$, as long as we do not choose one of the the special Δt just mentioned.

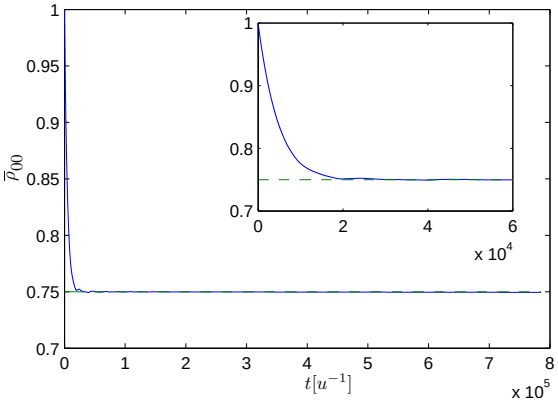

Figure 5.8.: Same as Fig. 5.3, but now with $\Delta t = \pi/\delta$. According to (5.8), we obtain the quasi-attractor state $\overline{\rho}_{00}^{\text{attr}} = 3/4$ (dashed line). As expected from our analytical considerations, this state, indeed, is stabilized and the relaxation to $\overline{\rho}_{00} = 1/2$ is almost completely suppressed.

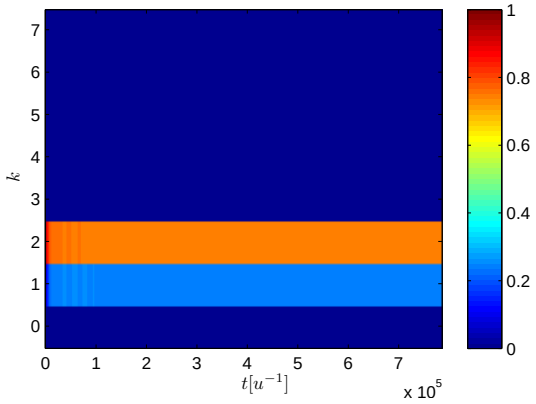

Figure 5.9.: Evolution of the band occupation probabilities p_k corresponding to Fig. 5.8. There exists only a shift from the initial band $k = 2$ to band $k = 1$. Other energy bands are not involved.

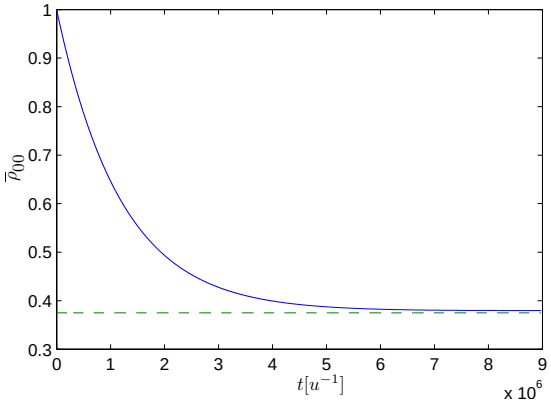

Figure 5.10.: Relaxation of the TLS to a state of negative temperature due to the periodic measurements of its environment (7 spins with initially 2 spins up). The final state is determined by (5.6) with $\beta_+ = \frac{1}{\delta_B} \ln\left(\frac{35}{21}\right)$, which yields $\overline{\rho}_{00}^{\text{attr}} \approx 0.3750$ (dashed green line). Chosen parameters: $\delta = 1\,u$, $\Omega = 0.7\,u$, $\lambda = 0.003\,u$, $\Delta t = 2\pi/\Omega$.

As we have discussed in Sect. 4.5.4, the off-resonant case allows us to create arbitrary thermal states (even with negative temperatures) by choosing appropriate parameters Δt and Ω. Fig. 5.10 shows that this, indeed, is even possible for small environments. Note, that in this regime only the anti-resonant terms of the interaction are responsible for the dynamics. These lead to an excitation or de-excitation in the system and the environment at the same time. Therefore, if the initial state is given by $\rho_{00} = 1$ for the system and occupation of band k_0 for the environment, the band $k_0 + 1$ gets occupied during the dynamics (cf. Fig. 5.11). Thus, the final state is determined by (5.6). Accordingly, the final state would be given by (5.5) for the initial state $\rho_{00} = 0$.

5.3. Dynamics with direct measurements of the TLS

Up to now we always considered the situation, where the energy (or magnetization) of the environment was measured. In this section we will discuss the dynamics of the TLS again coupled to the spin environment but now the energy of the TLS is being measured periodically, which is realized by applying

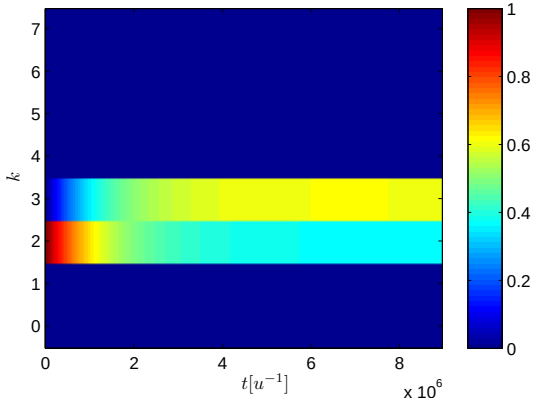

Figure 5.11.: Evolution of the band occupation probabilities p_k corresponding to Fig. 5.10. Due to the off-resonant terms in the interaction, the higher energy band gets occupied even though the TLS starts in its ground state.

the projection operators

$$\hat{P}_{|0\rangle} = |0\rangle\langle 0| \otimes \hat{1}_B \,, \tag{5.12}$$

$$\hat{P}_{|1\rangle} = |1\rangle\langle 1| \otimes \hat{1}_B \,. \tag{5.13}$$

Since such measurements always lead to a projection into ground or excited state, it is for sure that a single trajectory of the TLS will look different from the ones obtained by the indirect measurements, where also states different from $|0\rangle$ and $|1\rangle$ appear during the transient (cf. Fig. 4.1 and Fig. 4.2). Fig. 5.12 shows the trajectory of a TLS under periodic direct measurements. An interesting question now is, whether there exists some kind of relaxation for the ensemble average, similar to the case of indirect measurements. Indeed, as shown in Fig. 5.13 this relaxation occurs. Furthermore, we find that the first phase of the dynamics is almost identical to the case where we measure the environment. The evolution differs only in the second phase, since the measurements of the TLS do not lead to a suppression of the drift of the occupation probabilities in the environment as shown in Fig. 5.14.

Thus, for large environments we can expect that direct and indirect measurements lead to almost the same dynamics of the TLS, since the change of the TLS state due to the drift in the second phase is very slow (β only changes slowly with the band index k).

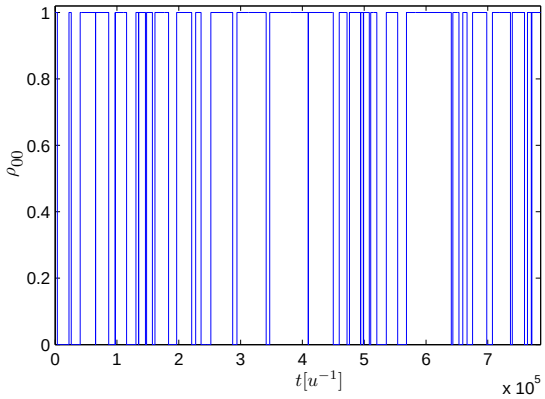

Figure 5.12.: Trajectory of the TLS under direct periodic measurements with $\Delta t = \pi/\delta$. The TLS is coupled to an environment of 7 spins with initially 2 spins up. Other parameters: $\delta = \delta_B = 1\,u$, $\lambda = 0.003\,u$, $\rho_{00}(0) = 0.8$.

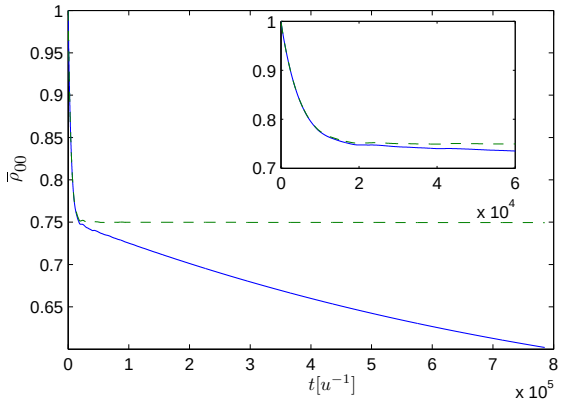

Figure 5.13.: Ensemble average of ρ_{00} for the TLS under direct periodic measurements with $\Delta t = \pi/\delta$ (blue line) compared to the dynamics under the influence of indirect measurements (dashed green line). As shown in the inset, the initial relaxation is almost the same, whereas in the second phase the TLS approaches the totally mixed state in contrast to the case with indirect measurements. The parameters are the same as for the simulation shown in Fig. 5.12 except for the initial state $\rho_{00}(0) = 1$.

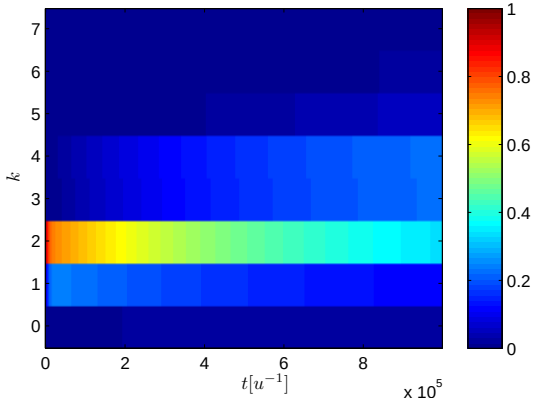

Figure 5.14.: Evolution of the band occupation probabilities p_k corresponding to Fig. 5.13. In contrast to the case of indirect measurements shown in Fig. 5.9, there exists a drift towards the center bands.

For small environments however, indirect measurements have the advantage that states of finite temperature can be stabilized by suppressing the drift of environmental occupation probabilities, which is not possible for direct measurements.

5.4. Explicit measurement model based on a CNOT-gate

So far the measurements performed on the environment or in the last section on the TLS have mathematically been realized by applying projection operators on the state of the system according to the measurement postulate of quantum mechanics. In this section we will discuss a concrete model for the measurement apparatus/detector (cf. Sect. 3.3) to test whether our results still remain valid for measurements with finite duration[2].

The main idea is to realize the detector D by an additional TLS, whose state allows us to draw conclusions about the state of the TLS S. In doing

[2]The considerations in this section were motivated by a paper of N. Erez et al. [12], in which a CNOT gate was used as model for a detector in a closely related model. However, there seems to be a typo in their formula for time-dependent part of the Hamiltonian, which is inconsistent with the Hamiltonian we will derive here. A detailed comparison of both models with respect to the attractor state is presented in Chap. 6.

so, the state of the detector, however, should not influence the state of S (so-called back-action evasion [6, 48]). This can be realized for example by using a "Controlled NOT" gate (CNOT) [23], which has the property that the TLS D flips, if S is in its excited state, whereas its state does not change if S is in the ground state:

$$|1\rangle_D |1\rangle_S \rightarrow |0\rangle_D |1\rangle_S , \tag{5.14}$$
$$|0\rangle_D |1\rangle_S \rightarrow |1\rangle_D |1\rangle_S , \tag{5.15}$$
$$|1\rangle_D |0\rangle_S \rightarrow |1\rangle_D |0\rangle_S , \tag{5.16}$$
$$|0\rangle_D |0\rangle_S \rightarrow |0\rangle_D |0\rangle_S . \tag{5.17}$$

In our chosen representation, the CNOT gate is given by the matrix

$$\hat{U}_{\mathrm{CNOT}} = \begin{pmatrix} 0 & 0 & 1 & 0 \\ 0 & 1 & 0 & 0 \\ 1 & 0 & 0 & 0 \\ 0 & 0 & 0 & 1 \end{pmatrix} , \tag{5.18}$$

such that, e.g.,

$$\hat{U}_{\mathrm{CNOT}} |1\rangle_D |1\rangle_S = \begin{pmatrix} 0 & 0 & 1 & 0 \\ 0 & 1 & 0 & 0 \\ 1 & 0 & 0 & 0 \\ 0 & 0 & 0 & 1 \end{pmatrix} \begin{pmatrix} 1 \\ 0 \\ 0 \\ 0 \end{pmatrix} = \begin{pmatrix} 0 \\ 0 \\ 1 \\ 0 \end{pmatrix} = |0\rangle_D |1\rangle_S , \tag{5.19}$$

and so forth.

Thus, after applying $\hat{U}_{\mathrm{CNOT}}$, the state of S is correlated with the state of D ("pre-measurement"), and therefore could be inferred by determining the detector state. However, since we are only interested in the effect of the measurement on system S, in the following we do not model the measurement of the detector state, but just trace out the detector, which yields us the ensemble averaged state of S after the measurement.

5.4.1. Hamiltonian for the CNOT gate

Since our goal is to study the dynamics of system S coupled to spin-environment B under periodic measurements by detector D, we first have to find a suitable Hamiltonian for the CNOT gate. Thereby, our attempt is not to find the most general form but just a rather simple one. First, it is important to avoid an energy exchange between D and S, because the detector should not influence the system as mentioned above. This can be realized if both states $|0\rangle_D$ and $|1\rangle_D$ have the same energy. Therefore, we simply choose $\hat{H}_D = 0$. To keep

the interaction Hamiltonian as simple as possible, we assume that it is of the form

$$\hat{H}_{DS}(t) = h_{DS}(t)\hat{H}^0_{DS}\,, \tag{5.20}$$

where $h_{DS}(t)$ is a phenomenological function describing the time-dependent coupling of system and detector. Defining

$$\tilde{h}_{DS} := \int_0^\tau h_{DS}(t)\mathrm{d}t\,, \tag{5.21}$$

with τ being the duration of the interaction between D and S, we can rewrite $h_{DS}(t)$ as

$$h_{DS}(t) = \tilde{h}_{DS}\frac{f(t)}{\int_0^\tau f(t')\mathrm{d}t'}\,. \tag{5.22}$$

Here, $f(t)$ is an arbitrary, phenomenological function. The next step is now to determine $\tilde{h}_{DS}$ and $\hat{H}^0_{DS}$ such that the corresponding time evolution operator equals $\hat{U}_{\mathrm{CNOT}}$:

$$\hat{U}_{DS} = \mathrm{e}^{-\mathrm{i}\int_0^\tau \hat{H}_{DS}(t)\mathrm{d}t} \stackrel{!}{=} \hat{U}_{\mathrm{CNOT}}\,. \tag{5.23}$$

The Taylor expansion of the time evolution operator reads

$$\hat{U}_{DS} = \hat{1} + \sum_{m=1}^{\infty}\frac{(-\mathrm{i}\tilde{h}_{DS})^m}{m!}\left(\hat{H}^0_{DS}\right)^m\,. \tag{5.24}$$

With the ansatz $\left(\hat{H}^0_{DS}\right)^2 = \chi\hat{H}^0_{DS}$ we get $\left(\hat{H}^0_{DS}\right)^m = \chi^{m-1}\hat{H}^0_{DS}$ and therefore

$$\begin{aligned}\hat{U}_{DS} &= \hat{1} + \frac{\hat{H}^0_{DS}}{\chi}\sum_{m=1}^{\infty}\frac{(-\mathrm{i}\tilde{h}_{DS}\chi)^m}{m!}\\ &= \hat{1} + \frac{1}{\chi}\left(\mathrm{e}^{-\mathrm{i}\tilde{h}_{DS}\chi} - 1\right)\hat{H}^0_{DS}\,.\end{aligned} \tag{5.25}$$

Since, the matrix representation of $\hat{U}_{\mathrm{CNOT}}$ only contains real entries, we can for simplicity demand that χ, $\tilde{h}_{DS}$ and the entries of $\hat{H}^0_{DS}$ are all real, too. In order to get a real, non-vanishing factor in front of $\hat{H}^0_{DS}$ in (5.25) we then have to fulfill the condition

$$\mathrm{e}^{-\mathrm{i}\tilde{h}_{DS}\chi} \stackrel{!}{=} -1\,, \tag{5.26}$$

which leads to

$$\tilde{h}_{DS} = \pm(2n-1)\frac{\pi}{\chi}, \quad n = 1, 2, 3, \ldots . \tag{5.27}$$

Entering this into (5.25) and using $\hat{U}_{DS} = \hat{U}_{\mathrm{CNOT}}$ leads us to

$$\hat{H}^0_{DS} = \frac{\chi}{2}\left(\hat{1} - \hat{U}_{\mathrm{CNOT}}\right) . \tag{5.28}$$

Thus we finally end up with the following Hamiltonian for the CNOT gate

$$\hat{H}_{DS}(t) = h_{DS}(t)\hat{H}^0_{DS} = \pm\frac{(2n-1)\pi}{2}\frac{f(t)}{\int_0^\tau f(t')\mathrm{d}t'}\begin{pmatrix} 1 & 0 & -1 & 0 \\ 0 & 0 & 0 & 0 \\ -1 & 0 & 1 & 0 \\ 0 & 0 & 0 & 0 \end{pmatrix} . \tag{5.29}$$

As already mentioned, the function as CNOT gate is here guarantied for arbitrary choice of $f(t)$, modeling the time-dependent interaction between D and S. One may think, for example, of a function which is constant for some time τ and zero elsewhere, to consider measurements of finite duration τ (for the projective measurement $f(t)$ would be a δ-peak at the time of the measurement).

5.4.2. Dynamics of the TLS under periodic application of the CNOT-operation

In this section we replace the projective, direct measurements of the TLS discussed in Sect. 5.3 by periodic applications of the CNOT-gate. This allows us to test whether our results are robust against finite duration of the measurements.

In our simulations, we use the Runge Kutta method [42] to find the solution of the time-dependent Heisenberg equation. We consider a TLS S coupled to an environment B, which is even smaller than in the last section, consisting of only two spins. Actually, this is the smallest environment of which we can expect to lead to a quasi-attractor state with finite temperature, since it has only one energy level in the first and third and two levels in the second "energy band" (to use the notion we introduced for large spin environments. Of course there are no "bands" in the usual sense in this limit). Additionally S is coupled to the detector TLS D being initially in $|0\rangle_D$. The coupling between S and D is described by the Hamiltonian (5.29) with $f(t)$ being constant for the duration τ of the "measurement" starting at time t_0 and $f(t) = 0$ elsewhere

$$f(t) = \Theta(t - t_0) \cdot \Theta(\tau - (t - t_0)) , \tag{5.30}$$

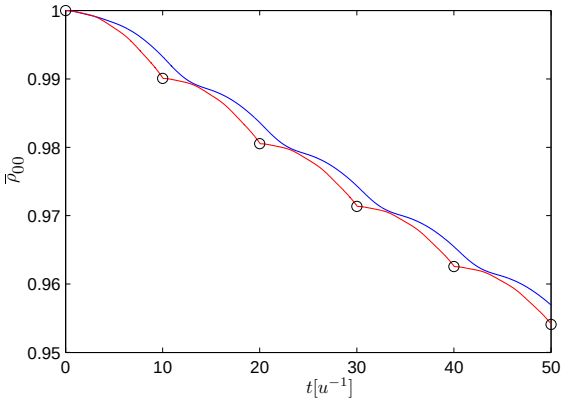

Figure 5.15.: Evolution of $\overline{\rho}_{00}$ of S under periodic "CNOT-measurements" with $\tau = 1/2\Delta t$ (blue) and $\tau = 1/100\Delta t$ (red) compared to the values after projective measurements (black circle). Chosen parameters: $\delta = \delta_B = 1\,u$, $\lambda = 0.01\,u$, $\Delta t = 10\,u^{-1}$.

with the Heaviside step function Θ. This interaction between D and S leads to an entanglement between system and detector. For example the initial state $|\psi_0\rangle = \frac{1}{\sqrt{2}} |1\rangle_D (|1\rangle_S + |0\rangle_S)$ yields

$$\hat{U}_{\mathrm{CNOT}} |\psi_0\rangle = \frac{1}{\sqrt{2}} (|1\rangle_D |0\rangle_S + |0\rangle_D |1\rangle_S) \,. \tag{5.31}$$

A measurement of the detector state then would cause a collapse in one of the states $|1\rangle_D |0\rangle_S$ or $|0\rangle_D |1\rangle_S$. If we consider the ensemble average of the state of S, we just have to trace out the detector. However, if we want to consider repeated measurements, we have to reset the detector after the measurement by preparing it in $|0\rangle_D$ again (Landauer principle).

One may wonder, why this additional spin should affect the dynamics at all, since it does not influence the state of S directly, as mentioned before. Indeed, these measurements affect the dynamics by periodically destroying correlations between system S and its environment B.

Fig. 5.15 shows the dynamics of S coupled to B under this periodic influence of D for different τ compared to the result of projective measurements. As one can see, for $\tau = 1/100\Delta t$ the state after time Δt is almost the same as for a projective measurement, whereas for "measurements" with longer duration we obtain some deviation. Nevertheless, this deviation seems to stay approximately constant with increasing number of measurements. Thus, we

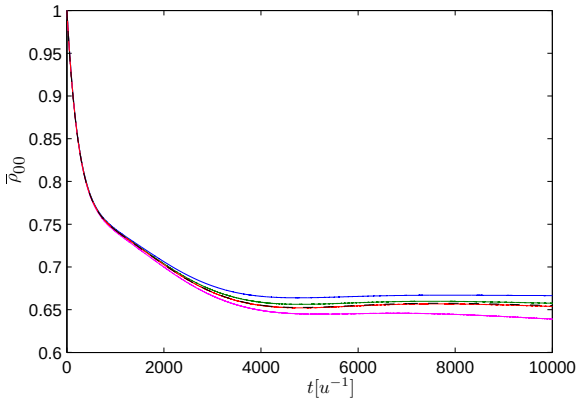

Figure 5.16.: First phase of the evolution of $\overline{\rho}_{00}$ of S under periodic "CNOT-measurements" with $\tau = 1/2\Delta t$ (blue), $\tau = 1/3\Delta t$ (green), $\tau = 1/6\Delta t$ (magenta) and $\tau = 1/100\Delta t$ (red) compared to the values after projective measurements (dashed black): In this phase all curves are approximately identical. Chosen parameters are the same as in Fig. 5.15.

can expect that the main dynamics on larger timescales will be approximately the same. Indeed, this is the case for the first phase of the dynamics (cf. Sect. 5.2) as shown in Fig. 5.16: The relaxation to the quasi-attractor state, which is given by $\overline{\rho}_{00}^{\text{attr}} \approx 0.6657$ according to (5.5), is almost the same for projective measurements and "measurements" with finite duration using the CNOT-gate. In contrast, the relaxation to the totally mixed state in phase two depends on the duration of the measurement and is suppressed for large τ as shown in Fig. 5.17.

Thus, we can conclude that the results we derived analytically for the projective measurements and large environments are rather robust, since they remain applicable even down to very small environments consisting of only two spins and are appropriate also to measurements with finite duration: The dynamics in the first phase of the relaxation turns out to be almost independent of the duration of the measurements.

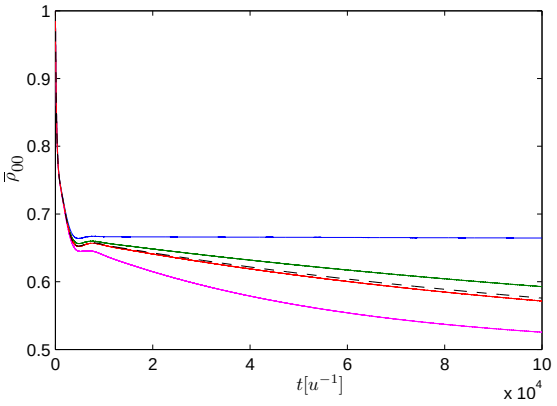

Figure 5.17.: Evolution of $\overline{\rho}_{00}$ shown in Fig. 5.16 for longer times. The relaxation in phase two depends on the duration τ: It can be faster or slower than for projective measurements. For large τ this relaxation is almost suppressed.

6. Comparison with the model of Kurizki et al.

Recently, the group of G. Kurizki has published a series of papers [5, 12, 18, 19], where they considered a qubit coupled to a bath of harmonic oscillators and proposed cooling of this qubit by different methods as highly frequent phase shifts or periodic non-selective QND (quantum non-demolition) measurements of the qubit. Since this model is related to ours, it is worthwhile to compare the results of both models, restricting ourselves to the case of periodic measurements.

For this reason, let us first present a brief summary of their model and their results: The Hamiltonian reads

$$\hat{H}_{\text{tot}} = \hat{H}_S + \hat{H}_B + \hat{H}_{SB}, \tag{6.1}$$

where the Hamiltonians for the spin and the oszillator bath are given by

$$\hat{H}_S = \frac{\delta}{2}\hat{\sigma}_z\,, \quad \hat{H}_B = \sum_m \omega_m \hat{b}_m^\dagger \hat{b}_m\,, \tag{6.2}$$

with $\hat{b}_m$ and $\hat{b}_m^\dagger$ being the annihilation and creation operators of the bath oscillators, respectively. For the spin-boson model the interaction part reads

$$\hat{H}_{SB} = \sum_m \eta_m \left(\left(\hat{b}_m \hat{\sigma}^+ + \hat{b}_m^\dagger \hat{\sigma}^- \right) + \left(\hat{b}_m \hat{\sigma}^- + \hat{b}_m^\dagger \hat{\sigma}^+ \right) \right), \tag{6.3}$$

where η_m denotes the coupling rates. As one can see, this interaction also contains both resonant and anti-resonant terms as in the interaction we consider in our model (cf. Sect. 2.2.2). As we have seen, these anti-resonant terms become important for the dynamics under periodic measurements.

Kurizki et al. then derive a rate equation for the occupation probabilities of the TLS, which describes the dynamics between the measurements j (at $t = 0$) and $j + 1$ (at $t = \Delta t$)

$$\dot{\rho}_{11}(t) = R_0(t)\rho_{00} - R_1(t)\rho_{11}\,, \tag{6.4}$$

with the transition rates

$$R_{1(0)}(t) = 2t \int_{-\infty}^{\infty} G_T(\omega)\mathrm{sinc}\left((\omega \mp \delta)t\right) \mathrm{d}\omega\,, \tag{6.5}$$

where $\mathrm{sinc}(x) := \sin(x)/x$. The temperature-dependent coupling spectrum is given by

$$G_T(\omega) = \left(\eta_T(\omega) + 1\right) G_0(\omega) + \eta_T(-\omega) G_0(-\omega)\,, \tag{6.6}$$

with the zero-temperature coupling spectrum $G_0(\omega)$ and $\eta_T(\omega) = 1/(\mathrm{e}^{\beta\omega} - 1)$.

In [18] they derive an explicit expression for the attractor state under periodic measurements, obtaining

$$\overline{\rho}_{11}^{\mathrm{attr}}(\Delta t) = \frac{\int_0^{\Delta t} R_0(t')\mathrm{d}t'}{\int_0^{\Delta t}(R_0(t') + R_1(t'))\mathrm{d}t'}\,. \tag{6.7}$$

For the spin boson-model this attractor reads

$$\overline{\rho}_{11}^{\mathrm{attr}}(\Delta t) = \frac{\int_{-\infty}^{\infty} G_T(\omega)\mathrm{sinc}^2\left((\omega + \delta)\Delta t/2\right) \mathrm{d}\omega}{\int_{-\infty}^{\infty} G_T(\omega)\left[\mathrm{sinc}^2\left((\omega + \delta)\Delta t/2\right) + \mathrm{sinc}^2\left((\omega - \delta)\Delta t/2\right)\right] \mathrm{d}\omega}\,. \tag{6.8}$$

Note, that the factors 1/2 in the sinc-functions are missing in their paper. But one can easily check that this has to be a typo, since

$$\begin{aligned}
\int_0^{\Delta t} R_{0(1)}(t')\mathrm{d}t' &= \int_0^{\Delta t} 2t' \int_{-\infty}^{\infty} G_T(\omega)\mathrm{sinc}((\omega \mp \delta)t')\mathrm{d}\omega\mathrm{d}t' \\
&= 2\int_0^{\Delta t} \int_{-\infty}^{\infty} G_T(\omega)\frac{\sin((\omega \mp \delta)t')}{\omega \mp \delta}\mathrm{d}\omega\mathrm{d}t' \\
&= 2\int_{-\infty}^{\infty} G_T(\omega)\frac{1 - \cos((\omega \mp \delta)\Delta t)}{(\omega \mp \delta)^2}\mathrm{d}\omega \\
&= 4\int_{-\infty}^{\infty} G_T(\omega)\frac{\sin^2((\omega \mp \delta)\Delta t/2)}{(\omega \mp \delta)^2}\mathrm{d}\omega \\
&= \Delta t^2 \int_{-\infty}^{\infty} G_T(\omega)\mathrm{sinc}^2((\omega \mp \delta)\Delta t/2)\mathrm{d}\omega\,.
\end{aligned} \tag{6.9}$$

Thus, as in our model they obtain an attractor state which depends on the time Δt between the measurements. The concrete value depends on $G_T(\omega)$, i.e., on the temperature and spectrum of the oscillator bath. In their papers Kurizki

et al. consider a Lorentzian coupling spectrum and numerically determine the Δt which minimizes the temperature of the TLS.

In order to compare the results of both models, we choose a different spectrum namely

$$G_0(\omega) = \delta(\omega - \omega_0)\,, \tag{6.10}$$

that is, all oscillators in the environment have the same frequency ω_0. This matches most closely the situation in our model, where all environmental spins have approximately the same splitting δ_B.

With this special choice, we can calculate (6.8) easily: With

$$G_T(\omega) = \left(1/(\mathrm{e}^{\beta\omega} - 1) + 1\right)\delta(\omega - \omega_0) + 1/(\mathrm{e}^{-\beta\omega} - 1)\delta(-\omega - \omega_0) \tag{6.11}$$

we get

$$\begin{aligned}\overline{\rho}_{00}^{\mathrm{attr}}(\Delta t) &= 1 - \frac{\mathrm{e}^{\beta\omega_0}\mathrm{sinc}^2((\omega_0+\delta)\Delta t/2) + \mathrm{sinc}^2((\omega_0-\delta)\Delta t/2)}{(\mathrm{e}^{\beta\omega_0}+1)\left(\mathrm{sinc}^2((\omega_0+\delta)\Delta t/2) + \mathrm{sinc}^2((\omega_0-\delta)\Delta t/2)\right)} \\ &= \frac{\mathrm{e}^{\beta\omega_0/2}\frac{\sin^2\left(\frac{\Omega}{2}\Delta t\right)}{\Omega^2} + \mathrm{e}^{-\beta\omega_0/2}\frac{\sin^2\left(\left(\delta+\frac{\Omega}{2}\right)\Delta t\right)}{(2\delta+\Omega)^2}}{2\cosh(\beta\omega_0/2)\left(\frac{\sin^2\left(\frac{\Omega}{2}\Delta t\right)}{\Omega^2} + \frac{\sin^2\left(\left(\delta+\frac{\Omega}{2}\right)\Delta t\right)}{(2\delta+\Omega)^2}\right)}\end{aligned} \tag{6.12}$$

with $\Omega := \omega_0 - \delta$. Remarkably, this is exactly the same result as obtained in our model (cf. (4.93)), even though we consider two quite different situations: On the one hand a TLS coupled according to the spin-boson model to an environment of harmonic oscillators under the influence of direct, periodic measurements of the TLS and on the other hand a TLS coupled via random interaction to a spin-environment, where the energy of the environment is measured periodically.

This demonstrates that details of the model are not that important for the dynamics we discussed here. The basic prerequisite seems to be the periodic disturbance of the system, be it by measurements of the system itself, its environment or something else, which causes a destruction of the correlations between system and environment. The possibility of cooling the TLS to temperatures beyond $1/\beta$ originates from the different energy splittings of the system and its environment. The obtained attractor state is rather stable, even if there exists more than one energy difference for the environmental transitions, as in the model of Kurizki et al. Indeed, if one chooses, for example, a Lorentzian coupling spectrum as done in their papers

$$G_0(\omega) = \lambda\frac{\omega}{\delta}\frac{\gamma^2}{\gamma^2 + (\omega - \omega_0)^2}\,, \tag{6.13}$$

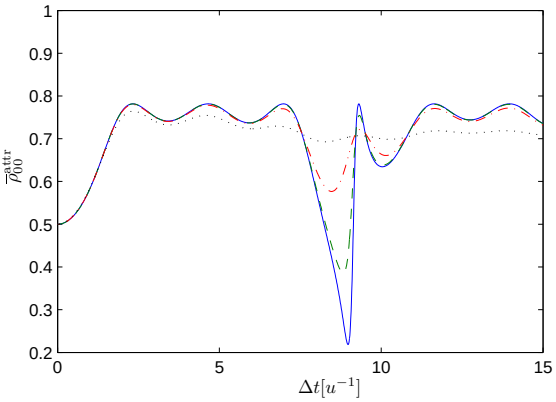

Figure 6.1.: Analytically obtained attractor (6.12) for $G_0(\omega) = \delta(\omega - \omega_0)$ (solid blue) compared to the numerically calculated attractor (6.8) with Lorentzian coupling spectrum for $\gamma = 0.001\,u$ (dashed green), $\gamma = 0.01\,u$ (dash-dotted red) and $\gamma = 0.1\,u$ (dotted black). Other parameters: $\delta = 1\,u$, $\Omega = 0.7\,u$, $\beta = 0.75\,u^{-1}$.

one still obtains an attractor state which is approximately given by (6.12), as long as the width of the distribution, which is specified by γ, stays relatively small, as shown in Fig. 6.1. Only the negative temperature regime seems to be rather sensitive, vanishing relatively fast for increasing γ. This may be the reason, why the possibility of creating negative temperatures was not discussed in the mentioned papers.

Part II.

Temperature estimation: Fluctuations arising from quantum measurements

7. Temperature estimation for modular systems

Fluctuations of extensive and intensive thermodynamic variables [9, 30] as well as of heat and work [28, 38, 45] have long since attracted considerable interest. However, the origin and operational accessibility of such fluctuations remains rather unclear. Especially the concept of temperature fluctuations has caused long-standing controversies [29, 35] that have not been resolved satisfactorily to this day [50].

In this second part of the thesis we try to shed new light on this problem. Based on statistical mechanics, there exist different, rather formal approaches to this topic [11, 30], which lead to the well-known relation for temperature fluctuations

$$\Delta T^2 = \frac{k_B T^2}{\mathfrak{C}}\,, \tag{7.1}$$

with $\mathfrak{C}$ being the heat capacity of the respective system and k_B the Boltzmann constant.

From the point of view of quantum thermodynamics [15] such fluctuations proper cannot exist for an individual system appropriately embedded in a large environment, since the environment enforces a quasi-stationary state on the system as we have discussed in Sect. 2.1, which means that system properties such as energy and temperature will remain constant.[1]

Thus, the question arises, if and in which sense one can talk about fluctuations or even derive the formula (7.1) in a quantum thermodynamical setting (after equilibrium has been reached).

Our approach to this problem will again be based on including a measurement scenario into the quantum thermodynamical system. In this case, however, we need independent individual measurements, i.e., the time between the measurements has to be long enough to allow for thermalization of the measured system: Strict periodicity is irrelevant (in contrast to the small

[1] Note, that the fluctuations of the occupation probabilities shown in Fig. 2.1 are due to the relatively small size of the environment used in the simulation and cannot be associated with the fluctuations (7.1), which depend on the heat capacity of the system.

Δt-regime, which we discussed up to now). The time series of individual measurement results will allow us to give fluctuations (in time) a well-defined, i.e., operational meaning.

7.1. Repeated temperature estimations: Average and fluctuations

Temperature is not an observable, that is, it cannot be measured directly but only indirectly by measuring an observable which depends on temperature. All thermometers are based on this idea, e.g., a mercury thermometer for which temperature is determined through the volume of the mercury fluid.

Here, our aim is to determine the temperature of a quantum system coupled to a thermalizing environment by measuring its energy. Therefore, we assume the mean energy to be a bijective function of temperature

$$\langle E \rangle = f(T)\,, \tag{7.2}$$

that is, we can write[2]

$$T = f^{-1}(\langle E \rangle)\,. \tag{7.3}$$

Thus, according to (7.3) one may identify the temperature by determining the average energy of the system. However, this average energy can only be obtained by carrying out (in principle infinitely) many measurements. Hence, the question arises, how to get an estimate for the temperature after a single energy measurement. Since the best guess for a random variable is its average [49], an obvious estimate for the temperature in case of having measured energy E_m is

$$T_{\mathrm{est}} = f^{-1}(E_m)\,. \tag{7.4}$$

At this point it is already clear, that the so-defined temperature estimate T_{est} will fluctuate, since a quantum measurement of energy will cause the system to collapse into one of the energy eigenstates E_m, implying different values T_{est}. Thus, fluctuations of the measured energy and the estimated temperature are directly correlated. In the following, we will calculate the expectation value and the fluctuations of this estimated temperature under quite general conditions.

[2] Note that there must not necessarily exist an explicit expression for this inverse function.

To do so, the first step is to make an approximation for the occupation probabilities $\mathfrak{p}(E)$. In general, the thermalizing environment leads to a Boltzmann distribution

$$\mathfrak{p}(E) = g(E)\mathrm{e}^{-E/T}\,, \tag{7.5}$$

where $g(E)$ denotes the degeneracy (k_B is set to unity). To keep our model as general as possible, our only assumption concerning the system is that it is modular, i.e., composed of n identical parts. This is no strong restriction, since such a modular structure is typical in nature as discussed in [15]: For example, almost any macroscopic system can be split up into small parts with identical properties, especially all parts having the same spectrum.

This allows us to apply the so-called central limit theorem [7], which states that a random variable, which is a sum of n identically distributed random variables, is in good approximation normally distributed if n is sufficiently large.

For a modular system the energy of the total system is given by the sum of the energies of its identical subsystems. Thus, the distribution of occupation probabilities for the total system can be approximated by a Gaussian distribution, if the number of subsystems is large enough:

$$\mathfrak{p}(E) \approx \frac{1}{\sqrt{2\pi}\sigma}\mathrm{e}^{-\frac{1}{2}\left(\frac{E-\langle E\rangle}{\sigma}\right)^2}\,. \tag{7.6}$$

With this, the expectation value for the temperature estimate is given by

$$\langle T_{\mathrm{est}}\rangle = \int_{-\infty}^{\infty}\mathfrak{p}(E)T_{\mathrm{est}}(E)\mathrm{d}E\,. \tag{7.7}$$

In general, $T_{\mathrm{est}}(E)$ may be a complicated function which means that this integral typically cannot be solved analytically. However, since the normal distribution (7.6) is peaked at $\langle E\rangle$, we can perform a Taylor expansion of $T_{\mathrm{est}}(E) = f^{-1}(E)$ around this point in energy space. Therefore, we use the fact that the derivative of the inverse function can be expressed as

$$\frac{\mathrm{d}}{\mathrm{d}E}f^{-1}(E) = \frac{1}{f'(f^{-1}(E))}\,, \tag{7.8}$$

and that $f^{-1}(\langle E\rangle) = T$ according to (7.3). This leads to the expansion up to

fourth order

$$\begin{aligned} T_{\text{est}}(E) &= T + \frac{1}{f'(T)}(E - \langle E\rangle) - \frac{f''(T)}{2(f'(T))^3}(E - \langle E\rangle)^2 \\ &\quad + \frac{3(f''(T))^2 - f'(T)f'''(T)}{6(f'(T))^5}(E - \langle E\rangle)^3 \\ &\quad + \frac{-15(f''(T))^3 + 10f'(T)f''(T)f'''(T) - (f'(T))^2 f^{(4)}(T)}{24(f'(T))^7} \\ &\quad \times (E - \langle E\rangle)^4 + \mathcal{O}\left((E - \langle E\rangle)^5\right) . \end{aligned} \tag{7.9}$$

Plugging this into (7.7) leads to integrals of the form

$$I_a = \frac{1}{\sqrt{2\pi}\sigma} \int_{-\infty}^{\infty} (x - \mu)^a \mathrm{e}^{-\frac{1}{2}\left(\frac{x-\mu}{\sigma}\right)^2} \mathrm{d}x \,. \tag{7.10}$$

Using

$$\int_0^{\infty} x^a \mathrm{e}^{-bx^2} \mathrm{d}x = \frac{\Gamma\left(\frac{a+1}{2}\right)}{2b^{\frac{a+1}{2}}} \tag{7.11}$$

(cf. [7]) we get the analytical solutions

$$I_a = \frac{1}{\sqrt{\pi}} 2^{\frac{a}{2}-1} \left(1 + (-1)^a\right) \sigma^a \Gamma\left(\frac{a+1}{2}\right) , \tag{7.12}$$

which are zero for odd a. For even a we can use

$$\Gamma\left(n + \frac{1}{2}\right) = \frac{(2n)!\sqrt{\pi}}{n! 2^{2n}} , \quad n = 0, 1, 2, \ldots , \tag{7.13}$$

to get the non-vanishing integrals in our expansion, which read

$$I_0 = 1 , \quad I_2 = \sigma^2 , \quad I_4 = 3\sigma^4 . \tag{7.14}$$

σ can be expressed by the heat capacity $\mathfrak{C} = \frac{\mathrm{d}\langle E\rangle}{\mathrm{d}T} = f'(T)$, using a standard method of statistical mechanics: Rewriting the average energy and the average of E^2 by means of the partition sum

$$\langle E\rangle = \frac{-\frac{\mathrm{d}Z}{\mathrm{d}\beta}}{Z} = T^2 \frac{\frac{\mathrm{d}Z}{\mathrm{d}T}}{Z} , \tag{7.15}$$

$$\langle E^2\rangle = \frac{\frac{\mathrm{d}^2 Z}{\mathrm{d}\beta^2}}{Z} = T^2 \frac{2T\frac{\mathrm{d}Z}{\mathrm{d}T} + T^2 \frac{\mathrm{d}^2 Z}{\mathrm{d}T^2}}{Z} \tag{7.16}$$

$$\tag{7.17}$$

we have

$$\sigma^2 = \langle E^2\rangle - \langle E\rangle^2 = T^2\frac{2TZ\frac{\mathrm{d}Z}{\mathrm{d}T} + T^2 Z\frac{\mathrm{d}^2Z}{\mathrm{d}T^2} - T^2(\frac{\mathrm{d}Z}{\mathrm{d}T})^2}{Z^2}\,. \tag{7.18}$$

On the other hand, the heat capacity is given by

$$\mathfrak{C} = \frac{\mathrm{d}\langle E\rangle}{\mathrm{d}T} = \frac{2TZ\frac{\mathrm{d}Z}{\mathrm{d}T} + T^2 Z\frac{\mathrm{d}^2Z}{\mathrm{d}T^2} - T^2(\frac{\mathrm{d}Z}{\mathrm{d}T})^2}{Z^2}\,. \tag{7.19}$$

Thus, we get

$$\sigma^2 = T^2\mathfrak{C}(T)\,. \tag{7.20}$$

Together with (7.9) and (7.14), this leads to the expectation value for the temperature estimate

$$\begin{aligned}\langle T_{\mathrm{est}}\rangle &= T - T^2\frac{\mathfrak{C}'(T)}{2(\mathfrak{C}(T))^2}\\ &\quad -T^4\frac{15(\mathfrak{C}'(T))^3 - 10\mathfrak{C}(T)\mathfrak{C}'(T)\mathfrak{C}''(T) + (\mathfrak{C}(T))^2\mathfrak{C}'''(T)}{8(\mathfrak{C}(T))^5}\\ &\quad +\ldots\,.\end{aligned} \tag{7.21}$$

As one can see, the expectation value of T_{est} would equal the true temperature T in case of a constant heat capacity. Otherwise, there will be deviations which increase with decreasing subsystem number n since $\mathfrak{C}$ is extensive (i.e., the first correction term is of the order $1/n$, the second one of the order $1/n^2$, and so forth). The higher order terms typically become more important for higher temperatures, because of the factors T^2, T^4,... . However, this is no systematic expansion in T since also the heat capacity $\mathfrak{C}$ depends on the temperature.

Our next step is to determine the fluctuations of the estimated temperature characterized by $\Delta T^2_{\mathrm{est}} = \langle T^2_{\mathrm{est}}\rangle - \langle T_{\mathrm{est}}\rangle^2$. $\langle T^2_{\mathrm{est}}\rangle$ can be calculated in the same way as done for $\langle T_{\mathrm{est}}\rangle$: First we have to calculate the expansion for T^2_{est}, which yields

$$\begin{aligned}T^2_{\mathrm{est}}(E) &= T^2 + \frac{2T}{f'(T)}(E-\langle E\rangle) + \frac{f'(T) - Tf''(T)}{(f'(T))^3}(E-\langle E\rangle)^2\\ &\quad +\frac{-3f'(T)f''(T) + 3T(f''(T))^2 - Tf'(T)f'''(T)}{3(f'(T))^5}(E-\langle E\rangle)^3\\ &\quad +\Big(15f'(T)(f''(T))^2 - 15T(f''(T))^3 - 4(f'(T))^2 f'''(T)\\ &\quad +10Tf'(T)f''(T)f'''(T) - T(f'(T))^2 f^{(4)}(T)\Big)\\ &\quad \times\frac{1}{12(f'(T))^7}(E-\langle E\rangle)^4 + \mathcal{O}\left((E-\langle E\rangle)^5\right)\,.\end{aligned} \tag{7.22}$$

With this, we can calculate the average

$$\langle T_{\mathrm{est}}^2 \rangle = \int_{-\infty}^{\infty} \mathfrak{p}(E) T_{\mathrm{est}}^2(E) \mathrm{d}E \,, \tag{7.23}$$

again using (7.12). We obtain

$$\begin{aligned} \langle T_{\mathrm{est}}^2 \rangle \;=\; & T^2 + \frac{T^2 f'(T) - T^3 f''(T)}{(f'(T))^2} \\ & - \Big(15T^5 (f''(T))^3 - 5T^4 f'(T) f''(T)(3f''(T) + 2T f'''(T)) \\ & - T^4 (f'(T))^2 (4f'''(T) + T f^{(4)}(T)) \Big) \frac{1}{4(f'(T))^5} \\ & + \dots \,. \end{aligned} \tag{7.24}$$

Replacing $f'(T) = \mathfrak{C}(T)$ as well as the higher order derivatives and using (7.21) finally leads us to the fluctuations of the temperature estimate

$$\Delta T_{\mathrm{est}}^2 = \frac{T^2}{\mathfrak{C}(T)} + T^4 \left(\frac{7(\mathfrak{C}'(T))^2}{2(\mathfrak{C}(T))^4} - \frac{\mathfrak{C}''(T)}{(\mathfrak{C}(T))^3} \right) + \dots \,. \tag{7.25}$$

Remarkably, in lowest order, this is exactly the well-known fluctuation formula (7.1). Moreover, the formula would be exact, if the heat capacity $\mathfrak{C}(T)$ was temperature independent, since all higher order terms contain derivatives of $\mathfrak{C}(T)$. This is for example the case for the classical ideal gas. Also in some classical derivations of the fluctuation formula (7.1), such a constant heat capacity is implicitly assumed [11]. Due to the extensivity of $\mathfrak{C}$, the lowest order of the fluctuations (7.25) is proportional to $1/n$, whereas the next order correction is already proportional to $1/n^2$. Thus, we can expect that (7.1) describes the fluctuations of the temperature estimate for sufficiently large systems. A detailed discussion of the bounds within which (7.1) holds can be found in Sect. 7.1.1.

As we have seen, these fluctuations of the temperature estimate are directly connected to the fluctuations of measured energy. Both fluctuations can be combined to formulate a kind of "thermodynamic uncertainty relation" [16, 33]: Using (7.20) and (7.25) we get

$$\Delta E^2 \Delta T_{\mathrm{est}}^2 = T^4 + \mathcal{O}\left(\frac{1}{n}\right) . \tag{7.26}$$

For given thermal state with temperature T this uncertainty product is fixed. The relation indicates that any increase of fluctuations in energy (e.g. by increasing the size of the thermometer system and thus increasing the heat capacity $\mathfrak{C}$) has to be counterbalanced by a reduction of the fluctuations of the temperature estimate.

7.1.1. Bounds for the validity of the fluctuation formula

As we have seen, the fluctuations of the temperature estimate (7.25) are in lowest order given by the well known formula (7.1). However, if the heat capacity is temperature dependent, there exist higher order terms, which contribute to the fluctuations. Thus, formula (7.1) remains valid only as long as the higher order terms are negligible. This is the case, if the ratio between the 2nd order term and the first order term is very small. Thus, we can get an estimate for the high-temperature bound, beyond which the (7.1) breaks down, by demanding

$$\frac{T_{\max}^4\left(\frac{7(\mathfrak{C}'(T_{\max}))^2}{2(\mathfrak{C}(T_{\max}))^4}-\frac{\mathfrak{C}''(T_{\max})}{(\mathfrak{C}(T_{\max}))^3}\right)}{\frac{T_{\max}^2}{\mathfrak{C}(T_{\max})}}=T_{\max}^2\left(\frac{7(\mathfrak{C}'(T_{\max}))^2}{2(\mathfrak{C}(T_{\max}))^3}-\frac{\mathfrak{C}''(T_{\max})}{(\mathfrak{C}(T_{\max}))^2}\right)\stackrel{!}{=}\varepsilon\,, \tag{7.27}$$

with some $\varepsilon \ll 1$ determining the tolerated deviations from (7.1).

Furthermore, the validity range of (7.1) is not only limited from above but also from below: At low temperatures the occupation probabilities can no longer be described by a normal distribution. This means that in this regime the approximation (7.6) we used to derive (7.25) breaks down for finite systems, which typically also leads to a deviation of the fluctuations from (7.1).

How can we get an estimate for the lower bound? Let us set the energy of the ground state to zero. Then, of course, the exact Boltzmann distribution for the system has non-vanishing values only for $E \geq 0$. Thus, in order to be a good approximation, the normal distribution (7.6) should only have negligibly small occupation probabilities for $E < 0$. To estimate the low-temperature bound beyond which this holds, we demand the expectation value of the distribution to be larger than three times the standard deviation: $\langle E\rangle \geq 3\sigma$. This guarantees that about $99,87\%$ of the occupation probability are at $E > 0$ (cf. App. G). With (7.20) and

$$\langle E\rangle = \int_0^T \mathfrak{C}(T')\mathrm{d}T' \tag{7.28}$$

we can express this condition in terms of the heat capacity, which gives us a criterion for the minimal temperature $T_{\min}$, below which the fluctuation formula (7.1) may break down:

$$3T_{\min}\sqrt{\mathfrak{C}(T_{\min})} = \int_0^{T_{\min}} \mathfrak{C}(T')\mathrm{d}T'\,. \tag{7.29}$$

Both of the bounds (7.27) and (7.29) will be studied in Sect. 7.2 for a concrete example.

7.1.2. Temperature estimation by using more than one measurement

Until now, we always considered temperature estimations based on a single energy measurement. If one wants to improve this estimate (e.g. for small systems, where the fluctuations of T_{est} tend to become large), one has to perform more measurements: It is clear that for modular systems with n parts the probability of obtaining the total energy $E = E^{(1)} + E^{(2)} + ... + E^{(m)}$ after m independent measurements equals the probability for measuring energy E for a system of $m \cdot n$ parts after a single measurement: $\mathfrak{p}^{(n,m)}(E) = \mathfrak{p}^{(m\cdot n,1)}(E)$. This means that calculating the temperature by averaging over several measurements amounts to an effective increase of the system size, thus reducing the fluctuations.

In turn, this demonstrates that the formula (7.1) can be applicable only for temperature estimations based on a single measurement: Whenever an average over more measurements is used, the fluctuations of estimated temperature will also depend on the number of measurements. However, the average over several independent measurements requires that the system has enough time to equilibrate after each measurement, which means that temperature is not determined local in time. In this sense, formula (7.1) can be understood as representing a fundamental limit for the instantaneous determination of temperature.

7.2. Example: The n spin model

In this section we like to illustrate our general considerations of Sect. 7.1 with a concrete example: We consider a modular system consisting of n non-interacting spins with energy splitting δ, i.e., the spectrum of the system is given by

$$E_k = \delta k\,, \quad k = 0, 1, 2, \dots\,. \tag{7.30}$$

This is a model for a paramagnetic salt which is, indeed, used experimentally as thermometer [10].

According to our general theory we first have to determine the average energy $\langle E\rangle = f(T)$, which reads

$$\langle E\rangle = \frac{1}{Z}\sum_{k=0}^{n}\binom{n}{k}\mathrm{e}^{-\delta k/T}\delta k\,. \tag{7.31}$$

The partition sum Z can be rewritten using the binomial theorem

$$(a+b)^n = \sum_{k=0}^{n} \binom{n}{k} a^{n-k} b^k \,, \tag{7.32}$$

obtaining

$$Z = \sum_{k=0}^{n} \binom{n}{k} \mathrm{e}^{-\delta k/T} = \left(1 + \mathrm{e}^{-\delta/T}\right)^n \,. \tag{7.33}$$

With this, we can calculate the average energy using (7.15), which yields

$$\langle E \rangle = \frac{n\delta}{1 + \mathrm{e}^{\delta/T}} \,. \tag{7.34}$$

Thus, when measuring energy E_m, our temperature estimate (7.4) is given by[3]

$$T_{\mathrm{est}}(E_m) = \frac{\delta}{\ln\left(\frac{n\delta}{E_m} - 1\right)} \,. \tag{7.35}$$

The so-defined temperature estimate diverges at $k = n/2$, which would yield an infinite temperature average, even if the probability to measure this state is very small. To get a meaningful average, we have to avoid such a divergence. This can be done by introducing a cutoff energy E_{cut}. For energies $E > E_{\mathrm{cut}}$, the temperature is redefined by $T_{\mathrm{est}}(E) = T_{\mathrm{est}}(E_{\mathrm{cut}})$. Thus, if we choose for example $E_{\mathrm{cut}} = E_{n/2-1}$, the singularity in the temperature estimate is removed. Introducing this cutoff, however, makes sense only, if the calculated average does not depend on the particular choice of the cutoff. This, indeed, is the case for sufficiently low temperatures, where the occupation probabilities for $E > E_{\mathrm{cut}}$ are negligible.

With this definition of the temperature estimate we are now able to study the average and the fluctuations of T_{est} for various system sizes n and temperatures T.

7.2.1. Average temperature estimate

The average of the temperature estimate reads

$$\langle T_{\mathrm{est}} \rangle = \frac{1}{Z} \sum_{k=0}^{n} \binom{n}{k} \mathrm{e}^{-E_k/T} T_{\mathrm{est}}(E_k) \,. \tag{7.36}$$

[3] Remarkably, we have $T_{\mathrm{est}}(E_m) = 1/\beta(E_m)$ (cf. (2.10)). If the system is sufficiently large, this means that – after measuring E_m – it would serve as thermalizing environment to a coupled TLS, leading to a temperature which equals the temperature estimate $T_{\mathrm{est}}(E_m)$.

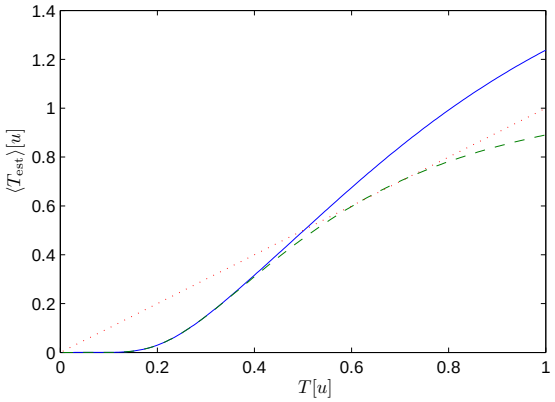

Figure 7.1.: Average of the estimated temperature (7.36) for $n = 10$ spins with $\delta = 1\,u$. The solid blue line corresponds to $E_{\rm cut} = (n/2-1)\delta$ and the dashed green line to $E_{\rm cut} = (n/2-2)\delta$, which leads to very different estimates for $T > 0.3\,u$. The average temperature estimate also strongly deviates from the real temperature T (dotted red line: $\langle T_{\rm est}\rangle = T$), which means this method for estimating temperature does not work for such small systems.

It is clear, that only if $\langle T_{\rm est}\rangle \approx T$ holds, our temperature estimation is useful. This, indeed, is only the case for sufficiently large systems within a certain temperature region: Fig. 7.1 shows the average temperature estimate (7.36) for $n = 10$ for two different choices of the cutoff energy energy $E_{\rm cut}$. As one can see, the average is only independent of the cutoff for very low temperatures, where the estimated temperature varies tremendously from the real temperature. Thus, for such small systems the temperature estimation via a single measurement does not work appropriately. If we turn to larger systems as shown in Fig. 7.2 for $n = 100$, we indeed find a temperature range, where the average temperature estimate is close to the real temperature independent of the choice of the cutoff. This region gets the bigger, the larger the system is chosen as shown in Fig. 7.3 for $n = 1000$.

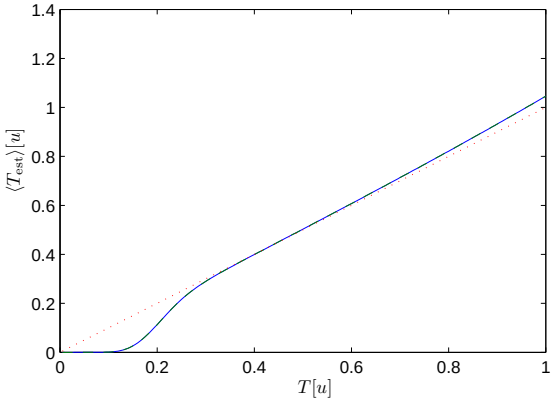

Figure 7.2.: Same as Fig. 7.1, but now for $n = 100$ spins. The average temperature estimate does no longer depend on the choice of the cutoff energy (as long as it is not too small). There exists a temperature range, where $\langle T_{\rm est}\rangle \approx T$ holds.

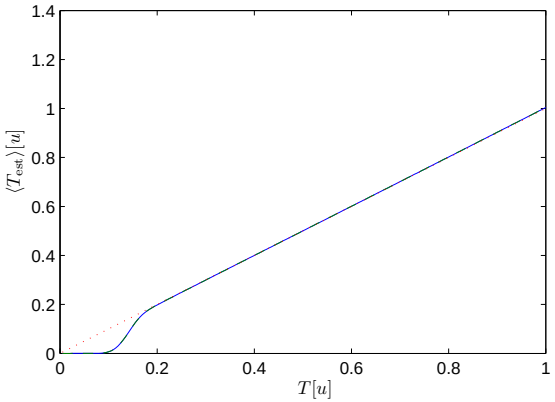

Figure 7.3.: Same as Fig. 7.1, but now for $n = 1000$ spins. Here, $\langle T_{\rm est}\rangle \approx T$ holds already within a quite large temperature range.

7.2.2. Fluctuations of the estimated temperature

Let us now turn to the fluctuations of our temperature estimate, which are given by

$$\begin{aligned}\Delta T_{\mathrm{est}}^2 &= \frac{1}{Z}\sum_{k=0}^{n}\binom{n}{k}\mathrm{e}^{-E_k/T}T_{\mathrm{est}}^2(E_k) \\ &\quad -\left(\frac{1}{Z}\sum_{k=0}^{n}\binom{n}{k}\mathrm{e}^{-E_k/T}T_{\mathrm{est}}(E_k)\right)^2 . \end{aligned} \tag{7.37}$$

As predicted by our general theory in Sect. 7.1, these fluctuations should approximately be given by the fluctuation formula (7.1) within a certain temperature range, if the systems are sufficiently large. Using (7.34), we have

$$\mathfrak{C} = \frac{n\delta^2\mathrm{e}^{\delta/T}}{T^2\left(1+\mathrm{e}^{\delta/T}\right)^2} , \tag{7.38}$$

and formula (7.1) reads ($k_B = 1$)

$$\Delta T^2 = \frac{T^2}{\mathfrak{C}} = \frac{T^4\left(1+\mathrm{e}^{\delta/T}\right)^2}{n\delta^2\mathrm{e}^{\delta/T}} . \tag{7.39}$$

Note that this formula diverges for $T \to 0$. However, this is not a problem, because for too low temperatures the formula does no longer hold, anyway: According to our considerations in Sect. 7.1.1, there exists a lower bound for the temperature $T_{\min}$, under which (7.39) may break down. Entering (7.38) in (7.29) leads to

$$T_{\min} = \frac{\delta}{\ln\left(\frac{n}{9}\right)} . \tag{7.40}$$

Equation (7.27) for the upper bound reads

$$\begin{aligned}\varepsilon &= \frac{1}{2n\delta^2}\mathrm{e}^{-\delta/T_{\max}}\Big(16\left(1+\mathrm{e}^{\delta/T_{\max}}\right)^2 T_{\max}^2 - 16\left(\mathrm{e}^{2\delta/T_{\max}}-1\right)\delta T \\ &\quad + \left(5-6\mathrm{e}^{\delta/T_{\max}}+5\mathrm{e}^{2\delta/T_{\max}}\right)\delta^2\Big) , \end{aligned} \tag{7.41}$$

which cannot be solved analytically. However, if we assume that $T_{\max}$ is large enough such that $\mathrm{e}^{-\delta/T_{\max}} \approx 1 \approx \mathrm{e}^{\delta/T_{\max}}$, (7.41) simplifies to

$$\varepsilon \approx \frac{32T_{\max}^2 + 2\delta^2}{n\delta^2} , \tag{7.42}$$

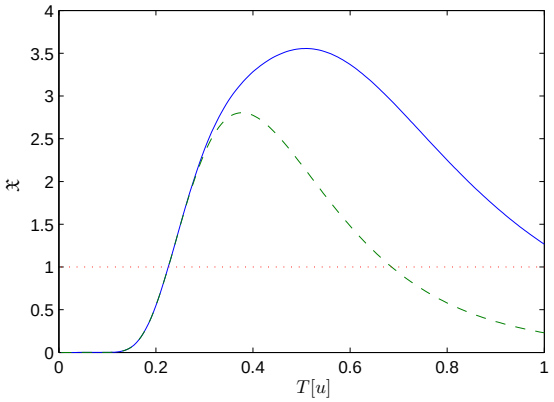

Figure 7.4.: Ratio $\mathfrak{X} = \Delta T_{\text{est}}^2 / \frac{T^2}{\mathfrak{C}}$ for $n = 10$ corresponding to the two average temperature relations as shown in Fig. 7.1: The fluctuations cannot be described by $\Delta T_{\text{est}}^2 = \frac{T^2}{\mathfrak{C}}$ (red dotted line) for such small systems.

which leads to the upper bound

$$T_{\max} \approx \frac{\delta}{4\sqrt{2}} \sqrt{n\varepsilon - 2}\,. \tag{7.43}$$

Thus, for large n the upper bound increases proportional to $\sqrt{n}$.

Fig. 7.4–Fig. 7.6 show the ratio $\mathfrak{X} = \Delta T_{\text{est}}^2 / \frac{T^2}{\mathfrak{C}}$ for different system sizes corresponding to the average temperature estimates shown Fig. 7.1–Fig. 7.3.

As one can see, for small systems, the fluctuations cannot be described by $\Delta T_{\text{est}}^2 = T^2/\mathfrak{C}$, on the one hand because the Gaussian approximation is not justified for such few subsystems and on the other hand because higher order terms become important. For increasing system size, however, there exists a temperature range in which this formula holds. At low temperatures we find strong deviations from (7.1), as expected due to the fact that the Gaussian approximation breaks down here. Indeed, the predicted lower bound $T_{\min}$ according to (7.40) describes quite nicely the end of the strong deviation peak, which shifts as expected towards lower temperatures with increasing n. Also the upper bound – moving to higher temperatures with increasing n – can be estimated by (7.41). For sufficiently large n the solution of (7.41) converges to the value determined by approximation (7.43).

Remarkably, this temperature range in which the fluctuation formula $\Delta T_{\text{est}}^2 = \frac{T^2}{\mathfrak{C}}$ is valid corresponds to the temperature range in which the average tem-

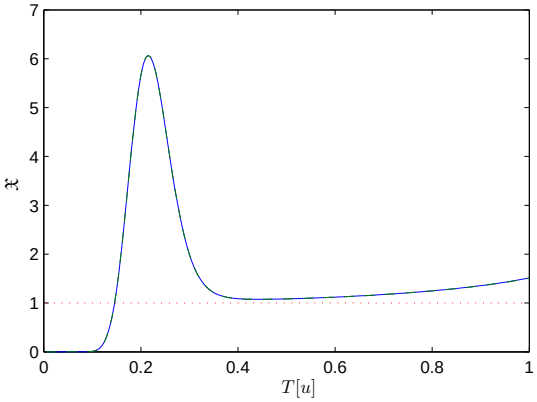

Figure 7.5.: Ratio $\mathfrak{X} = \Delta T_{\mathrm{est}}^2 / \frac{T^2}{\mathfrak{C}}$ for $n = 100$ corresponding to the average temperature shown in Fig. 7.2: After strong deviations at low T caused by the non-Gaussian distribution, there exists a temperature range in which the fluctuations approximately fulfill $\Delta T_{\mathrm{est}}^2 = \frac{T^2}{\mathfrak{C}}$. For higher temperatures, the deviations again increase due to the higher order terms in (7.25). According to (7.40), the lower bound is given by $T_{\mathrm{min}} \approx 0.415\,u$ and the upper bound (7.41) for accuracy $\varepsilon = 0.1$ lies at $T_{\mathrm{max}} \approx 0.670\,u$.

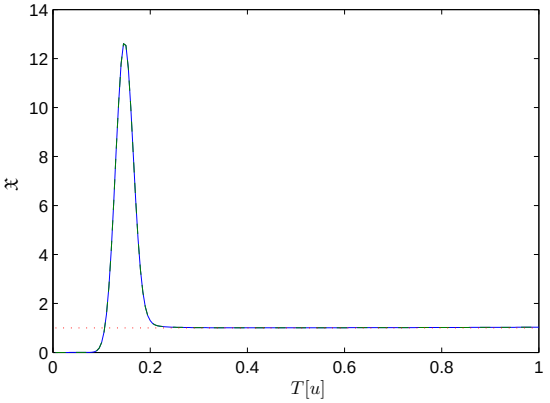

Figure 7.6.: Ratio $\mathfrak{X} = \Delta T_{\text{est}}^2 / \frac{T^2}{\mathfrak{C}}$ for $n = 1000$ corresponding to the average temperature shown in Fig. 7.3: Here, the temperature range in which the fluctuations fulfill $\Delta T_{\text{est}}^2 = \frac{T^2}{\mathfrak{C}}$ is already quite large. According to (7.40), the lower bound is given by $T_{\min} \approx 0.212\,u$ and the upper bound (7.41) for accuracy $\varepsilon = 0.1$ lies at $T_{\max} \approx 1.819\,u$.

perature estimate coincides with the temperature T. Thus, we can conclude that the fluctuation formula is valid whenever our temperature estimation by a single measurement is useful to determine the temperature.

7.2.3. Temperature estimation with several measurements

We have argued in Sect. 7.1.2 that the probability to measure the total energy $E_{\text{tot}} = E^{(1)} + E^{(2)} + ... + E^{(m)}$ after m measurements for a modular system with n subsystems, equals the probability to measure E_{tot} in a single measurement of a modular system of the same kind with $n \cdot m$ subsystems. This can also be shown directly for our example, the n-spin environment.

The probability to measure the total energy E_{tot} after m measurements, is given by

$$\mathfrak{p}^{(n,m)}\left(E_{\text{tot}}\right) = \sum_{E^{(1)}=0}^{E_{\text{tot}}} \sum_{E^{(2)}=0}^{E_{\text{tot}}-E^{(1)}} \cdots \sum_{E^{(m-1)}=0}^{E_{\text{tot}}-\sum_{i=1}^{m-2} E^{(i)}} \mathfrak{p}\left(E^{(1)}\right) \times \mathfrak{p}\left(E^{(2)}\right) \ldots \mathfrak{p}\left(E^{(m-1)}\right) \mathfrak{p}\left(E_{\text{tot}} - \sum_{i=1}^{m-1} E^{(i)}\right) \quad (7.44)$$

with

$$\mathfrak{p}\left(E^{(i)}\right) := \mathfrak{p}^{(n,1)}\left(E^{(i)}\right) = \binom{n}{k_{E^{(i)}}} \frac{\mathrm{e}^{-E^{(i)}/T}}{Z} \,. \tag{7.45}$$

We can also express the probabilities after measurement $m+1$ iteratively by the probabilities after measurement m as

$$\mathfrak{p}^{(n,m+1)}\left(E_{\mathrm{tot}}\right) = \sum_{E'=0}^{E_{\mathrm{tot}}} \mathfrak{p}^{(n,m)}\left(E_{\mathrm{tot}} - E'\right) \mathfrak{p}\left(E'\right) \,, \tag{7.46}$$

which can be shown easily by inserting $\mathfrak{p}^{(n,m)}$ according to (7.44) and renaming the energies $E' \to E^{(1)}$, $E^{(1)} \to E^{(2)}$, ..., $E^{(m-1)} \to E^{(m)}$.

We now show that $\mathfrak{p}^{(n,m)}(E_{\mathrm{tot}})$ given by (7.44), indeed, is identical to $\mathfrak{p}^{(m\cdot n,1)}(E_{\mathrm{tot}})$, that is, the probability to measure E_{tot} after a single measurement in a modular system with $m \cdot n$ subsystems.

Let us start with the probabilities after two measurements. According to (7.46), we get

$$\begin{aligned}
\mathfrak{p}^{(n,2)}\left(E_{\mathrm{tot}}\right) &= \sum_{E'=0}^{E_{\mathrm{tot}}} \mathfrak{p}^{(n,1)}\left(E_{\mathrm{tot}} - E'\right) \mathfrak{p}\left(E'\right) \\
&= \sum_{E'=0}^{E_{\mathrm{tot}}} \frac{1}{Z^2} \binom{n}{k_{E_{\mathrm{tot}}} - k_{E'}} \binom{n}{k_{E'}} \mathrm{e}^{-\left(E_{\mathrm{tot}} - E'\right)/T} \mathrm{e}^{-E'/T} \\
&= \frac{1}{Z^2} \binom{2n}{k_{E_{\mathrm{tot}}}} \mathrm{e}^{-E_{\mathrm{tot}}/T} \,,
\end{aligned} \tag{7.47}$$

where in the last step we used the so-called Vandermonde identity [2]

$$\sum_{j=0}^{k} \binom{m}{j} \binom{n}{k-j} = \binom{m+n}{k} \,. \tag{7.48}$$

In the same way we get

$$\begin{aligned}
\mathfrak{p}^{(n,3)}\left(E_{\mathrm{tot}}\right) &= \sum_{E'=0}^{E_{\mathrm{tot}}} \mathfrak{p}^{(n,2)}\left(E_{\mathrm{tot}} - E'\right) \mathfrak{p}\left(E'\right) \\
&= \frac{1}{Z^3} \binom{3n}{k_{E_{\mathrm{tot}}}} \mathrm{e}^{-E_{\mathrm{tot}}/T} \,,
\end{aligned} \tag{7.49}$$

and so forth. Finally, after m measurements we obtain

$$\mathfrak{p}^{(n,m)}\left(E_{\mathrm{tot}}\right) = \frac{1}{Z^m} \binom{m\cdot n}{k_{E_{\mathrm{tot}}}} \mathrm{e}^{-E_{\mathrm{tot}}/T} = \mathfrak{p}^{(m\cdot n,1)}\left(E_{\mathrm{tot}}\right) \,, \tag{7.50}$$

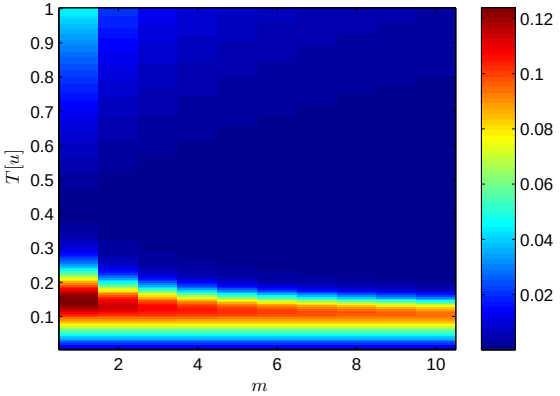

Figure 7.7.: Deviation of the average temperature estimate from the real temperature $|\langle T_{\text{est}} \rangle - T|$ depending on the temperature T and the number of measurements m used for the temperature estimation ($n = 100$).

as expected. Thus, the temperature estimation for a n spin system after m independent measurements, indeed, equals the temperature estimation for a $m \cdot n$ spin system after a single measurement.

Fig. 7.7 shows the error of the average temperature estimate of a system with fixed size of $n = 100$ spins with increasing number of measurements, whereas Fig. 7.8 shows the corresponding fluctuations of the temperature estimate. As one can see, the error of the average temperature estimate and its fluctuations at high temperature reduce very fast with increasing number of measurements, whereas accurate temperature estimation at low temperature would require an average over many measurements.

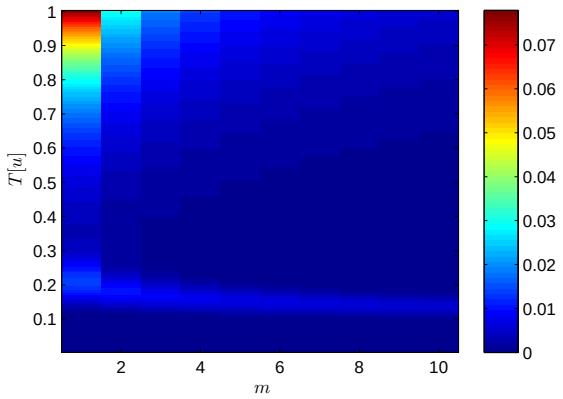

Figure 7.8.: Fluctuations ΔT^2_{est} of the temperature estimate depending on the temperature T and the number of measurements m used for the temperature estimation ($n = 100$).

8. Conclusion

Quantum thermodynamics intends to explain, how thermalization for a quantum systems may emerge from pure Schrödinger dynamics due to the coupling to an environment. This even applies to a single system within its individual environment. However, in the standard theory of quantum thermodynamics no measurements are included so far; the total system consisting of system and environment is assumed to be isolated from the rest of the universe, especially from any external observer. In quantum mechanics observation is not for free but has to be modeled explicitly. In this thesis, we investigated the aspect of external observation by including (ideal, projective) quantum measurements in the quantum thermodynamical models.

In the first part of the thesis, our concrete model consisted of a two-level system (TLS) with splitting δ coupled via random interaction to a spin-environment with splitting δ_B. For this model, we first illustrated the thermalization of the TLS under undisturbed Heisenberg dynamics for the resonant case $\delta = \delta_B$.

Then, we have built in the external observation by including instantaneous periodic measurements of the environmental magnetization/energy (waiting time Δt). The effect of any such measurement is threefold: First, it causes a projection into one of the environment energy bands. Second, it destroys correlations between system and environment, which have been created in the undisturbed dynamics between the measurements. And third, it also directly changes the state of the TLS, an effect known as co-jump. We analyzed the dynamics of the TLS under these periodic measurements analytically using perturbation theory valid for small Δt. It turned out that due to the measurements, a single TLS no longer relaxes to a thermal state but shows some kind of quasi-classical trajectory, always jumping between its ground and excited state. As in statistical mechanics, thermalization and temperature here only have a meaning in terms of an ensemble average or a long-time average. Indeed, by calculating these averages, we were able to show ergodicity for this model, i.e., the ensemble average equals the long-time average.

Interestingly, the temperature of the obtained attractor state depends on the time Δt between the measurements as well as on the detuning of the environment $\Omega \equiv \delta_B - \delta$. For very fast repeated measurements, two at first apparently contradicting results emerge: On the one hand, the relaxation

constant, which determines the velocity of the relaxation, tends to zero. This is well known as the so-called Zeno-effect: Fast measurements suppress the dynamics. On the other hand, however, we find that the temperature for the attractor state becomes infinitely high in this limit. Of course, the limit $\Delta t = 0$ is not reachable. However, for any small but finite Δt this means that the initial state will be approximately conserved for quite a long time due to the Zeno-effect, but finally a state of very high temperature will be reached.

In the resonant case $\Omega = 0$, the lowest possible temperature equals the temperature the system would get due to the coupling to its environment *without* measurements ($T = 1/\beta$). Remarkably, this turns out to be the case for times Δt, for which the environment also serves as a *perfect* measuring device, i.e., the correlations between measurement results and state of the TLS are maximized. In contrast, these correlations vanish for very fast measurements, which means the measurements no longer provide information about the system. In this sense, we can argue that the increase of entropy for the TLS at fast repeated measurements coincides with the additional, subjective lack of knowledge of the observer.

In the off-resonant case $\Omega \neq 0$, we found that the TLS can even be cooled below $T = 1/\beta$ by choosing appropriate values for the detuning and measurement frequency. Furthermore, here it is also possible to prepare states of negative temperatures, i.e., to create inversion or to freeze the initial state just by measuring appropriately frequently.

We have tested our results numerically also for relatively small environments (up to seven spins), for which the numerical calculation of the dynamics under periodic measurements could be done exactly. It turned out that our results in some sense remain applicable even for such small environments: In ensemble average there also exists some kind of attractor state, which however depends on the initial state. Nevertheless, given the initial state, it is possible to predict this attractor using the analytical results obtained for the large environments. We also tested the influence of direct, projective measurements of the TLS and "measurements" with finite duration using a CNOT-gate. We found that the dynamics of the ensemble average is almost identical to the dynamics under measurements of the environment, i.e., does not depend on the concrete realization of the measurement process.

In the second part of the thesis we turn to repeated measurements in the limit of long waiting times Δt: We have discussed the appearance and meaning of "temperature fluctuations" in a quantum thermodynamical setting. According to quantum thermodynamics, an embedded quantum system relaxes to a stationary thermal state. Therefore, fluctuations of temperature cannot exist. However, temperature itself is not an observable, which means it cannot be determined directly. Thus, one has to measure an observable which is

suitable to get an estimate for the temperature. Here, we chose the energy of the system as this observable.

We considered a quite general model, namely the class of modular systems, which are typical in nature. For these, we were able to show that, indeed, the temperature estimate from a single projective measurement will fluctuate from measurement to measurement according to the well known formula $\Delta T^2 = \frac{k_B T^2}{\mathfrak{C}}$ under some conditions: The system has to be sufficiently large and the equilibrium temperature should neither be too low nor too high. For too low temperatures, the occupation probabilities will no longer be Gaussian distributed. This deviation from the Gaussian distribution typically also leads to a deviation of the fluctuations from the above formula. For too high temperatures on the other hand, the higher order correction terms we derived, will become important. To illustrate our general results, we finally considered a concrete modular system consisting of n non-interacting spins.

In conclusion, by studying the influence of quantum measurements in a quantum thermodynamical setting, we have shown how several principles and concepts known from statistical mechanics may arise from this "quantum thermodynamics under observation", although they do not have any meaning in the "unobserved" quantum thermodynamics: In the small Δt-limit quasi-classical trajectories necessitate introducing ensemble and long-time averages. Considering the ensemble of systems, we obtained thermalization and confirmed ergodicity in our model. Furthermore, we discussed two aspects of statistical mechanics, which often lead to confusion or misunderstandings: Firstly, we presented a connection between the objective entropy of the system and the subjective lack of knowledge of the observer. Secondly, we explained how "temperature fluctuations" (for large Δt) can be interpreted as representing a fundamental limit for the instantaneous determination of temperature.

Going beyond the quantum thermodynamical model by introducing some detuning between system and environment, we also demonstrated, how periodic measurements could be used to cool the system or to create inversion. Since both cooling and creating inversion are of particular relevance in modern physics, this may also be an interesting feature for practical applications in the future.

Part III.

Appendices

A. Numerical test of the approximations for the total state after the measurement

In Sect. 4.1 we have applied the following two approximations to simplify the state of the total system after a measurement:

- Approximation 1: We neglect the correlations, which may be present after the incomplete measurement (our measurements are incomplete, since we project on one of the environmental energy bands and not on a single state). That is, we replace the exact state after the measurement $\hat{\rho}_{\mathrm{tot}} = \hat{\tilde{P}}_k \hat{\rho}'_{\mathrm{tot}} \hat{\tilde{P}}_k / \mathrm{Tr}_B \left\{ \hat{P}_k \hat{\rho}'_B \right\}$ by $\mathrm{Tr}_B\{\hat{\rho}_{\mathrm{tot}}\} \otimes \mathrm{Tr}_S\{\hat{\rho}_{\mathrm{tot}}\}$.

- Approximation 2: The second approximation is to replace the exact state of the environment after the measurement of band k by a simple one of the form

$$\hat{\rho}^0_B(k) = \frac{1}{N_k} \sum_{n_k} |n_k\rangle\langle n_k| \; . \tag{A.1}$$

These approximations are the prerequisite to derive the analytical results for the dynamics of the system under periodic measurements. To test their validity, we undertake some numerical simulations for a TLS coupled to a five-band environment on which we periodically apply the projections. Between the projections, the total system evolves under undisturbed Heisenberg dynamics. To imitate the situation which would occur due to periodic measurements, we project many times on the same band before projecting on a different one, since the occupation probability of the band on which was projected at the last measurement will be much larger than for its next neighbor bands.

One may imagine these five bands to be the part of the spectrum of a much larger environment, which is important for the dynamics. We need five bands and not only three as in Sect. 2.3, since we also have to test the validity of our approximations when measuring a different band: For example, if we start

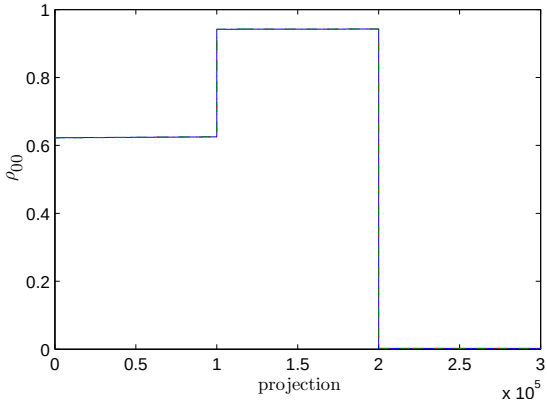

Figure A.1.: Evolution of ρ_{00} for the TLS coupled to the 5-band environment with 201 levels under the periodic influence of projections: numerically exact (blue), using approximation 1 (dashed green) and using both approximations (dotted red). First we apply 10^5 projections, on band 3, followed by 10^5 projections on band 4 and finally again 10^5 projections on band 3. Used parameters: $\delta = \delta_B = 1\,u$, $\beta = 0.5\,u^{-1}$, $\lambda = 1 \cdot 10^{-4}$, $\Delta\varepsilon_k = 4.5 \cdot 10^{-4}$.

in the middle band 3, bands 2, 3 and 4 are involved in the dynamics. If we project on band 4 at some point of the simulation, bands 3, 4 and 5 will become involved and so on.

We will then compare the evolution of the system under the exact dynamics, i.e., the state after each projection is given by $\hat{\rho}_{\mathrm{tot}} = \hat{\tilde{P}}_k \hat{\rho}'_{\mathrm{tot}} \hat{\tilde{P}}_k / \mathrm{Tr}_B \left\{ \hat{P}_k \hat{\rho}'_B \right\}$, with the cases where we apply approximation one only or both of them after each projection. If the approximations are justified, there should not be much difference between these simulations.

Fig. A.1 shows the evolution of ρ_{00} for such a simulation. As one can see, all three curves almost coincide, confirming the validity of the approximations. If we look at the deviations shown in Fig. A.2, we can see that there, indeed, exists a small error due to the approximations. However, as tested in similar simulations with different environmental size, this error further decreases, if the size of the environment is increased.

In addition to the state of the TLS we also have to ensure that the occupation probabilities of the environmental energy bands are correctly calculated when applying the approximations. This is exemplarily demonstrated for the occupation probability of band 3 in Fig. A.3. The error according to approxi-

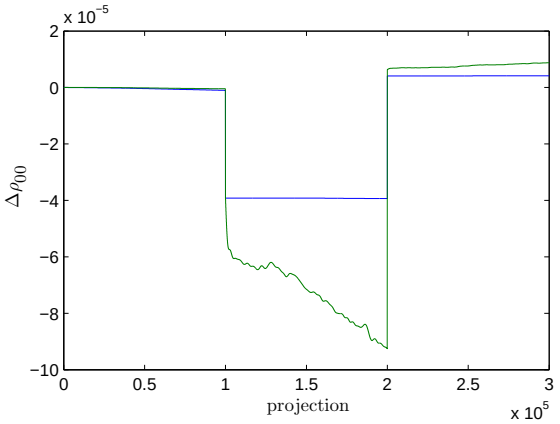

Figure A.2.: Deviations of the ρ_{00} shown in Fig. A.1: Error caused by approximation 1 (blue) and by both approximations (green).

mation 1 is negligible small, being of the order of 10^{-10} in this simulation. The error due to approximation 2 is relatively large directly after projecting on a different energy band, but then p_3 under the exact dynamics relaxes very fast to the value obtained by applying the approximations. The small fluctuations around this value again decrease for increasing size of the environment.

Thus, the approximations 1 and 2 are, indeed, justified to describe the dynamics of the system. As expected, the approximations get the better the larger the environments are.

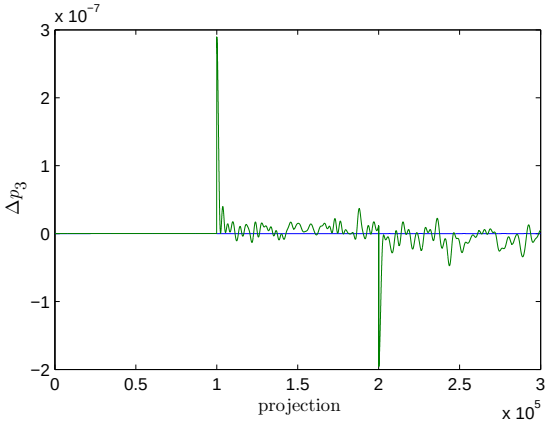

Figure A.3.: The deviations of occupation probability of band 3 from the exact values caused by approximation 1 (blue) are negligible small. The error caused by both approximations (green) is relatively large immediately after projecting into a different band, but reduces very fast after some projections of the same band. The used parameters are the same as in Fig. A.1.

B. Short-time approximation

When calculating the dynamics of the TLS in 2nd order perturbation theory, we obtain terms which consist of a double sum over many oscillating terms with slightly different frequency $\alpha + \omega(m_a, n_b)$ and random amplitudes $|C_{a,b}(m_a, n_b)|^2$:

$$\sum_{m_a,n_b} |C_{a,b}(m_a,n_b)|^2 \cos\left((\alpha+\omega(m_a,n_b))\tilde{t}\right) =: \mathfrak{S}_{a,b}\left(\alpha,\tilde{t}\right) \tag{B.1}$$

with $\tilde{t} := t' - t''$. In this section we like to demonstrate that these terms can be simplified according to (4.19) as long as $\tilde{t}$ is sufficiently small (short-time approximation).

For sufficiently short times, all cosine functions with similar frequencies are almost in phase. Thus, if the sum goes over sufficiently many cosine functions (which is the case, if there are many levels within the bands of small width), this sum can be approximated by the sum over cosine functions which all have the average amplitude $\tilde{c}_{a,b}$.

Thus, for large environments we have

$$\mathfrak{S}_{a,b}\left(\alpha,\tilde{t}\right) \approx \sum_{m_a,n_b} \tilde{c}_{a,b} \cos\left((\alpha+\omega(m_a,n_b))\tilde{t}\right) . \tag{B.2}$$

For the further calculation let us assume that bands a and b have the width $\Delta\varepsilon_a$ and $\Delta\varepsilon_b$, respectively, and the levels within the bands are approximately uniformly distributed. Then, we can approximate the sums by integrals of the form

$$\mathfrak{S}_{a,b}\left(\alpha,\tilde{t}\right) \approx N_a N_b \tilde{c}_{a,b} \int_0^1 \int_0^1 \cos\left((\alpha+\Delta\varepsilon_a\tilde{m}_a - \Delta\varepsilon_b\tilde{n}_b)\tilde{t}\right) \mathrm{d}\tilde{m}_a \mathrm{d}\tilde{n}_b . \tag{B.3}$$

Carrying out the integrations leads to

$$\begin{aligned} \mathfrak{S}_{a,b}\left(\alpha,\tilde{t}\right) \;\approx\; & \frac{A_{a,b}}{\Delta\varepsilon_a\Delta\varepsilon_b\tilde{t}^2}\big[\cos\left(\alpha\tilde{t}\right) + \cos\left((\alpha+\Delta\varepsilon_a-\Delta\varepsilon_b)\tilde{t}\right) \\ & - \cos\left((\alpha-\Delta\varepsilon_b)\tilde{t}\right) - \cos\left((\alpha+\Delta\varepsilon_a)\tilde{t}\right)\big] , \end{aligned} \tag{B.4}$$

where we have introduced the abbreviation $A_{a,b} := N_a N_b \tilde{c}_{a,b}$. Using the trigonometric relations $\cos(x) + \cos(y) = 2\cos((x+y)/2)\cos((x-y)/2)$,

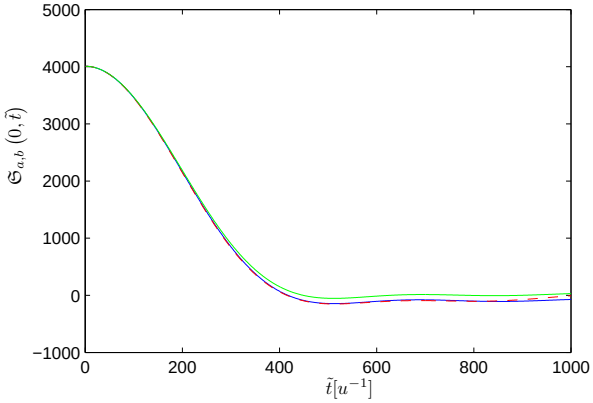

Figure B.1.: Example for the exact function (B.1) with $\alpha = 0$ (blue) compared to the approximations (B.2) (dashed red) and (B.5) (green). For this example we considered two bands with widths $\Delta\varepsilon_1 = 0.01\,u$ and $\Delta\varepsilon_2 = 0.014\,u$ and $N_1 = 40$ and $N_2 = 50$ levels randomly distributed within the bands (uniform distribution). The values $C_{1,2}(m_1, n_2)$ were chosen randomly from a Gaussian distribution such that $\tilde{c}_{1,2} = 2$.

$\cos(x+y) = \cos(x)\cos(y) - \sin(x)\sin(y)$ and $2\sin(x)\sin(y) = \cos(x-y) - \cos(x+y)$, we can rewrite the expression as

$$\begin{aligned}\mathfrak{S}_{a,b}(\alpha,\tilde{t}) \;\approx\; & A_{a,b}\mathrm{sinc}\left(\frac{\Delta\varepsilon_a}{2}\tilde{t}\right)\mathrm{sinc}\left(\frac{\Delta\varepsilon_b}{2}\tilde{t}\right) \\ & \times\left[\cos\left(\alpha\tilde{t}\right)\cos\left(\frac{\Delta\varepsilon_a-\Delta\varepsilon_b}{2}\tilde{t}\right) - \sin\left(\alpha\tilde{t}\right)\sin\left(\frac{\Delta\varepsilon_a-\Delta\varepsilon_b}{2}\tilde{t}\right)\right]\end{aligned} \tag{B.5}$$

Fig. B.1 illustrates these approximations.

If we restrict ourselves to short times corresponding to the initial "plateau" domain of $\mathfrak{S}_{a,b}\left(0,\tilde{t}\right)$ in Fig. B.1, we only need to consider the lowest order of (B.5) in $\Delta\varepsilon_{a,b}\tilde{t}$, which yields

$$\mathfrak{S}_{a,b}\left(\alpha,\tilde{t}\right) \approx A_{a,b}\cos\left(\alpha\tilde{t}\right) + \mathcal{O}\left(\Delta\varepsilon_{a,b}\tilde{t}\right)\,. \tag{B.6}$$

Thus, $\mathfrak{S}_{a,b}\left(\alpha,\tilde{t}\right) \approx A_{a,b}\cos\left(\alpha\tilde{t}\right)$ is a good approximation, if $\Delta\varepsilon_{a,b}\tilde{t}$ is sufficiently small, which is the case for small band widths $\Delta\varepsilon_{a,b}$ and not too long times $\tilde{t}$. As an illustration Fig. B.2 shows the zeroth-order approximation compared with the exact $\mathfrak{S}_{a,b}\left(\alpha,\tilde{t}\right)$ for $\alpha = 2\,u$ and $\alpha = 0\,u$.

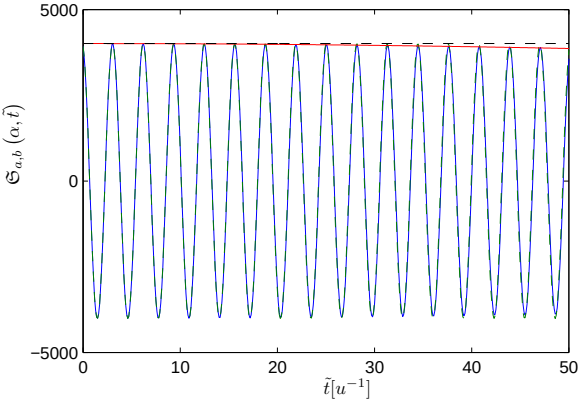

Figure B.2.: Short time approximation (B.6) compared with the exact $\mathfrak{S}_{a,b}\left(\alpha,\tilde{t}\right)$ given by (B.1) for the same simulation as in Fig. B.1. The red and black dashed lines correspond to $\alpha = 0\,u$ and the blue and dashed green lines correspond to $\alpha = 2\,u$.

One may assume that next neighbor bands typically will have approximately the same width. This further improves the approximation, since for $\Delta\varepsilon_a = \Delta\varepsilon_b$ the first order correction vanishes, i.e., $\mathfrak{S}_{a,b}(\alpha) \approx A_{a,b}\cos\left(\alpha\tilde{t}\right) + \mathcal{O}\left(\left(\Delta\varepsilon_{a,b}\tilde{t}\right)^2\right)$.

Of course, this approximation also works for similar sums over sin-functions as they appear in the interaction energy. In lowest order we then have

$$\sum_{m_a,n_b} |C_{a,b}(m_a,n_b)|^2 \sin\left((\alpha+\omega(m_a,n_b))\tilde{t}\right) \approx A_{a,b}\sin\left(\alpha\tilde{t}\right)\,. \tag{B.7}$$

C. Interaction energy

The interaction energy is given by

$$E_{\mathrm{int}}(t) = \mathrm{Tr}\Big\{\lambda \hat{V}(t)\hat{\rho}_{\mathrm{tot}}(t)\Big\}\,. \tag{C.1}$$

To calculate the interaction energy up to 2nd order in interaction strength λ, we have to consider $\hat{\rho}_{\mathrm{tot}}(t)$ up to first order:

$$\begin{aligned}\hat{\rho}_{\mathrm{tot}}(t) &= \hat{\rho}_{\mathrm{tot}}(0) + \mathrm{i}\lambda\int_0^t [\hat{\rho}_{\mathrm{tot}}(0), \hat{V}(t')]\mathrm{d}t' \\ &= \hat{\rho}_{\mathrm{tot}}(0) + \mathrm{i}\lambda\int_0^t \hat{\rho}_{\mathrm{tot}}(0)\hat{\sigma}^+\hat{B}(t') + \hat{\rho}_{\mathrm{tot}}(0)\hat{\sigma}^-\hat{B}^\dagger(t') \\ &\qquad -\hat{\sigma}^+\hat{B}(t')\hat{\rho}_{\mathrm{tot}}(0) - \hat{\sigma}^-\hat{B}^\dagger(t')\hat{\rho}_{\mathrm{tot}}(0)\mathrm{d}t'\,, \end{aligned}\tag{C.2}$$

where $\hat{\rho}_{\mathrm{tot}}(0) = \hat{\rho}(0)\otimes\hat{\rho}_B^0(k)$ is the initial product state with band k being occupied (cf. (4.5)). With this, we get

$$\begin{aligned}E_{\mathrm{int}}(t) &= \mathrm{i}\lambda^2\int_0^t \mathrm{Tr}\Big\{\hat{\sigma}^-\hat{B}^\dagger(t)\hat{\rho}_{\mathrm{tot}}(0)\hat{\sigma}^+\hat{B}(t') + \hat{\sigma}^+\hat{B}(t)\hat{\rho}_{\mathrm{tot}}(0)\hat{\sigma}^-\hat{B}^\dagger(t') \\ &\qquad -\hat{\sigma}^-\hat{B}^\dagger(t)\hat{\sigma}^+\hat{B}(t')\hat{\rho}_{\mathrm{tot}}(0) - \hat{\sigma}^+\hat{B}(t)\hat{\sigma}^-\hat{B}^\dagger(t')\hat{\rho}_{\mathrm{tot}}(0)\Big\}\mathrm{d}t'\,. \end{aligned}\tag{C.3}$$

All other terms do not contribute to the trace. Using (4.9), (4.16) as well as (4.36) leads to

$$\begin{aligned}E_{\mathrm{int}}(t) &= \frac{-2\lambda^2}{N_k}\int_0^t \sum_{m_k,n_{k+1}} |C_{k,k+1}(m_k,n_{k+1})|^2 \\ &\qquad \times\Big[\rho_{11}(0)\sin(\Omega+\omega(n_{k+1},m_k)(t-t')) \\ &\qquad\quad +\rho_{00}(0)\sin(2\delta+\Omega+\omega(n_{k+1},m_k)(t-t'))\Big] \\ &\qquad -\sum_{m_k,n_{k-1}} |C_{k,k-1}(m_k,n_{k-1})|^2 \\ &\qquad \times\Big[\rho_{11}(0)\sin(2\delta+\Omega+\omega(m_k,n_{k-1})(t-t')) \\ &\qquad\quad +\rho_{00}(0)\sin(\Omega+\omega(m_k,n_{k-1})(t-t'))\Big]\mathrm{d}t'\,. \end{aligned}\tag{C.4}$$

Applying the short-time approximation (B.7) and carrying out the integration finally yields the interaction energy

$$E_{\mathrm{int}}(t) = \frac{4\lambda^2}{N_k}\Bigg[(\rho_{11}A_{k,k-1} - \rho_{00}A_{k,k+1}) \frac{1}{2\delta+\Omega} \sin^2\left(\frac{2\delta+\Omega}{2}t\right) + (\rho_{00}A_{k,k-1} - \rho_{11}A_{k,k+1}) \frac{1}{\Omega} \sin^2\left(\frac{\Omega}{2}t\right)\Bigg]. \quad \text{(C.5)}$$

D. Evolution of ρ_{00} for periodic measurement of the same energy band

In order to proof the monotonicity of ρ_{00} as long as the same energy band is being measured, we consider (4.33)

$$\rho_{00,0}(j) \approx \rho_{00}(j-1)\left(1 - 4\frac{\lambda^2}{N_{k_j}}\rho_{11}(j-1)(A_{k_j,k_j-1} - A_{k_j,k_j+1})\,(\zeta_1 - \zeta_2)\right), \tag{D.1}$$

$A_{k_j,k_j-1} - A_{k_j,k_j+1}$ is a fixed value, thus having a fixed sign, since the band index k does not change. This sign may be positive or negative, depending on the chosen interaction. The sign of the expression

$$\zeta_1 - \zeta_2 = \frac{\sin^2\left(\frac{\Omega}{2}\Delta t\right)}{\Omega^2} - \frac{\sin^2\left(\left(\delta + \frac{\Omega}{2}\right)\Delta t\right)}{(2\delta + \Omega)^2} \tag{D.2}$$

depends on the chosen parameters δ, Ω and Δt, but is also fixed. For the resonant case $\Omega = 0$ this factor is always positive for $\Delta t > 0$, since

$$\lim_{\Omega \to 0} \zeta_1 - \zeta_2 = \Delta t^2 - \frac{\sin^2(\delta \Delta t)}{\delta^2} > 0\,. \tag{D.3}$$

Thus, the term $4\frac{\lambda^2}{N_{k_j}}\rho_{00}(j-1)\rho_{11}(j-1)(A_{k_j,k_j-1} - A_{k_j,k_j+1})\,(\zeta_1 - \zeta_2)$, which determines the change of ρ_{00}, always has a fixed sign, when the concrete model parameters are chosen. This means, ρ_{00}, indeed, shows a monotonic behavior as long as the same energy band is measured.

It is also noteworthy that $\rho_{00}(j-1)$ determines how large the change will be. The closer $\rho_{00}(j-1)$ gets to the values 1 or 0, the smaller becomes the change of ρ_{00}. There is no change at all if the ground state or excited state is reached. Hence, both these states are rather stable as long the same band is measured, despite the monotonicity.

E. Vanishing of the off-diagonal elements

In this appendix we discuss the attractor of the off-diagonal elements, i.e., the we investigate the limit $\lim_{j\to\infty}|\overline{\rho}_{10}(j)|$, where $|\overline{\rho}_{10}(j)|$ is given according to (4.74) as

$$\begin{aligned}|\overline{\rho}_{10}(j)| &= \left(\Re(j)^2+\Im(j)^2\right)^{1/2}\\ &= \frac{\mathrm{e}^{c_1 j}}{\gamma}\Big[\big((c_3\sinh(\gamma j)+\gamma\cosh(\gamma j))\,\Re(0)+(c_4-c_2)\sinh(\gamma j)\Im(0)\big)^2\\ &\quad+\big((c_2+c_4)\sinh(\gamma j)\Re(0)+(-c_3\sinh(\gamma j)+\gamma\cosh(\gamma j))\,\Im(0)\big)^2\Big]^{1/2}.\end{aligned} \tag{E.1}$$

Therefore, we have to distinguish two cases, namely those, for which $\gamma=\sqrt{-c_2^2+c_3^2+c_4^2}$ becomes imaginary and those, where it becomes real. Both cases can occur, depending on the chosen parameters.

Let us start with γ being imaginary. In this case, we can rewrite all terms in the square bracket in (E.1) replacing

$$\sinh(\gamma j)=\mathrm{i}\sin(\mathrm{Im}\,(\gamma)\,j)\,,\quad \gamma\cosh(\gamma j)=\mathrm{i}\mathrm{Im}\,(\gamma)\cos(\mathrm{Im}\,(\gamma)\,j)\,. \tag{E.2}$$

Hence, all terms in this bracket are oscillating, which means that $\lim_{j\to\infty}|\overline{\rho}_{10}(j)|=0$ holds, if the prefactor $\mathrm{e}^{c_1 j}$ vanishes for $j\to\infty$, that is, if c_1 defined in (4.66) is negative. It is obvious that

$$\begin{aligned}c_1 &= -2\lambda^2\cosh(\beta\delta_B/2)\left(\frac{1-\cos(\Omega\Delta t)}{\Omega^2}+\frac{1-\cos((2\delta+\Omega)\Delta t)}{(2\delta+\Omega)^2}\right)\\ &\leq 0\,,\end{aligned} \tag{E.3}$$

since $1-\cos(\Omega\Delta t)\geq 0$ and $1-\cos((2\delta+\Omega)\Delta t)\geq 0$. Only if both of this expressions are 0, $c_1=0$ holds. This is the case only, if $\Delta t=n\frac{\pi}{\delta}$ and $\Omega=\frac{2m\pi}{\Delta t}$, $n=0,1,2,...$, $m=1,2,....$ For this choise of the parameters, we also get $c_3=0$ and $c_4=0$ (cf. (4.68) and (4.69)). The only non-vanishing

coefficient is c_2 (4.67). This leads to

$$\begin{aligned}
|\overline{\rho}_{10}(j)|^2 &= -\frac{1}{c_2^2}\left[\left(\sqrt{-c_2^2}\cosh\left(\sqrt{-c_2^2}j\right)\Re(0) - c_2\sinh\left(\sqrt{-c_2^2}j\right)\Im(0)\right)^2\right. \\
&\quad \left. + \left(c_2\sinh\left(\sqrt{-c_2^2}j\right)\Re(0) + \sqrt{-c_2^2}\cosh\left(\sqrt{-c_2^2}j\right)\Im(0)\right)^2\right] \\
&= \left(\cosh^2\left(\sqrt{-c_2^2}j\right) - \sinh^2\left(\sqrt{-c_2^2}j\right)\right)(\Re(0)+\Im(0)) \\
&= \Re(0)+\Im(0) \\
&= |\overline{\rho}_{10}(0)|^2 \qquad \text{(E.4)}
\end{aligned}$$

Thus, for this very special choice of the parameters, $|\overline{\rho}_{10}(j)|$, indeed, becomes constant. As discussed in Sect. 4.5.2, also the relaxation constant R (4.84) for the diagonal-elements vanishes in these cases, i.e., it is possible to freeze the state of the TLS by appropriate periodic measurements.

However, for all other choices of the parameters, $c_1 < 0$ holds, and therefore the off-diagonal elements will vanish after sufficiently many measurements if γ is imaginary.

The second case, γ being real, is more difficult to analyze. If γ is real, it is also positive. Thus, all terms of (E.1) containing $\mathrm{e}^{-\gamma j}$ will vanish for $j \to \infty$. However, in order to show that $\lim_{j\to\infty}|\overline{\rho}_{10}(j)| = 0$ holds, one has to ensure that $\mathrm{e}^{(c_1+\gamma)j} \to 0$, i.e., that $c_1 + \gamma < 0$. Indeed, as checked numerically this is the case for arbitrary $\Omega > -\delta$ and $\Delta t > 0$.

For an analytical proof, we restrict ourselves to the resonant case $\Omega = 0$. Introducing the abbreviation $x = \delta\Delta t$, we have

$$\begin{aligned}
c_1 + \gamma &= \underbrace{\frac{-\lambda^2}{\delta^2}\cosh(\beta\delta/2)}_{<0}\left[x^2 + \sin^2(x)\right. \\
&\quad \left. - \sqrt{-\left(x - \frac{1}{2}\sin(2x)\right)^2 + x^2\sin^2(2x) + 4x^2\sin^4(x)}\right]. \qquad \text{(E.5)}
\end{aligned}$$

Thus, we need to show that

$$x^2 + \sin^2(x) \geq \sqrt{-\left(x - \frac{1}{2}\sin(2x)\right)^2 + x^2\sin^2(2x) + 4x^2\sin^4(x)} \qquad \text{(E.6)}$$

holds. Since we consider the case where $\gamma > 0$, both sides of the equation are positive, which allows us to consider the square of both sides. Hence, we have

to prove the following inequality

$$f(x) \;=\; \left(x^2+\sin^2(x)\right)^2 - \left(-\left(x-\frac{1}{2}\sin(2x)\right)^2 + x^2\sin^2(2x) + 4x^2\sin^4(x)\right)$$
$$\geq\; 0 \qquad \text{(E.7)}$$

We rewrite this expression by using the trigonometric relations $\sin(2x) = 2\sin(x)\cos(x)$, $\sin^2(x)+\cos^2(x)=1$, $\sin^2(x)=\frac{1}{2}(1-\cos(2x))$ and $\cos^2(x)-\sin^2(x)=\cos(2x)$, obtaining

$$f(x) = x^4 + \frac{1}{2} + \left(x^2-\frac{1}{2}\right)\cos(2x) - x\sin(2x)\,. \qquad \text{(E.8)}$$

As one can see easily, $f(0)=0$ holds. The final step to prove our inequality is to show that $f(x)$ is strictly monotonically increasing. If this is the case, $f(x)>0$ will hold for any $x>0$. Thus, we consider the derivative of $f(x)$, which reads

$$\frac{\mathrm{d}f(x)}{\mathrm{d}x} = 4x^2(x-\sin(x)\cos(x))\,. \qquad \text{(E.9)}$$

Finally using $\sin(x)\cos(x) \leq |\sin(x)|$ and $|\sin(x)| < x$ for $x>0$, we get

$$\frac{\mathrm{d}f(x)}{\mathrm{d}x} \geq 4x^2(x-|\sin(x)|) > 0\,, \quad \text{for} \quad x>0\,. \qquad \text{(E.10)}$$

This completes our proof that $c_1+\gamma<0$ for any $\Delta t>0$ and therefore, $\lim_{j\to\infty}|\overline{\rho}_{10}(j)|=0$ is valid also for the case of γ being real.

F. POVM measurements of the TLS

As we have discussed in Sect. 3.2, a projective measurement of the total system can be described by a generalized POVM measurement for a subsystem. This is also the case in our model, i.e., we can describe the influence of the measurements of the environment as POVM measurements of the TLS.

For that purpose we have to find the POVM elements $\hat{E}_i$ corresponding to the measurement of energy band up, band down or the same band. Thus, the $\hat{E}_i$ have to fulfill (3.11) with the probabilities given by (4.61)–(4.63), that is,

$$\mathrm{Tr}\left\{\hat{\rho}\hat{E}_+\right\} = p_+(j) = 4\lambda^2 \mathrm{e}^{\beta\delta_B/2}\left(\rho_{11}\zeta_1 + \rho_{00}\zeta_2\right), \tag{F.1}$$

$$\mathrm{Tr}\left\{\hat{\rho}\hat{E}_-\right\} = p_-(j) = 4\lambda^2 \mathrm{e}^{-\beta\delta_B/2}\left(\rho_{00}\zeta_1 + \rho_{11}\zeta_2\right), \tag{F.2}$$

$$\mathrm{Tr}\left\{\hat{\rho}\hat{E}_0\right\} = p_0(j) = 1 - p_+(j) - p_-(j). \tag{F.3}$$

One can easily check that these conditions are fulfilled for

$$\hat{E}_+ = 4\lambda^2 \mathrm{e}^{\beta\delta_B/2}\left(\zeta_1 |1\rangle\langle 1| + \zeta_2 |0\rangle\langle 0|\right), \tag{F.4}$$

$$\hat{E}_- = 4\lambda^2 \mathrm{e}^{-\beta\delta_B/2}\left(\zeta_2 |1\rangle\langle 1| + \zeta_1 |0\rangle\langle 0|\right), \tag{F.5}$$

$$\hat{E}_0 = \hat{1} - \hat{E}_+ - \hat{E}_-. \tag{F.6}$$

In general, none of these elements are orthogonal. However, if we choose appropriate parameters such that ζ_2 or ζ_1 vanishes, $\hat{E}_+$ and $\hat{E}_-$, indeed, become orthogonal. This corresponds to the cases, where we get a strict correlation or anticorrelation between the state of the TLS and measuring band up or band down, as discussed in Sect. 4.6.2.

It is also possible to construct the measurement operators $\hat{M}_i$ describing the influence of the measurements on the TLS. For example, the measurement operator corresponding to the measurement of energy band up, reads

$$\hat{M}_+ = 2\lambda \mathrm{e}^{\beta\delta_B/4}\left(\frac{\mathrm{e}^{\mathrm{i}\delta t}\sin((\delta+\frac{\Omega}{2})\Delta t)}{2\delta+\Omega}|1\rangle\langle 0| + \frac{\sin(\frac{\Omega}{2}\Delta t)}{\Omega}|0\rangle\langle 1|\right). \tag{F.7}$$

This operator fulfills the condition (3.13)

$$\hat{M}_+^\dagger \hat{M}_+ = \hat{E}_+ \tag{F.8}$$

and

$$\hat{\rho}_+(j) = \frac{\hat{M}_+ \hat{\rho}(j-1) \hat{M}_+^\dagger}{\mathrm{Tr}\left\{ \hat{M}_+ \hat{\rho}(j-1) \hat{M}_+^\dagger \right\}} \tag{F.9}$$

yields the correct state of the TLS after the measurement (cf. (4.34) and (4.42)).

G. Lower limit for the Gaussian approximation

In Sect. 7.1 we have approximated the Boltzmann distribution by the Gaussian distribution (7.6). If the ground state energy is set to zero, this can only be a good approximation, if (7.6) yields negligibly small occupation probabilities for $E < 0$. Thus, we have to ensure that

$$f(\mu) = \frac{1}{\sqrt{2\pi}\sigma} \int_0^\infty \mathrm{e}^{-\frac{1}{2}\left(\frac{x-\mu}{\sigma}\right)^2} \mathrm{d}x \approx 1\,, \tag{G.1}$$

which implies that μ has to be sufficiently large for given σ. With the substitution $y = \frac{x-\mu}{\sigma}$ we can rewrite (G.1) as

$$\begin{aligned} f(\mu) &= \frac{1}{\sqrt{2\pi}} \int_{-\mu/\sigma}^\infty \mathrm{e}^{-\frac{1}{2}y^2} \mathrm{d}y \\ &= \frac{1}{\sqrt{2\pi}} \int_0^\infty \mathrm{e}^{-\frac{1}{2}y^2} \mathrm{d}y + \frac{1}{\sqrt{2\pi}} \int_0^{\mu/\sigma} \mathrm{e}^{-\frac{1}{2}y^2} \mathrm{d}y\,. \end{aligned} \tag{G.2}$$

The first term yields $1/2$ whereas the second term can be rewritten by the substitution $z = y/\sqrt{2}$, leading to

$$f(\mu) = \frac{1}{2}\left(1 + \mathrm{erf}\left(\frac{\mu}{\sqrt{2}\sigma}\right)\right)\,, \tag{G.3}$$

with the so-called error function $\mathrm{erf}(x) = \frac{2}{\sqrt{\pi}} \int_0^x \mathrm{e}^{-z^2} \mathrm{d}z$. The value of $\mathrm{erf}(x)$ has to be calculated numerically or can be found in various book as e.g. [24]. We get for example

μ	$f(\mu)$
1σ	0.8413
2σ	0.9773
3σ	0.9987

Thus, we can take $\mu \gtrsim 3\sigma$ as a criterion for our Gaussian approximation to hold.

H. German summary - Deutsche Zusammenfassung

Die klassische Thermodynamik besitzt einen sehr breiten Einsatzbereich: Ursprünglich entwickelt für die Beschreibung von Wärmekraftmaschinen, finden die thermodynamischen Konzepte z.B. auch bei der Beschreibung chemischer Reaktionen oder in der Kosmologie Anwendung. Dabei ist die Thermodynamik selbst eine phänomenologische Theorie, welche auf einigen axiomatisch eingeführten Hauptsätzen basiert.

Die Entwicklung der statistischen Mechanik lieferte eine mikroskopische Begründung der Thermodynamik, basierend auf der klassischen Mechanik. Allerdings wurden dabei zusätzliche Annahmen, wie z.B. die Ergoden Hypothese, benötigt. Mit der Entwicklung der Quantenmechanik stellte sich heraus, dass die klassische Mechanik als Grenzfall dieser neuen Theorie gesehen werden kann und somit die Quantenmechanik die grundlegendere Theorie darstellt. Damit stellte sich die Frage, ob sich die Thermodynamik ohne weitere Zusatzannahmen direkt aus der Quantenmechanik ableiten ließe. Erst vor wenigen Jahren gelang es schließlich, eine solche Begründung der Thermodynamik aus der Quantenmechanik zu finden [15, 17, 41]. So konnte im Rahmen der Quantenthermodynamik gezeigt werden, dass sich ein Quantensystem, welches schwach an eine typische Umgebung gekoppelt ist, praktisch zu jedem Zeitpunkt in einem thermischen Gleichgewichtszustand befindet, selbst wenn für das Gesamtsystem ein reiner Zustand vorliegt. Dies gilt auch im Grenzfall sehr kleiner Systeme, wie z.B. einem einzelnen Zwei-Niveau-System bei Kopplung an eine geeignete Umgebung. Das Gesamtsystem bestehend aus System und Umgebung wird dabei in der Quantenthermodynamik zunächst als abgeschlossenes System betrachtet. Insbesondere existiert keine Wechselwirkung mit externen Beobachtern. Nun wissen wir aber, dass Messungen in der Quantenmechanik das gemessene System beeinflussen. Daher stellt sich die Frage, welchen Einfluss solche Messungen in einem quantenthermodynamischen Modell nach sich ziehen. Die Untersuchung dieser Fragestellung ist Inhalt der vorliegenden Arbeit. Dabei zeigt sich, wie verschiedene, aus der statistischen Mechanik bekannte Konzepte aus der "beobachteten Quantenthermodynamik" hervorgehen, was zum tieferen Verständnis dieser Konzepte beiträgt. Darüber hinaus wird untersucht, inwiefern sich die Messungen zur

Kühlung, Erwärmung und Erzeugung von Inversion oder zur Stabilisierung eines Zustandes nutzen lassen.

H.1. Das quantenthermodynamische Modell

Grundsätzlich betrachtet man in der Quantenthermodynamik ein System, welches an eine Umgebung gekoppelt ist. Unter gewissen Grundvoraussetzungen können dann für das eingebettete System thermische Eigenschaften auftreten: Die Wechselwirkung zwischen System und Umgebung muss schwach sein, d.h. die Wechselwirkungsenergie muss viel kleiner sein als die Energien der Teilsysteme. Dies ist auch eine Grundannahme in den allen gewöhnlichen, thermodynamischen Überlegungen. Darüber hinaus muss die Wechselwirkung einen Energieaustausch zwischen System und Umgebung ermöglichen. Dazu werden resonante Übergänge benötigt. Damit das System tatsächlich in einen thermischen Zustand relaxiert, welcher unabhängig vom Anfangszustand ist, muss die Umgebung eine mit der Energie exponentiell ansteigende Zustandsdichte aufweisen. Dies ist der Fall für modulare Systeme, welche in der Natur typisch sind [15].

Im ersten Teil dieser Arbeit betrachten wir ein konkretes quantenthermodynamisches Modell, nämlich ein Zwei-Niveau-System (TLS) mit Aufspaltung δ gekoppelt an eine Umgebung, bestehend aus n Spins jeweils mit Aufspaltung $\delta_B = \delta + \Omega$. Im resonanten Fall ist $\Omega = 0$. In allen folgenden Betrachtungen setzen wir $\hbar = 1$. Der Hamilton-Operator für das Gesamtsystem lautet

$$\hat{H}_{\text{tot}} = \frac{\delta}{2}\hat{\sigma}_z \otimes \hat{1}_B + \hat{1}_S \otimes \hat{H}_B + \lambda \hat{V} \,. \tag{H.1}$$

Falls die Umgebungsspins nicht untereinander wechselwirken, ist das Spektrum der Umgebung einfach gegeben durch

$$E_k = \delta_B k \,, \quad k = 0, 1, \ldots, n \tag{H.2}$$

mit der Entartung

$$N_k = \binom{n}{k} \,. \tag{H.3}$$

Bei einer schwachen Wechselwirkung zwischen den Spins, wird diese Entartung aufgehoben und die Niveaus werden zu Energiebändern mit endlichen Breiten $\Delta\varepsilon_k \ll \delta_B$.

Laut Quantenthermodynamik liegt eine thermalisierende Umgebung (d.h. eine Umgebung, welche das angekoppelte System in einen thermischen Zustand überführt) vor, wenn ihre Zustandsdichte exponentiell mit der Energie ansteigt. Relevant sind dabei nur die Energieniveaus, für welche während

der Dynamik eine nicht verschwindende Besetzungswahrscheinlichkeit vorliegt. Nehmen wir an, zur Zeit $t = 0$ sei ein bestimmtes Niveau/Band k_0 besetzt, dann lässt sich für hinreichend große Umgebungen die binomiale Entartung um dieses Niveau durch eine exponentielle Entartung approximieren. Man erhält dabei

$$N_k \approx \mathcal{N} \mathrm{e}^{\beta \delta_B k} \tag{H.4}$$

mit

$$\beta(k_0) \approx \frac{1}{\delta_B} \ln\left(\frac{n}{k_0} - 1\right) . \tag{H.5}$$

Die Wechselwirkung zwischen System und Umgebung ist in unserem Modell gegeben als

$$\hat{V} = \left(\hat{\sigma}^+ + \hat{\sigma}^-\right) \otimes \hat{B} , \tag{H.6}$$

mit

$$\begin{aligned} \hat{B} = \sum_k \sum_{n_k, m_{k+1}} & \quad C_{k+1,k}(m_{k+1}, n_k) \, |n_k\rangle\langle m_{k+1}| \\ & + \quad C_{k,k+1}(n_k, m_{k+1}) \, |m_{k+1}\rangle\langle n_k| , \end{aligned} \tag{H.7}$$

wobei mit $\hat{\sigma}^+ = |1\rangle\langle 0|$ und $\hat{\sigma}^- = |0\rangle\langle 1|$ der Erzeugungs- bzw. Vernichtungsoperator des TLS bezeichnet wird. Um das Modell möglichst allgemein zu halten, betrachten wir die $C_{i,j}$ als einen Satz von Zufallsmatrizen mit gaußverteilten Einträgen. Diese Wechselwirkung erlaubt einen Energieaustausch zwischen System und Umgebung. Außerdem soll die Wechselwirkung schwach sein, was sich durch geeignete Wahl der Wechselwirkungsstärke λ erreichen lässt.

Im resonanten Fall $\delta = \delta_B$ sind also alle Bedingungen für ein typisches quantenthermodynamische Modell erfüllt. Eine Präparation der Umgebung in einem bestimmten Band k_0 bewirkt damit bei ungestörter Heisenbergdynamik des Gesamtsystems eine Relaxation des TLS in einen thermischen Zustand mit Temperatur $T = 1/\beta$. Dieses Verhalten lässt sich auch numerisch verifizieren. Dazu wird die Zeitentwicklung des Gesamtsystems mit Hilfe exakter Diagonalisierung bestimmt und anschließend die Umgebung ausgespurt. Wenn zu Beginn nur ein einzelnes Energieband besetzt ist, sind während der Dynamik maximal drei Bänder relevant (das ursprünglich besetzte und seine Nachbarbänder). Die Umgebung kann also durch ein Dreiband-Modell beschrieben werden, wodurch sich die Größe des Gesamt-Hilbertraums soweit reduzieren lässt, dass die exakte Diagonalisierung möglich wird. Abbildung H.1 zeigt das

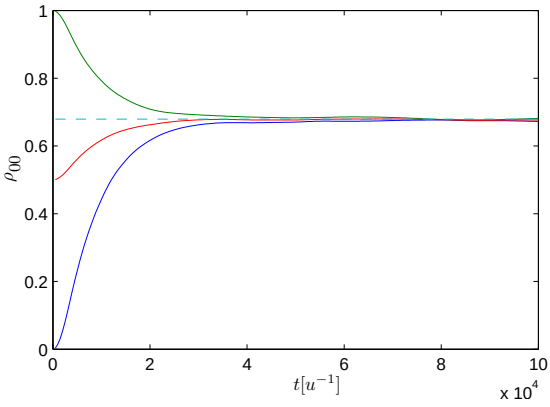

Abbildung H.1.: Relaxation des TLS mit Aufspaltung $\delta = \delta_B = 1\,u$ in einen thermischen Zustand mit Temperatur $T = 1/\beta = 4/3\,u$ für drei verschiedene Anfangszustände. Bei der Umgebung ist zu Beginn nur das mittlere Band besetzt: $\hat{\rho}_B(0) = \frac{1}{N_2}\sum_{n_2}|n_2\rangle\langle n_2|$. Die Wechselwirkungsstärke ist $\lambda = 10^{-4}\,u$ und die Breite der Bänder $\Delta\varepsilon = 0.001\,u$.

Ergebnis einer solchen Simulation. Tatsächlich relaxiert das TLS unabhängig von seinem Anfangszustand in einen thermischen Zustand, welcher durch die Entartungsstruktur der Umgebung festgelegt ist.

H.2. Der Einfluss periodischer Messungen

H.2.1. Kurzzeitdynamik und Trajektorien

Das zuvor eingeführte quantenthermodynamische Modell wird nun ergänzt durch periodische Messungen der Umgebungsenergie bzw. -magnetisierung.

Nach dem Mess-Postulat der Quantenmechanik wird eine solche Messung beschrieben durch eine Projektion in den gemessenen Zustand. Der dazugehörige Projektor lautet

$$\hat{\tilde{P}}_k = \hat{1}_S \otimes \hat{P}_k\,, \quad \hat{P}_k = \sum_{n_k} |n_k\rangle\langle n_k|\ . \tag{H.8}$$

Die Messung bewirkt also eine Projektion in das jeweils gemessene Energieband k der Umgebung. Darüber hinaus hat sie auch eine Zerstörung der zuvor

aufgebauten Korrelationen $\hat{C}_{SB}$ zwischen System und Umgebung zur Folge und führt zu einer Änderung des Systemzustandes, wie man durch Ausspuren der Umgebung erkennen kann:

$$\hat{\rho} = \frac{\mathrm{Tr}_B\left\{\hat{\rho}' \otimes \hat{P}_k \hat{\rho}'_B \hat{P}_k + \hat{\hat{P}}_k \hat{C}_{SB} \hat{\hat{P}}_k\right\}}{\mathrm{Tr}_B\left\{\hat{P}_k \hat{\rho}'_B\right\}} = \hat{\rho}' + \frac{\mathrm{Tr}_B\left\{\hat{\hat{P}}_k \hat{C}_{SB}\right\}}{\mathrm{Tr}_B\left\{\hat{P}_k \hat{\rho}'_B\right\}} \,. \tag{H.9}$$

$\hat{\rho}$ bezeichnet hier den Zustand des Systems nach der Messung und $\hat{\rho}'$ den Zustand vor der Messung. Näherungsweise kann der Zustand des Gesamtsystems nach der Messung beschrieben werden durch

$$\hat{\rho}_{\mathrm{tot}} \approx \hat{\rho} \otimes \hat{\rho}^0_B(k) \,. \tag{H.10}$$

mit

$$\hat{\rho}^0_B(k) = \frac{1}{N_k} \sum_{n_k} |n_k\rangle\langle n_k| \,. \tag{H.11}$$

Nach der Messung entwickelt sich das Gesamtsystem dann wieder ungestört, bis nach der Zeit Δt die nächste Messung erfolgt, usw.

Um die Zeitentwicklung des Gesamtsystems unter dem Einfluss dieser periodischen Messungen zu bestimmen, berechnen wir zunächst die Kurzzeitdynamik nach einer Messung mithilfe der zeitabhängigen Störungstheorie. Es zeigt sich dabei, dass es für jede Messung drei mögliche Ergebnisse gibt: Entweder es wird das gleiche Band wie zuvor gemessen (dies ist der wahrscheinlichste Fall), oder aber ein Band höher oder ein Band niedriger. Abhängig davon erhält man auch nach jeder Messung drei mögliche Werte für den Zustand des TLS:

$$\rho_{00,0}(j) \approx \rho_{00}(j-1)\left(1 - 4\frac{\lambda^2}{N_{k_j}} \rho_{11}(j-1)(A_{k_j,k_j-1} - A_{k_j,k_j+1})\,(\zeta_1 - \zeta_2)\right) , \tag{H.12}$$

$$\rho_{00,+}(j) \approx \frac{\rho_{11}(j-1)\zeta_1}{\rho_{11}(j-1)\zeta_1 + \rho_{00}(j-1)\zeta_2} \,, \tag{H.13}$$

$$\rho_{00,-}(j) \approx \frac{\rho_{11}(j-1)\zeta_2}{\rho_{11}(j-1)\zeta_2 + \rho_{00}(j-1)\zeta_1} \,. \tag{H.14}$$

mit

$$\zeta_1 \equiv \frac{\sin^2\left(\frac{\Omega}{2}\Delta t\right)}{\Omega^2} \,, \tag{H.15}$$

$$\zeta_2 \equiv \frac{\sin^2\left(\left(\delta + \frac{\Omega}{2}\right)\Delta t\right)}{(2\delta + \Omega)^2} \,. \tag{H.16}$$

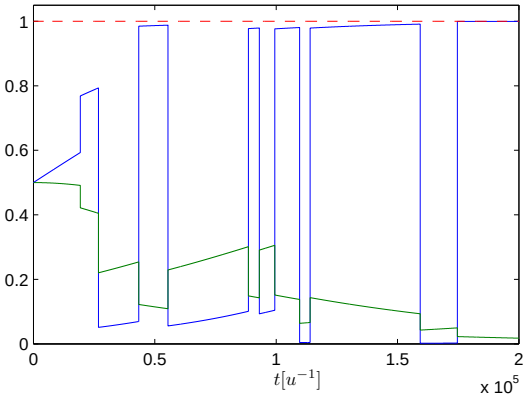

Abbildung H.2.: Trajektorie des TLS für den reinen Anfangszustand $|\psi\rangle = 1/\sqrt{2}(|1\rangle + |0\rangle)$: Nach einiger Zeit befindet sich das TLS immer entweder im Grundzustand oder im angeregten Zustand. Die blaue Linie zeigt den Verlauf von ρ_{00}. Die Nicht-Diagonalelemente (die grüne Linie zeigt $|\rho_{10}|$) verschwinden derart, dass die Reinheit (purity $\mathcal{P}$) des TLS immer nahe 1 bleibt (gestrichelte rote Linie). Verwendete Parameter: $\delta = 1\,u$, $\Delta t = 2\,u^{-1}$, $\beta = 0.75\,u^{-1}$, $\lambda = 4 \cdot 10^{-3}\,u$, $\Omega = 0\,u$.

Eine analoge Rechnung lässt sich auch für die Nicht-Diagonalelemente durchführen. Wie man sieht, bewirkt das Messen des gleichen Bandes nur eine kleine ($\propto \lambda^2$), aber streng monotone Änderung im Zustand des TLS, d.h. das TLS nähert sich bei jeder dieser Messungen mehr und mehr dem Grundzustand oder angeregten Zustand an. Welcher Fall eintritt hängt dabei von den konkreten Modellparametern ab. Im Gegensatz dazu bewirkt die Messung eines anderen Energiebandes eine massive Änderung des TLS Zustandes (z.B. führt $\rho_{00}(j-1) \approx 0$ zu $\rho_{00,\pm}(j) \approx 1$ und umgekehrt). Zusammenfassend folgt daraus, dass sich das TLS nach hinreichend vielen Messungen immer entweder im Grundzustand oder im angeregten Zustand befinden wird. Es durchläuft dann also eine Art quasi-klassischer Trajektorie, völlig im Gegensatz zum quantenthermodynamischen Modell ohne Messungen. Abbildung H.2 zeigt ein Beispiel für solch eine Trajektorie, hervorgerufen durch die periodischen Messungen. Ähnlich wie in der statistischen Mechanik liegt nun also die Situation vor, dass sich ein einzelnes System nicht mehr in einem thermischen Zustand befindet, sondern eine Trajektorie durchläuft. Es stellt sich daher die Frage, ob analog zur statistischen Mechanik Thermalisierung auch hier durch Betrachtung des

Ensemblemittels definiert werden kann.

H.2.2. Ensemblemittelung: Relaxation und Attraktorzustand

Das Ensemblemittel von ρ_{ab} nach Messung j ergibt sich aus der Summe der drei möglichen Werte $\rho_{ab,0}(j)$, $\rho_{ab,+}(j)$ und $\rho_{ab,-}(j)$, jeweils gewichtet mit den Wahrscheinlichkeiten, dass das entsprechende Messergebnis auftritt, also

$$\overline{\rho}_{ab}(j) = p_0(j)\rho_{ab,0}(j) + p_+(j)\rho_{ab,+}(j) + p_-(j)\rho_{ab,-}(j)\,. \tag{H.17}$$

Die Wahrscheinlichkeiten p_0, p_+ und p_-, welche den Besetzungswahrscheinlichkeiten der Energiebänder der Umgebung entsprechen, lassen sich ebenfalls mithilfe der Störungstheorie berechnen.

Es zeigt sich, dass die Nicht-Diagonalelemente im Ensemblemittel typischerweise mit zunehmender Anzahl der Messungen verschwinden. Das Diagonalelement ρ_{00} (und entsprechend $\rho_{11} = 1-\rho_{00}$) nähert sich dagegen exponentiell einem endlichen Wert

$$\overline{\rho}_{00}(j) = \left(\rho_{00}(0) - \overline{\rho}_{00}^{\mathrm{attr}}\right) \mathrm{e}^{-Rj} + \overline{\rho}_{00}^{\mathrm{attr}}\,, \tag{H.18}$$

mit

$$R = 8\lambda^2 \cosh(\beta\delta_B/2)\,(\zeta_1 + \zeta_2) \tag{H.19}$$

und

$$\overline{\rho}_{00}^{\mathrm{attr}} = \frac{\mathrm{e}^{\beta\delta_B/2}\zeta_1 + \mathrm{e}^{-\beta\delta_B/2}\zeta_2}{2\cosh(\beta\delta_B/2)\,(\zeta_1+\zeta_2)}\,, \tag{H.20}$$

wobei ζ_1 und ζ_2 durch (H.15) bzw. (H.16) gegeben ist.

Im Ensemblemittel stellt sich also tatsächlich ein thermischer Attraktorzustand ein, und zwar nicht nur im resonanten Fall ($\Omega = 0$), wie es ohne Messungen der Fall ist, sondern für beliebige Ω. Der Wert von $\overline{\rho}_{00}^{\mathrm{attr}}$ bzw. die Temperatur dieses Attraktorzustandes hängt dabei von der Wahl des "Detunings" Ω sowie von der Zeit zwischen den Messungen Δt ab. Werden die Messungen sehr schnell nacheinander ausgeführt ($\Delta t \to 0$), so ergeben sich zwei Effekte: Zum einen erhält man für die Relaxationskonstante $R \to 0$. Eine solche Unterdrückung der Dynamik durch schnell wiederholte Messungen ist bekannt als der sogenannte Zeno-Effekt [22, 37]. Zum anderen erhält man allerdings in diesem Grenzfall $\overline{\rho}_{00}^{\mathrm{attr}} \to 1/2$, was einer Temperatur von $T \to \infty$ entspricht. Natürlich lässt sich der Grenzfall $\Delta t = 0$ nicht erreichen. Für jedes kleine, aber endliche Δt folgt aber eine langsame Relaxation zu einem Zustand hoher Temperatur.

Von besonderem Interesse ist oftmals das genaue Gegenteil, nämlich das Kühlen eines Systems. Betrachtet man zunächst den resonanten Fall $\Omega = 0$, so stellt sich heraus, dass die niedrigste Temperatur $T = 1/\beta$ erreicht wird für $\Delta t = \frac{n\pi}{\delta}$, $n = 1, 2, 3, ...$ Dies entspricht also genau jener Temperatur, welche für ein einzelnes System im quantenthermodynamischen Modell ohne Messungen vorliegen würde. Interessanterweise ergibt sich diese Temperatur genau dann, wenn die Umgebung als perfekter Messapparat fungiert: Der Zustand des TLS ist dabei streng korreliert mit dem Messergebnis. Bei zu schnellen Messungen nimmt diese Korrelation immer weiter ab, bis sie schließlich im Grenzfall $\Delta t \to 0$ völlig verschwindet. In diesem Sinne kann man sagen, dass der objektive Entropiezuwachs des TLS Zustandes im Einklang ist mit der Zunahme des subjektiven Informationsmangels des Beobachters, welcher die Messungen durchführt.

Bemerkenswerterweise liefert die Berechnung des Langzeitmittels über eine einzelne Trajektorie das gleiche Ergebnis wie die Ensemblemittelung. Das betrachtete System ist also ergotisch.

Möchte man einen Zustand mit Temperatur $T < 1/\beta$ erzeugen, so benötigt man ein endliches "Detuning" Ω der Umgebungsspins. In diesem nicht-resonanten Fall ergibt sich die niedrigst mögliche Temperatur zu

$$T_{\min} = \frac{\delta}{\delta_B} \frac{1}{\beta} . \tag{H.21}$$

Durch Vergrößerung der Aufspaltung δ_B (z.B. durch Anlegen eines externen Magnetfeldes) lassen sich auf diese Art prinzipiell sehr niedrige Temperaturen für das TLS erzeugen. Im nicht-resonanten Regime gibt es noch einen weiteren bemerkenswerten Grenzfall: Hier ist auch die Erzeugung negativer Temperaturen durch periodisches Messen möglich. Für $\Delta t = 2n\pi/|\Omega|$ erhält man die maximale Inversion mit einer negativen Temperatur von

$$T_{\max} = -\frac{\delta}{\delta_B} \frac{1}{\beta} . \tag{H.22}$$

Abbildung H.3 zeigt ein Beispiel für den Attraktorzustand des TLS in Abhängigkeit der Parameter Ω und Δt.

Außerdem ist es auch möglich, durch geeignete Wahl der Parameter Δt und Ω den Anfangszustand "einzufrieren", d.h. der Zustand des TLS bleibt durch die Messungen erhalten.

H.2.3. Periodische Messungen bei kleinen Spin-Umgebungen

Um eine näherungsweise exponentielle Entartungsstruktur zu erhalten, sind große Umgebungen notwendig. Auf dieser Voraussetzung basierte der zuvor

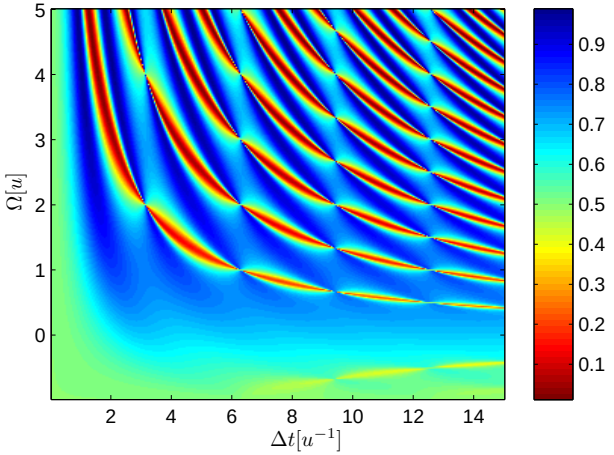

Abbildung H.3.: Attraktor der Grundzustandsbesetzung $\overline{\rho}_{00}^{\mathrm{attr}}$ in Abhängigkeit von Δt und Ω. Zustände niedriger Temperatur sind dunkelblau und solche mit hoher (negativer) Temperatur sind rot. Verwendete Parameter: $\delta = 1\,u$, $\beta = 0.75\,u^{-1}$.

diskutierte analytische Zugang. Man kann sich jedoch fragen, ob sich die diskutierten Effekte auch bei kleinen Umgebungen beobachten lassen. Zur Beantwortung dieser Frage betrachten wir ein TLS, das an Umgebungen gekoppelt ist, die nur aus wenigen (typischerweise 7) Spins bestehen. Für diese Systeme lässt sich die Dynamik unter dem Einfluss periodischer Messungen durch numerisch exakte Diagonalisierung simulieren. Dabei zeigt sich, dass im Ensemblemittel durch die periodischen Messungen tatsächlich ein quasi-stationärer Zustand entsteht, welcher nun zwar vom Anfangszustand abhängt, sich jedoch bei Kenntnis dieses Anfangszustandes mithilfe der analytischen Ergebnisse berechnen lässt. Auf einer deutlich größeren Zeitskala relaxiert das TLS schließlich (aufgrund einer Drift der Besetzungswahrscheinlichkeiten in der Umgebung in Richtung der mittleren Bänder) in einen vollständig gemischten Zustand. Der quasi-stationäre Zustand zeigt dieselben Abhängigkeiten von den Parametern Ω und Δt wie bei der großen Umgebung. So ist es z.B. auch bei kleinen Umgebungen möglich, durch geeignete Wahl der Parameter eine Inversion beim TLS zu erzeugen.

Alternativ zur bisherigen Messung der Umgebungsenergie, lässt sich auch der Einfluss direkter, periodischer Messungen des TLS untersuchen. Dabei zeigt sich, dass die Dynamik des Ensemblemittels zum quasi-stationären Zu-

stand praktisch gleich bleibt. Das gleiche Bild ergibt sich auch, wenn man die Messungen mithilfe eines CNOT-Gatters realisiert. Dies zeigt, dass die Ergebnisse nicht nur für idealisierte projektive Messungen gelten, sondern robust gegenüber einer endlichen Messdauer sind.

H.2.4. Vergleich mit dem Modell von Kurizki et al.

In einer Reihe kürzlich erschienener Paper [5, 12, 18, 19] wurde ein ähnliches Modell diskutiert. Betrachtet wurde hierbei ein TLS gekoppelt an ein Oszillatorbad. Dabei wurden periodisch "quantum non-demolition" Messungen an dem TLS ausgeführt. Über einen Zugang, basierend auf einer nicht-Markovschen Mastergleichung, gelang es den Autoren, den Attraktorzustand des TLS unter dem Einfluss dieser Messungen zu berechnen. Dieser hängt unter anderem von der Verteilung der Oszillatoren im Bad ab.

Betrachten wir den Spezialfall, dass bei allen Oszillatoren dieselbe Frequenz vorliegt, so erhalten wir den gleichen Attraktorzustand wie in unserem Modell. Dies ist bemerkenswert, zeigt es doch, dass das hier diskutierte Verhalten nicht von der speziellen Wahl des Modells abhängt, sondern allgemeinere Gültigkeit besitzt.

H.3. Temperaturschätzung und Fluktuationen

Im zweiten Teil dieser Arbeit versuchen wir neues Licht auf die langanhaltende Diskussion um die Existenz bzw. Bedeutung von "Temperaturfluktuationen" zu werfen [29, 35]. Basierend auf der statistischen Mechanik existieren verschiedene, eher formale Zugänge zu dieser Fragestellung [11, 30], welche schließlich zu der bekannten Formel

$$\Delta T^2 = \frac{k_B T^2}{\mathfrak{C}} \tag{H.23}$$

zur Beschreibung der Temperaturfluktuationen führen. Dabei ist k_B die Boltzmann-Konstante und $\mathfrak{C}$ die Wärmekapazität des betrachteten Systems. Die physikalische Bedeutung dieser Größe ΔT bleibt dabei oft unklar. So wird auch die Meinung vertreten, dass Temperaturfluktuationen ein Widerspruch in sich sind [29].

Vom Standpunkt der Quantenthermodynamik aus betrachtet, existieren solche Temperaturfluktuationen tatsächlich nicht. Wie wir bereits gesehen haben, führt die Kopplung eines Systems an eine geeignete Umgebung zu einem quasistationären, thermischen Zustand, was bedeutet, dass Energie und Temperatur des Systems konstant sind. Allerdings lässt sich diese Temperatur nicht

ohne weiteres bestimmen, denn die Temperatur ist keine Observable, sondern kann nur durch Messung geeigneter Observablen erschlossen werden. Im Folgenden untersuchen wir daher die Abschätzung der Temperatur in einem quantenthermodynamischen System durch Messung der Energie.

H.3.1. Temperaturschätzung durch Energiemessung: Erwartungswert und Fluktuationen

Als Grundannahme setzen wir voraus, dass der Energieerwartungswert des Systems eine bijektive Funktion der Temperatur ist $\langle E\rangle = f(T)$, sich also umkehren lässt zu

$$T = f^{-1}(\langle E\rangle)\,. \tag{H.24}$$

Bei Kenntnis des Energieerwartungswertes ließe sich daraus die Temperatur exakt berechnen. Allerdings sind zur Bestimmung von $\langle E\rangle$ sehr viele Messungen (im Prinzip unendlich viele) notwendig. Daher stellt sich die Frage, ob sich die Temperatur auch mithilfe einer einzelnen Messung abschätzen lässt. Da der Mittelwert den besten Schätzwert für eine Zufallsvariable darstellt, ist es naheliegend, die Temperatur bei Messung der Energie E_m durch

$$T_{\text{est}} = f^{-1}(E_m) \tag{H.25}$$

abzuschätzen. An diesem Punkt wird schon klar, dass dieser Temperaturschätzwert T_{est} fluktuieren wird, da sich je nach gemessenem Energieeigenwert E_m ein anderer Wert T_{est} ergibt. Um konkrete Aussagen über den Erwartungswert von T_{est} und seine Fluktuationen treffen zu können, betrachten wir als Modell die Klasse der modularen Systeme. Wie bereits zuvor erwähnt, sind in der Natur vorkommende Systeme typischerweise modular, wodurch dieses Modell einen weiten Gültigkeitsbereich besitzt. Die Besonderheit hinreichend großer modularer Systeme ist, dass die Besetzungswahrscheinlichkeiten in sehr guter Näherung gaußverteilt sind. Dies folgt direkt aus dem Zentralen Grenzwertsatz der Statistik. Unter Verwendung dieser Gaußverteilung und einer Entwicklung des Temperaturschätzwertes (H.25) um den Energieerwartungswert lässt sich der Erwartungswert $\langle T_{\text{est}}\rangle$ sowie die dazugehörigen Fluktuationen ΔT_{est}^2 berechnen. Es ergibt sich (mit $k_B = 1$)

$$\begin{aligned}\langle T_{\text{est}}\rangle \;=\; & T - T^2\frac{\mathfrak{C}'(T)}{2(\mathfrak{C}(T))^2} \\ & -T^4\frac{15(\mathfrak{C}'(T))^3 - 10\mathfrak{C}(T)\mathfrak{C}'(T)\mathfrak{C}''(T) + (\mathfrak{C}(T))^2\mathfrak{C}'''(T)}{8(\mathfrak{C}(T))^5} \\ & +\dots\,,\end{aligned} \tag{H.26}$$

d.h. der Erwartungswert von T_{est} entspricht der tatsächlichen Temperatur T, falls die Wärmekapazität $\mathfrak{C}$ temperaturunabhängig ist. Ansonsten ergeben sich Abweichungen, welche mit zunehmender Systemgröße jedoch immer abnehmen, da $\mathfrak{C}$ extensiv ist.

Entsprechend erhält man für die Fluktuationen den Ausdruck

$$\Delta T_{\mathrm{est}}^2 = \frac{T^2}{\mathfrak{C}(T)} + T^4 \left(\frac{7(\mathfrak{C}'(T))^2}{2(\mathfrak{C}(T))^4} - \frac{\mathfrak{C}''(T)}{(\mathfrak{C}(T))^3} \right) + \dots . \tag{H.27}$$

Bemerkenswerterweise ergibt sich also in niedrigster Ordnung gerade die bekannte Fluktuationsformel (H.23). Auch sie wäre für temperaturunabhängiges $\mathfrak{C}$ exakt. Die niedrigste Ordnung ist umgekehrt proportional zur Systemgröße n, während der nächsthöhere Korrekturterm schon proportional zu $1/n^2$ ist. Die höheren Ordnungen werden, aufgrund der Vorfaktoren T^2, T^4,..., typischerweise vor allem bei höheren Temperaturen relevant. Allerdings liegt hier keine systematische Entwicklung in T vor, da auch $\mathfrak{C}(T)$ temperaturabhängig ist.

Anhand der Entwicklung (H.27) könnte man zunächst annehmen, dass die Fluktuationsformel (H.23) insbesondere bei niedrigen Temperaturen gültig ist. Dies ist jedoch nicht der Fall, da bei zu niedrigen Temperaturen die gaußsche Näherung für die Boltzmannverteilung nicht mehr zulässig ist. Die Temperatur, unterhalb derer Abweichungen von (H.23) zu erwarten sind, lässt sich abschätzen über

$$3T_{\min}\sqrt{\mathfrak{C}(T_{\min})} = \int_0^{T_{\min}} \mathfrak{C}(T')\mathrm{d}T' . \tag{H.28}$$

Insgesamt lässt sich also sagen, dass die Fluktuationsformel (H.23) für hinreichend große Systeme innerhalb eines bestimmten Temperaturbereiches gilt, wobei dieser mit wachsender Systemgröße immer größer wird. Dies erklärt, wieso "Temperaturfluktuationen", die dieser Formel folgen, bei mesoskopischen Systemen experimentell tatsächlich gemessen wurden [10].

Eine Verbesserung des Temperatur-Schätzwerts ist durch die Mittelung über mehrerer Messungen möglich. Dabei entspricht das Ergebnis für ein modulares System der Größe n nach m Messungen gerade demjenigen eines Systems der Größe $m \cdot n$ nach einer einzelnen Messung. Dies zeigt, dass die Fluktuationsformel (H.23) nur für Temperaturschätzungen, die auf einer einzelnen Messung basieren, gültig ist.

Nach unserer Interpretation bedeuten die Fluktuationen also nicht, dass die Temperatur tatsächlich schwankt, sondern repräsentieren eher eine fundamentale Grenze für die instantane Bestimmbarkeit der Temperatur (durch eine einzelne Messung).

H.3.2. Konkretes Beispiel: Das n-Spin System

Als konkretes Beispiel der allgemeinen Überlegungen betrachten wir ein modulares System bestehend aus n nicht-wechselwirkenden Spins. Dabei bestätigt sich, dass die Fluktuationsformel (H.23) für Systeme ab ca. 100 Spins innerhalb eines gewissen Temperaturbereichs gültig ist. Für wachsende Anzahl der Spins wird dieser Gültigkeitsbereich schnell größer.

H.4. Fazit

In dieser Arbeit wurde gezeigt, wie sich verschiedenste Konzepte der statistischen Mechanik, welche in der Quantenthermodynamik zunächst keine Bedeutung haben, durch das Einbeziehen des quantenmechanischen Messprozesses in die quantenthermodynamischen Modelle ergeben: Dabei wurde die Entstehung quasi-klassischer Trajektorien untersucht und konnte die Gültigkeit der Ergodenhypothese für das betrachtete Systems bewiesen werden. Des Weiteren wurden zwei Aspekte der statistischen Mechanik beleuchtet, welche häufig zu Verwirrungen oder Missverständnissen führen: Zum einen wurde ein Zusammenhang zwischen der objektiven Entropie des Systems und der subjektiven Unkenntnis des Beobachters aufgezeigt und zum anderen diskutiert, wie sich "Temperaturfluktuationen" als fundamentale Grenze für die instantane Bestimmbarkeit der Temperatur interpretieren lassen.

Darüber hinaus konnte im Rahmen des betrachteten Modells gezeigt werden, wie sich periodische Messungen nutzen lassen, um den Zustand des Systems zu konservieren oder aber das System zu kühlen, zu erwärmen oder Inversion zu erzeugen. Sowohl das Kühlen von Quantensystemen als auch die Erzeugung von Inversion ist auch experimentell von besonderer Bedeutung, weshalb die hier diskutierten Mechanismen möglicherweise zukünftig auch für praktische Anwendungen relevant werden könnten.

List of Symbols

Frequently used abbreviation:

TLS	Two-Level System
POVM	Positive Operator-Valued Measure

$\hat{\sigma}^-, \hat{\sigma}^+$	Annihilation, creation operator of the TLS
$\hat{B}$	Environmental part of the interaction $\hat{V}$
β	Inverse temperature
k_B	Boltzmann constant
$\mathrm{Corr}\,(X, Y)$	Correlation coefficient between X and Y
$\hat{C}_{SB}$	Correlations between S and B
δ_B	Energy splitting of the environmental spins
δ	Energy splitting of the TLS
$\hat{\rho}_B$	Density operator of the environment B
$\hat{\rho}$	Density operator of the system S
$\hat{\rho}_{\mathrm{tot}}$	Density operator of the total system
$\overline{\rho}_{ab}$	Ensemble average of ρ_{ab}
$\overline{\rho}_{ab}^{\mathrm{attr}}$	Attractor for $\overline{\rho}_{ab}$
Ω	$\delta_B - \delta$: Detuning of the environment
$\digamma(x)$	Digamma function
E_{int}	Interaction energy
E	Energy
u	arbitrary energy unit

$\langle X \rangle$	Expectation value of X
$\Gamma(x)$	Gamma function
$\hat{H}$	Hamilton operator
$\mathfrak{C}$	Heat capacity
$\hat{V}$	Interaction part of the Hamiltonian
k	Band index
δ_{ab}	Kronecker delta
λ	Coupling strength
τ	Duration of the measurements
n	Number of environmental spins / Number of identical parts in the modular system
N_k	Number of energy levels in band k
$\mathfrak{I}(j)$	Im $(\overline{p}_{10}(j))$
$\mathfrak{R}(j)$	Re $(\overline{p}_{10}(j))$
$\omega(m_{k+1}, n_k)$	Energy difference of level m in band $k+1$ and level n in band k minus δ_B
Z	Partition sum
$\hat{\sigma}_{x,y,z}$	Pauli operators
$\hbar$	reduced Planck constant
$p_{k_j}(j)$	Probability to measure band k_j in measurement j
$p_{0,+,-}$	Probability to measure the same band again, one band higher or one band lower
$\tilde{p}\,(X\|Y)$	Conditional probability of X given Y
$\mathfrak{p}(E)$	Probability to measure energy E (occupation probability)
$\mathfrak{p}^{(n,m)}(E)$	Probability to measure the total energy E for a modular system of n parts after m measurements

$\hat{P}_k$	Projection operator projecting into energy band k of the environment
$\hat{P}_{\|0(1)\rangle}$	Projection operator projecting into the ground (excited) state of the TLS
$\hat{\tilde{P}}_k$	$\hat{1}_S \otimes \hat{P}_k$
$\mathcal{P}$	Purity of the system
$C_{i,j}$	Set of random matrices in the interaction Hamiltonian
$\tilde{c}_{i,j}$	Normalization of the entries of random matrix $C_{i,j}$
$\mathfrak{X}$	$\Delta T_{\text{est}}^2 / \frac{T^2}{\mathfrak{C}}$
R	Relaxation constant for the ground state occupation probability
$\hat{\mathfrak{c}}$	$[[\hat{\rho}_{\text{tot}}(j-1), \hat{V}(t'')], \hat{V}(t')]$
$A_{a,b}$	$N_a N_b \tilde{c}_{a,b}$
ζ_1	$\frac{\sin^2\left(\frac{\Omega}{2}\Delta t\right)}{\Omega^2}$
ζ_2	$\frac{\sin^2\left(\left(\delta+\frac{\Omega}{2}\right)\Delta t\right)}{(2\delta+\Omega)^2}$
σ_X	Standard deviation of X
T_{est}	Temperature estimate
T	Temperature
t	Time
Δt	Time between the measurements
$\text{Tr}\left\{\hat{A}\right\}$	Trace of $\hat{A}$
$\text{Tr}_B\left\{\hat{A}\right\}$	Partial trace of $\hat{A}$ over B
$\hat{U}_{\text{CNOT}}$	Unitary operation corresponding to a CNOT gate
$\Delta\varepsilon_k$	Width of energy band k

Bibliography

[1] G. D. Anderson and S.-L. Qiu. A monotoneity property of the gamma function. *Proc. Amer. Math. Soc.*, **125**, 3355, (1997).

[2] R. Askey. *Orthogonal Polynomials and Special Functions*. Society for Industrial Mathematics, (1975).

[3] J. Audretsch. *Verschränkte Systeme - Die Quantenphysik auf neuen Wegen*. Wiley-VCH, (2005).

[4] L. B. Ballentine. *Quantum mechanics*. World Scientific, Singapore, second edition, (1998).

[5] G. Bensky, D D B. Rao, G. Gordon, N. Erez, and G. Kurizki. Non-Markovian control of qubit thermodynamics by frequent quantum measurements. *Physica E*, **42**, 477, (2010).

[6] V. B. Braginsky, Y. I. Vorontsov, and K. S. Thorne. Quantum Nondemolition Measurements. *Science*, **209**, 4456, (1980).

[7] I. N. Bronstein, K. A. Semendjajew, G. Musiol, and H. Mühlig. *Taschenbuch der Mathematik*. Verlag Harri Deutsch, seventh edition, (2008).

[8] H. B. Callen. *Thermodynamics and an Introduction to Thermostatistics*. John Wiley & Sons, second edition, (1985).

[9] D. Chowdhury and D. Stauffer. *Principles of Equilibrium Statistical Mechanics*. Wiley, Weinheim, New York, (2000).

[10] T. C. P. Chui, D. R. Swanson, M. J. Adriaans, J. A. Nissen, and J. A. Lipa. Temperature Fluctuations in the Canonical Ensemble. *Phys. Rev. Lett.*, **69**, 3005, (1992).

[11] G. L. De Haas-Lorentz. *Die Brownsche Bewegung und einige verwandte Erscheinungen*. Vieweg, (1913).

[12] N. Erez, G. Gordon, M. Nest, and G. Kurizki. Thermodynamic control by frequent quantum measurements. *Nature*, **452**, 724, (2008).

[13] J. Gemmer and M. Michel. Finite quantum environments as thermostats: an analysis based on the Hilbert space average method. *Eur. Phys. J. B*, **53**, 517, (2006).

[14] J. Gemmer and M. Michel. Thermalization of quantum systems by finite baths. *Europhys. Lett.*, **73**, 1, (2006).

[15] J. Gemmer, M. Michel, and G. Mahler. *Quantum Thermodynamics*. Springer, Berlin, Heidelberg, second edition, (2009).

[16] R. Gilmore. Uncertainty relations of statistical mechanics. *Phys. Rev. A*, **31**, 3237, (1985).

[17] S. Goldstein, J. L. Lebowitz, R. Tumulka, and N. Zanghi. Canonical typicality. *Phys. Rev. Lett.*, **96**, 050403, (2006).

[18] G. Gordon, G. Bensky, D. Gelbwaser-Klimovsky, D D B. Rao, N. Erez, and G. Kurizki. Cooling down quantum bits on ultrashort time scales. *New Journal of Physics*, **11**, 123025, (2009).

[19] G. Gordon, D D B. Rao, and G. Kurizki. Equilibration by quantum observation. *New Journal of Physics*, **12**, 053033, (2010).

[20] C. M. Granzow and G. Mahler. Quantum trajectories of interacting pseudo-spin-networks. *Appl. Phys. B*, **67**, 733, (1998).

[21] A. Greven, G. Keller, and G. Warnecke. *Entropy*. Princeton Univ Press, (2003).

[22] W. M. Itano, D. J. Heinzen, J. J. Bollinger, and D. J. Wineland. Quantum Zeno effect. *Phys. Rev. A*, **41**, 2295, (1990).

[23] G. Jaeger. *Quantum Information: An Overview*. Springer, (2007).

[24] E. Jahnke, F. Emde, and F. Lösch. *Tafeln Höherer Funktionen*. Teubner Stuttgart, (1966).

[25] T. Jahnke, S. Lanéry, and G. Mahler. An operational approach to fluctuations of thermodynamic variables in finite quantum systems. *Phys. Rev. E*, **83**, 011109, (2011).

[26] T. Jahnke and G. Mahler. Quantum thermodynamics under observation: The influence of periodic quantum measurements. *EPL*, **90**, 50008, (2010).

[27] M. Jammer. *The Philosophy of Quantum Mechanics: The Interpretations of Quantum Mechanics in Historical Perspective*. John Wiley & Sons, (1974).

[28] C. Jarzynski. Nonequilibrium Equality for Free Energy Differences. *Phys. Rev. Lett.*, **78**, 2690, (1997).

[29] C. Kittel. Temperature fluctuation: An oxymoron. *Phys. Today*, **41(5)**, 93, (1988).

[30] L. D. Landau and E. M. Lifshitz. *Course of theoretical physics, vol. 5: statistical physics pt. 1.* Pergamon, London, third edition, (1980).

[31] R. Landauer. Irreversibility and heat generation in the computing process. *IBM J. Res. Dev.*, **5**, 183, (1961).

[32] P. T. Landsberg. Negative Temperatures. *Physical Review*, **115**, 518, (1959).

[33] B. H. Lavenda and J. Dunning-Davies. Probability distributions of thermodynamic intensive variables. *Int. J. Theor. Phys.*, **30**, 907, (1991).

[34] H. S. Leff and A. F. Rex. *Maxwell's Demon 2.* IOP, Bristol, (2003).

[35] B. B. Mandelbrot. Temperature fluctuation: A well-defined and unavoidable notion. *Phys. Today*, **42(1)**, 71, (1989).

[36] K. Maruyama, F. Nori, and V. Vedral. Colloquium: The physics of Maxwell's demon and information. *Rev. Mod. Phys.*, **81**, 1, (2009).

[37] B. Misra and E. C. G. Sudarshan. The Zeno's paradox in quantum theory. *J. Math. Phys.*, **18**, 756, (1977).

[38] S. Mukamel. Quantum extension of the Jarzynski Relation: Analogy with Stochastic Dephasing. *Phys. Rev. Lett.*, **90**, 170604, (2003).

[39] M. A. Nielsen and I. L. Chuang. *Quantum Computation and Quantum Information.* Cambridge University Press, (2000).

[40] L. Papula. *Mathematik für Ingenieure und Naturwissenschaftler*, volume 3. Vieweg, fourth edition, (2001).

[41] S. Popescu, A. J. Short, and A. Winter. Entanglement and the foundations of statistical mechanics. *Nature Phys.*, **2**, 754, (2006).

[42] W. H. Press, S. A. Teukolsky, W. T. Vetterling, and B. P. Flannery. *Numerical Recipes: The Art of Scientific Computing.* Cambridge University Press, third edition, (2007).

[43] H. T. Quan, Y. D. Wang, Yu-xi Liu, C. P. Sun, and F. Nori. Maxwell's Demon Assisted Thermodynamic Cycle in Superconducting Quantum Circuits. *Phys. Rev. Lett.*, **97**, 180402, (2006).

[44] F. Schwabl. *Quantenmechanik.* Springer, (1988).

[45] U. Seifert. Entropy Production along a Stochastic Trajectory and an Integral Fluctuation Theorem. *Phys. Rev. Lett.*, **95**, 040602, (2005).

[46] D. Spehner and F. Haake. Quantum measurements without macroscopic superpositions. *Phys. Rev. A*, **77**, 052114, (2008).

[47] H. Stumpf and A. Rieckers. *Thermodynamik*, volume 1. Vieweg, (1976).

[48] K. S. Thorne, R. W. P. Drever, C. M. Caves, M. Zimmermann, and V. D. Sandberg. Quantum Nondemolition Measurements of Harmonic Oscillators. *Phys. Rev. Lett.*, **40**, 667, (1978).

[49] Y. Tikochinsky and R. D. Levine. Estimation of inverse temperature and other Lagrange multipliers: The dual distribution. *J. Math. Phys.*, **25**, 2160, (1984).

[50] J. Uffink and J. van Lith. Thermodynamic Uncertainty Relations. *Found. Phys.*, **29**, 655, (1999).

[51] W. Weidlich. *Thermodynamik und statistische Mechanik*. Akademische Verlagsgesellschaft, Wiesbaden, (1976).